Inaugural dissertation

for

obtaining the doctoral degree

of the

Combined Faculty of Mathematics, Engineering and Natural Sciences

of the

Ruprecht - Karls - University

Heidelberg

Presented by

Stephanie Ullrich, M.Sc.

born in Stuttgart, Germany

Oral examination: December 5th, 2024

A novel pulse-chase fluorescence imaging approach for the analysis of HIV-1 cell-to-cell transmission and spread

Referees: Prof. Dr. Hans-Georg Kräusslich

Prof. Dr. Oliver T. Fackler

I. Summary

Transmission of HIV-1 after particle assembly and budding from the membrane of infected T cells can occur by two different modes: cell-free infection, where particles are released into the extracellular space and traffic to susceptible cells by diffusion, and cell-associated transmission by direct cell-cell contacts via so-called virological synapses (VS). In this dissertation, I established a novel approach to visualize HIV-1 cell-to-cell transmission using pulse-chase labeling to separately identify viral transfer and productive infection. To this end, I successfully established and characterized a fully replication-competent labeled HIV-1 derivative, HIV-1$^{iSNAPf(opt)}$. I could demonstrate that this derivative exhibited near wild-type levels of infectivity and remarkably stable integration of SNAPf into the group-specific antigen (Gag), as evidenced by the detection of SNAPf-tag expression by flow cytometry and Western blot after prolonged passaging in A3.01 T cells. In addition, the effect of codon optimization within sfGFP and SNAPf upon insertion into Gag was investigated, based on the previous observation that an increased level of CpG dinucleotides leads to RNA degradation by the Zinc-finger Antiviral Protein (ZAP). No notable enhancement in replication kinetics or infectivity was observed for the codon-optimized derivatives, when a time course was conducted in infected A3.01 T cells and infectivity assays were performed in reporter cell lines.

Furthermore, I developed a real-time method for the detection of productive cell-to-cell transmission. This was accomplished by labeling Gag.SNAPf in the donor cell population with a cell-permeable benzylguanine (BG)-conjugated SNAP dye, followed by continuous observation of Gag.SNAPf expression in contacted target cells, in presence of a novel, highly fluorogenic dye “SNAP23”. Moreover, a semi-automated analytical pipeline, developed in collaboration with ZEISS Arivis, was utilized to quantitatively analyze the factors influencing the dynamics of VS formation and to establish a correlation between cell-to-cell transfer and Gag.SNAPf expression in contacted target cells. The results of the quantitative analyses indicated that a single contact was sufficient to induce new Gag expression in the target cell, regardless of the duration of the contact. Furthermore, new Gag.SNAPf expression was observed in target cells as early as 30 minutes after VS formation, indicating the potential for direct translation of incoming genomic RNA. In conclusion, pulse-chase labeling of HIV-1 infection and cell-to-cell transmission offers a versatile tool for studying the various stages of the HIV-1 replication cycle. In the context of VS, this is the first instance in which distinct contact events have been directly correlated with novel Gag.SNAPf(opt) expression in target cells.

II. Zusammenfassung

Übertragung von HIV-1 zwischen Zellen nach der Partikelbildung und Abknospung von der Membran infizierter T-Zellen kann auf zwei verschiedene Arten erfolgen: zellfreie Infektion, bei der Partikel in den extrazellulären Raum freigesetzt werden und durch Diffusion zu empfänglichen Zellen gelangen, sowie zellassoziierte Übertragung durch direkte Zell-Zell-Kontakte über sogenannte virologische Synapsen (VS). In dieser Dissertation habe ich einen neuartigen Ansatz zur Visualisierung der HIV-1-Übertragung von Zelle zu Zelle mit Hilfe von Puls-Chase-Markierung entwickelt, um den Virustransfer und die produktive Infektion getrennt zu identifizieren. Dafür habe ich erfolgreich ein vollständig replikationskompetentes markiertes HIV-1-Derivat, HIV1$^{iSNAPf(opt)}$, generiert und charakterisiert. Dieses Derivat zeichnete sich durch Infektiosität sehr nah der des Wildtyps aus. Des Weiteren konnte eine bemerkenswert stabile Integration von SNAPf in das gruppenspezifische Antigen (Gag) beobachtet werden. Nach 90 Tagen Passagierung in A3.01 T Zellen, konnte weiterhin Tag-Expression mittels Durchflusszytometrie nachgewiesen werden. Zusätzlich wurde die Auswirkung von Codon-Optimierung innerhalb von sfGFP und SNAPf in Gag untersucht. Dieser Ansatz basiert auf der Beobachtung, dass ein erhöhter Gehalt an CpG-Dinukleotiden zum RNA-Abbau durch ZAP (Zinc-Finger Antiviral Protein) führt. Im Rahmen des Zeitverlaufs in infizierten A3.01 T-Zellen sowie der Infektiositätstests in Reporterzelllinien konnte keine nennenswerte Verbesserung der Replikationskinetik oder der Infektiosität für die Cordon-optimierten Derivate beobachtet werden.

Außerdem wurde eine Methode zum Nachweis einer produktiven Infektion nach VS-Formation in Echtzeit entwickelt. Dazu wurde Gag.SNAPf in der Donor-Zellpopulation mit einem zellpermeablen, mit Benzyl Guanin (BG) konjugierten SNAP-Farbstoff markiert, gefolgt von einer fortlaufenden mikroskopischen Erfassung der Gag.SNAPf-Expression in den kontaktierten Zielzellen unter Verwendung des neuartigen, hoch fluorogenen Farbstoffs SNAP23. Darüber hinaus wurde eine halbautomatische analytische Pipeline, die in Zusammenarbeit mit ZEISS Arivis entwickelt wurde, eingesetzt, um die Faktoren, die die Dynamik der VS-Bildung beeinflussen, quantitativ zu analysieren und eine Korrelation zwischen dem Zell-zu-Zell-Transfer und der Gag.SNAPf-Expression in den kontaktierten Zielzellen herzustellen. Die Ergebnisse der quantitativen Analysen zeigten, dass ein einziger Kontakt ausreicht, um eine neue Gag-Expression in der Zielzelle zu induzieren, unabhängig von der Dauer des Kontakts. Darüber hinaus wurde neue Gag.SNAPf-Expression in den Zielzellen bereits 30 Minuten nach der VS-Bildung beobachtet, was auf eine mögliche direkte Translation der aufgenommenen genomischen RNA hinweist. Zusammenfassend lässt sich sagen, dass die Puls-Chase-Markierung der HIV-1

Zell-zu-Zell Übertragung ein vielseitiges Hilfsmittel zur Untersuchung der verschiedenen Stadien des HIV-1-Replikationszyklus darstellt. In Bezug auf die VS stellt dies den ersten Fall dar, in dem unterschiedliche Kontaktereignisse direkt mit einer neuen Gag.SNAPf(opt)-Expression in den Zielzellen korreliert werden konnten. Dennoch bleibt ungewiss, welcher Anteil der beobachteten Gag.SNAPf(opt)-Expression letztlich zu einer produktiven Infektion führte und welcher Anteil zu einer direkten Translation des übertragenen viralen Gag.SNAPf(opt).

III. Table of contents

1. Introduction

1.1 The human immunodeficiency virus Type 1 (HIV-1)

1.1.1 Taxonomy and Epidemiology of HIV-1

Viruses represent a unique subset of microorganisms, classified as obligate intracellular pathogens due to their dependence on the molecular machinery of host organisms for replication (1). In 1971, David Baltimore proposed a classification model for all viruses based on the mode of mRNA synthesis, which is still in use today (2). The Baltimore classification system divides viruses into seven categories: double-stranded (ds) DNA viruses, single-stranded (ss) DNA viruses, ds RNA viruses, positive sense ss RNA viruses, negative sense ss RNA viruses, positive sense ss RNA viruses with DNA intermediates, and ds DNA viruses with an RNA intermediate. In addition, morphological characteristics of the virion, such as capsid symmetry or the presence of an envelope are used for the taxonomic classification into distinct virus families. The human immunodeficiency virus (HIV) is classified as Baltimore class XI and is a member of the family *Retroviridae* within the subfamily *Orthoretroviridae* and the genus Lentivirus. *(3)*. The stand-out characteristic of retroviruses is the process of reverse transcription, where the RNA genome is converted into cDNA, by a viral RNA-dependent DNA polymerase. This enzyme was given the name reverse transcriptase (RT) following its identification in the context of Rous sarcoma (4) and Rauscher leukemia virus in 1970 (5). The dsDNA intermediate is subsequently integrated into host chromosomes, where host mechanisms can be exploited for gene expression or the establishment of a latent reservoir in the cell (6).

HIV-1 was first isolated in 1983 (7) from a patient exhibiting symptoms consistent with the acquired immune deficiency syndrome (AIDS) that had been described two years prior (8). Although the origin was initially unclear, the primary reservoir was subsequently identified as the chimpanzee species *Pan troglodytes troglodytes*. More than a century ago, a crossover of the closely related simian immunodeficiency virus (SIVcpz) to the human population occurred, resulting in HIV-1 (9, 10). Distinct crossover events resulted in four different HIV-1 groups, based on genomic variations (11): M (major), O (outlier) (12), N (non-M, non-O) (13), and P (putative) (14). Most prevalent in humans is the M group, the main causative of the HIV-1 pandemic, accounting for 98% of HIV-1 infections (15). The World Health Organization (WHO) estimates that 39 million individuals were living with HIV at the end of 2022, with 1.5 million of them being children under the age of 14. While mortality could be significantly reduced by improving antiretroviral therapy, still 630,000 people died from HIV-related causes worldwide in 2023, increasing the total

reported number of fatalities to 42.3 million (16). Disease progression in individuals without treatment can be separated into three different phases: the acute phase, the asymptomatic phase, and the symptomatic phase (17, 18). The stages are defined by laboratory markers for antibodies and viral components in the blood of patients, as well as the presence of characteristic symptoms (19). During the acute phase, increasing viral titers lead to a burst of inflammatory cytokines and apoptosis of infected CD4+ T cells. Additionally, the activation of natural killers (NK) and CD8+ T cells further deplete CD4+ T cells, resulting in a significant overall loss of CD4+ T cells in lymphoid organs (20, 21). Symptoms observed during the acute phase are typically nonspecific and mild, resembling those associated with a common cold (22). The subsequent asymptomatic phase occurs when continuous viral replication and clearance of the virus reach a steady state (23). In untreated HIV-1 infections, viral replication remains high throughout all stages of infection (24) which is counterbalanced by the clearance and generation of new CD4+ cells, prompting in an equilibrium. A proportion of infected cells undergo reversion to a resting state, retain the integrated HIV-1 genome and establish a latent reservoir for the virus (25, 26). Viral escape mutants and other factors can result in a more pronounced reduction of the CD4+ T cell population, as clearance of viral titers becomes insufficient to retain the steady state. Once CD4+ T cell depletion reaches a point at which adaptive immunity is no longer functional and opportunistic infections cannot be eradicated, patients progress to the final symptomatic phase of the disease. This phase, which is marked by a severely compromised immune system, is medically defined as AIDS (27).

Despite extensive research, HIV-1 infection remains incurable. Therapeutic efforts thus primarily focus on managing the disease by minimizing viral replication and suppressing the viral load to undetectable levels. In the absence of treatment, AIDS is lethal due to the severely suppressed immune system which becomes incapable of clearing opportunistic infections. The initial pharmaceutical agent employed against HIV-1 replication was zidovudine (AZT), which targeted reverse transcription (28). However, the drug caused major side effects and drug-resistant HIV-1 strains emerged rapidly. The predominant therapeutic strategy to date comprises of a combination of at least three pharmaceutical agents targeting distinct stages of the viral replication cycle, the combined antiretroviral therapy (cART) (29). The efficacy of cART in reducing viral replication is well documented. However, the treatment has limited impact on latently infected memory T cells, resulting in the need for lifelong therapy (30). One major culprit of cART are significant adverse effects, which can impede the adherence of treated patients and result in drug-related complications (31). Of particular concern are neuropsychiatric adverse effects, which are associated with both viral toxins and drug-related toxicity. They represent a substantial

challenge in the pursuit of a dosage and pharmacokinetic balance within the central nervous system (CNS) to circumvent the development of HIV-associated neurocognitive disorders (HAND) (32). A novel strategy for ART has recently been approved by the Food and Drug Administration (FDA) of the United States of America. This strategy consists of a long-acting, injectable combination of the integrase strand transfer inhibitor cabotegravir (CAB) and the non-nucleoside reverse transcriptase inhibitor (NNRTI) rilpivirine (RPV) (33). Long-acting CAB/RPV ART is administered via an intramuscular injection every two months. This novel approach was documented to increase patient adherence to the prescribed dosage regimen due to the higher convenience and more privacy provided by limiting the intake of the drug to a clinical setting, as reviewed in (34).

1.1.2 Morphology and Genome organization of HIV-1

HIV-1 is an enveloped, positive sense, ss RNA virus. Two copies of the 9.7 kb genome are packaged into a conical capsid, which is surrounded by a membranous barrier, forming the 145 nm spherical particles (35, 36). The genome is comprised of nine open reading frames (ORF), which are flanked by long terminal repeats (LTR) at both 3'- as well as 5'-terminal ends. Encoded proteins are divided into three distinct groups. The first comprises structural proteins: Group Specific Antigen (Gag), Polymerase (Pol) and Envelope Protein (Env). The second category includes regulatory proteins, such as Tat (Trans activator of Transcription) and Rev (Regulator of Virion). The third category encompasses accessory proteins, including Vif (Virion Infectivity Factor), Vpr (Viral Protein R), Vpu (Viral Protein U), and Nef (Negative Factor) (Figure 1).

Gag forms a curved lattice and promotes virion assembly and budding of viral particles at the plasma membrane of host cells. Gag comprises four domains: matrix (MA), capsid (CA), nucleocapsid (NC) protein, phosphoprotein p6 and two small spacer peptides (SP1 and SP2) (37). All proteins are expressed as a 55 kDa precursor, which is processed by the viral protease (PR) into the various proteins. The Pol ORF encodes the viral enzymes PR, RT, with the RNAse H domain, and integrase (IN). The viral PR is also responsible for processing the individual proteins after translation. Due to ribosomal frameshifting at the 3'-terminal end of Gag, Pol is expressed together with Gag as a 160 kDa fusion protein. Frameshifting occurs with a 10% efficiency, resulting in a Gag:GagPol ratio of 1:10 (38).

In contrast to Gag and Pol, the fusion protein Env is not processed by the viral PR but is cleaved by cellular Furin. This process occurs during trafficking to the plasma membrane, where the surface glycoprotein (gp)120 and transmembrane domain gp41 are separated (39). The

heterotrimeric gp120/gp41 complex functions as the initiator of HIV-1 entry, interacting and binding to target cell receptors (40).

The expression of the HIV-1 gene is regulated by Tat through the trans-activating response element (TAR) and post-transcriptionally by Rev, which induces the expression of structural proteins that are required for the cytopathic phase of the replication cycle (41). In addition, the HIV-1 genome encodes several accessory proteins, comprising Vif, Vpu, Vpr, and Nef. The primary function of these proteins is to interact with host cell ligands, thereby reprogramming the cellular molecular machinery to facilitate virus replication (42).

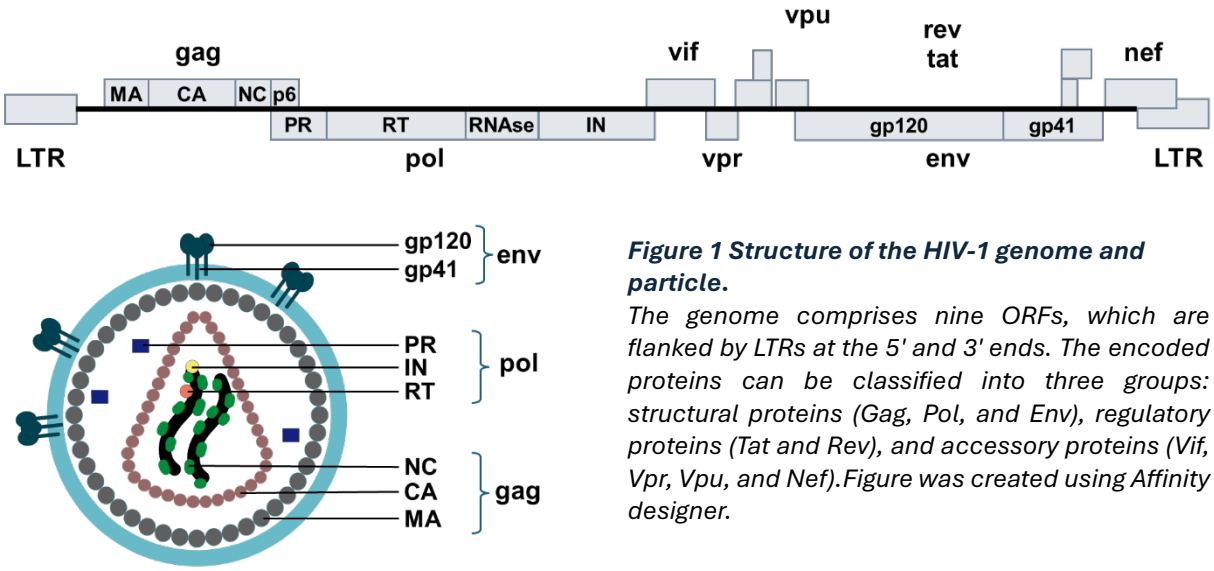

Figure 1 Structure of the HIV-1 genome and particle.
The genome comprises nine ORFs, which are flanked by LTRs at the 5' and 3' ends. The encoded proteins can be classified into three groups: structural proteins (Gag, Pol, and Env), regulatory proteins (Tat and Rev), and accessory proteins (Vif, Vpr, Vpu, and Nef).Figure was created using Affinity designer.

1.1.3 Replication cycle of HIV-1

Transmission of HIV occurs via direct contact with bodily fluids of an individual with a detectable viral load of HIV. Small lesions in the tissue allow entry of cell free or cell-associated viral particles into the bloodstream (46). The most prevalent transmission route is infection during sexual intercourse between people living with HIV and uninfected individuals. Especially in the early days of the AIDS pandemic, contaminated blood products were another common mode of transmission. In addition, vertical transmission from mother to child and the sharing of drug injection equipment play a key role in the spread of HIV-1 (47). The replication cycle of HIV-1 in infected host cells can be divided into eleven distinct steps, which are summarized in the following subchapters.

1.1.3.1 Entry, cytoplasmic trafficking, and nuclear import

Shortly after the discovery of HIV-1 as the primary causative agent of AIDS, CD4+ lymphocytes were identified as the primary target cells of HIV-1 infection (48). Binding of the surface unit of the gp120/gp41 trimer to the CD4 receptor results in refolding of the gp41 transmembrane segment.

The N-terminal fusion peptide translocates to the cell membrane and gp41 folds into a hairpin, initiating membrane fusion by the formation of a fusion pore (49). In addition to the receptor CD4, the chemokine receptors C-X-C motif chemokine receptor 4 (CXCR4) and C-C chemokine receptor type 5 (CCR5) were identified as main co-receptors required for virus fusion (50, 51). Based on the choice of co-receptor, HIV-1 isolates are classified as R5, X4 and R5X4-tropic (52). CXCR4 is used as a coreceptor on T lymphocytes, while CCR5 is expressed on macrophages, the other major target cells of HIV-1.

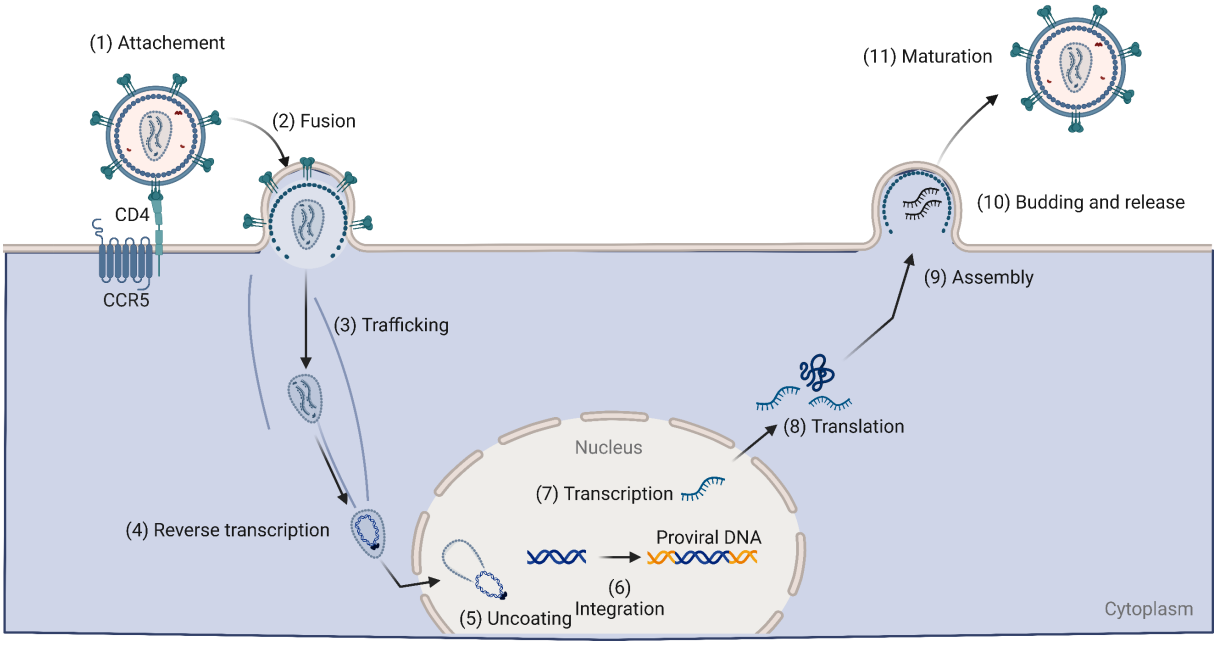

Figure 2 Schematic replication cycle of HIV-1.
Mature HIV-1 particles bind the cellular CD4 receptor with the Env trimer on their outer membrane and subsequently co-receptor CXCR4 or CCR5 (1), resulting in membrane fusion and entry into the cell (2). The capsid is released into the cytoplasm and targeted to the nuclear pore (3). During this process, reverse transcription is initiated (4). In the nucleus, the capsid uncoats (5), reverse transcription is completed, and the viral genome is integrated into the host chromosomal DNA (6). Viral transcripts are generated and exported to the cytoplasm (7), where they are translated by the host cellular machinery (8). Gag and unspliced genomic RNA assemble at the plasma membrane (9), particles bud (10), and Gag/GagPol polyproteins are cleaved by the viral PR (maturation 11). Figure was created with biorender.

Post entry, the viral capsid enters the cytoplasm and gets directed to the nucleus via the actin and microtubule network (53, 54). For a long time uncoating of the viral core and release of the viral genome was believed to occur during the transport to the nuclear pore complex (NPC) inside the cytoplasm (55–57). Other reports supported a model in which uncoating happens at the NPC, since CA could only be detected until binding of the NPC and nuclear entry (58–60). However, more recent data showed that intact capsids can enter the nucleus, suggesting that uncoating does not occur in the cytoplasm but after translocation through the NPC into the nucleus (61, 62). Nuclear import is mediated by capsid binding to phenylalanine-glycine (FG) repeats on the NPC

(63). Nevertheless, the exact location and timing of CA uncoating is still a controversial topic in the HIV-1 research community with evidence for uncoating within (64, 62), or outside the nucleus (65).

1.1.3.2 Reverse transcription

As stated earlier, the ability to reverse transcribe their genome is the defining characteristic common to all retroviruses. Since the discovery of the RNA-dependent DNA polymerase enzyme RT, it has been one of the major targets for antiviral therapy with 17 different FDA-approved drugs (as of march 2024 (66)) and has become a crucial tool in modern diagnostics and molecular biology (67). Initiation of dsDNA synthesis occurs early after entry into susceptible target cells during nuclear trafficking (68). Reverse transcription is initiated by the binding of host cell tRNA, specifically Lys3, near the 5' end of the retroviral genome, which serves as a primer for DNA synthesis. Negative strand DNA synthesis is completed to the 5' end, where strand transfer to the 3' end allows for continuous negative strand DNA synthesis based on the positive sense genomic RNA. The resulting RNA-DNA duplex is the substrate for the RNAse H domain of the RT, which subsequently degrades the viral RNA template. Plus-strand synthesis is primed at a purine-rich sequence that cannot be cleaved by RNase H (67). Removal of the tRNA primer by RNAse H allows for second-strand transfer and completion of the dsDNA. Plus-strand DNA synthesis exceeds the minus strand, which leads to LTRs flanking both ends of the ds viral DNA (vDNA) (69). The term reverse transcription complex (RTC) is used to describe the genome and associated proteins within the viral core during the active phase of reverse transcription. Upon successful synthesis of DNA intermediates, IN facilitates convergence of both vDNA ends by binding to them, thus forming the pre-integration complex (PIC). This allows vDNA to subsequently be integrated into the host genome (70).

1.1.3.3 Integration

Retroviral integration is defined as covalent attachment of the PIC to host cell chromosomal DNA. Integration of uncoated, reverse transcribed viral DNA into host chromatin occurs inside the nucleus and is mediated by the viral IN (71). An IN multimer binds the ends the vDNA and brings both ends of the linear viral transcripts together, leading to the formation of the intasom (72). The vDNA-associated IN enzyme removes the 3'-terminal dinucleotides, resulting in the formation of 3'-hydroxyl groups that are subsequently utilized as nucleophiles to cleave host chromosomes and target the 5'-phosphate groups. (73). The recombined DNA intermediate is repaired by the host cell machinery, resulting in an integrated provirus. While the overwhelming majority of integration events lead to active transcription of viral proteins in parallel with the host cell ORFs

during active replication, the integrated provirus may also become silent, creating a latent reservoir that is capable of activation upon stimulation (71).

1.1.3.4 Assembly, budding and release

Under the control of the regulatory protein Tat, transcription of viral genes and replication of the HIV-1 genome is conducted by the molecular host cell machinery (74). The export of unprocessed viral mRNAs from the nucleus into the cytoplasm is facilitated by Rev. Regulatory proteins are redirected to the nucleus, where they modulate transcription and replication after translation. Structural viral components and newly transcribed RNA genomes are directed to the plasma membrane, where they are assembled in specialized membrane microdomains. Virion assembly is driven by the Gag polyprotein, which is trafficked to the plasma membrane inner leaflet by the MA domain (75), followed by Env protein incorporation and genome packaging (76). Budding and release of immature viral particles is driven by the recruitment of the cellular endosomal complex required for transport (ESCRT) machinery by the p6 domain of Gag (77).

1.1.3.5 Maturation

Upon budding from the plasma membrane, the immature virion undergoes proteolytic cleavage. The Gag and GagPol precursor proteins are processed in order to generate infectious particles for the next round of infection, marking it a critical step in the HIV-1 replication cycle (78). In the immature state, Gag polyproteins are arranged in a curved radial lattice on the viral membrane. PR dimerizes after budding and cleaves at the flexible linkers to produce the functional active versions of MA, CA, NC, p6, PR, RT, and IN (76). The RNA genome is bound by NC to generate the condensed ribonucleoprotein particle (RNP). Subsequently, CA forms a conical core structure surrounding the NC-associated viral genome. Meanwhile, MA remains in close proximity to the viral membrane (79). Mature particles released from infected cells are subsequently capable of starting a new round of infection by binding the CD4 receptor of previously uninfected target cells.

1.2 Modes of HIV-1 transmission between cells

In the early days of molecular HIV research, understanding viral particle entry, mechanisms inside the cell, and particle release were the primary areas of interest. Extracellular pathways, other than cell type-specific limitations for the initial round of infection, were not well understood. Out of practicality and lack of intent to target cell-associated infection pathways, *in vitro* replication of HIV-1 was performed by inoculation of target cells with cell-free particles. It was soon discovered that HIV-1, like many other viruses, is capable of transmission by direct cell contacts, to circumvent environmental and biophysical constraints as well as host cell immune

system components in the extracellular space (80). In addition, cell-associated transmission includes the potential for long-distance transmission within the same host through the bloodstream. Furthermore, infection of new hosts is facilitated and more efficient when virions remain cell-associated and thus protected (61). However, cell-to-cell spread is not exclusively advantageous for viruses. It requires a higher degree of manipulation of host cell mechanisms and is only efficient for infection of cells in close proximity. Figure 3 provides a schematic illustration of the principal modes of HIV-1 transmission between T cells. Since cell-free transmission has already been covered in the general description of the viral replication cycle, the following sections will address contact-dependent HIV-1 transmission in greater detail, with particular emphasis on virological synapses (VS, plural VSs), which represent a primary area of interest in this thesis.

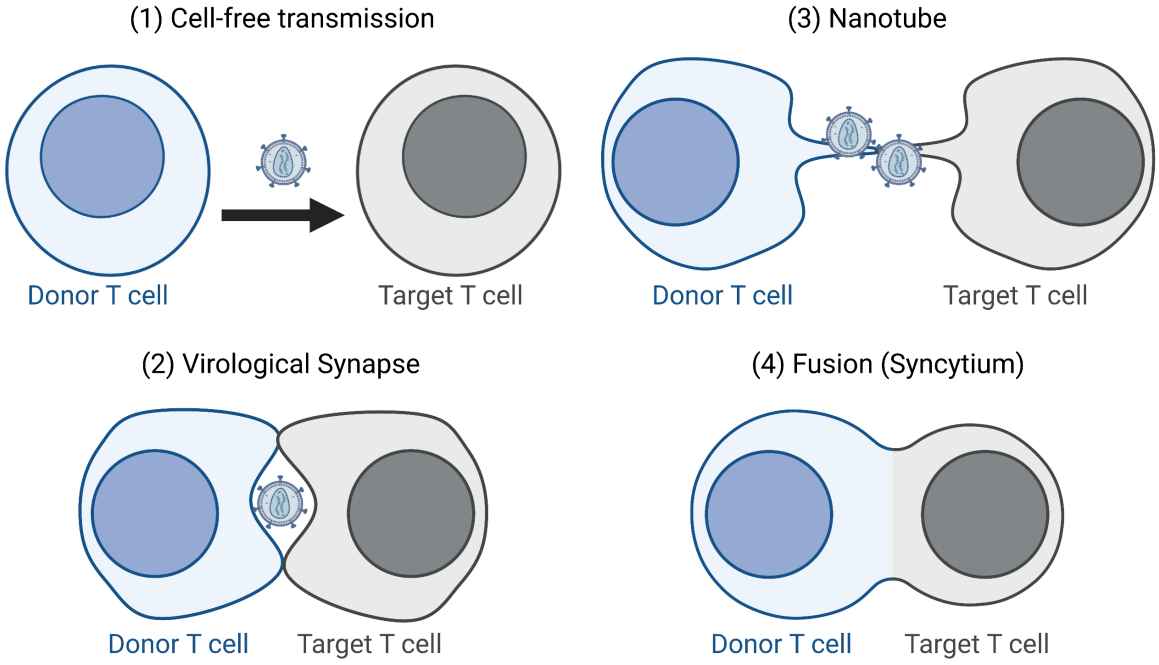

Figure 3 Different modes of in-host HIV-1 transmission between T cells.
(1) Viral particles are released from the infected cell into the extracellular space. The subsequent transit to target cells occurs via undirected diffusion. (2) An infected T cell establishes close contact with an uninfected target cell, forming a stable adhesive junction across which viral particles are transmitted. (3) Filamentous membrane protrusions form a nanotube between infected and uninfected cells, which HIV-1 particles then use to reach the target cell. (4) Env-dependent fusion of infected and uninfected T cells results in the formation of a multinucleated syncytium. Figure was created with biorender.

1.2.1 Cell-to-cell of transmission of HIV-1 via virological synapses

The phenomenon of cell-to-cell transmission, a cell-contact-dependent process that enables efficient viral spread, has been observed across numerous virus families. However, it appears to be exclusive to enveloped viruses (81). This can be attributed to the fact, that most naked viruses rely on cell lysis for release, however transmission through extracellular vesicles has been reported as another way of non-enveloped virus spread in recent years (82). Resulting quasi-envelopes can allow cell-to-cell spread, as demonstrated for the hepatitis A virus (HAV) (83). Cell-associated viral spread has been documented over five decades, with early descriptions dating back to the 1960s for rabies and herpes viruses (84, 85). The first reference to direct transmission between cells in the context of HIV-1 dates back to 1989, when spread of HIV-1 infection was observed in cocultured lymphocytes of seropositive individuals in the presence of Zidovudine (AZT) (80). Subsequent experiments revealed that drug resistance was not responsible for the observed effects, and neutralizing antibodies failed to prevent productive infection within the cocultures. As a result, it was hypothesized that direct cell-to-cell transmission, bypassing an extracellular phase, could account for the observed phenomenon. Furthermore, release and budding of HIV-1 particles at the interface between infected and uninfected T cells was observed in 1995 by transmission electron microscopy (TEM) (86). In 2003, the human T cell leukemia virus type 1 (HTLV-I) was the first retrovirus identified to undergo non-fusional cell-to-cell transmission (87). Infected cells established junctions with uninfected cells, causing viral proteins to polarize toward the contact zone, resulting in the targeted budding of viral particles and their directed transfer to the uninfected cell. The structure was referred to as a VS because of the similarities it exhibited with immunological synapses established between T cells and antigen-presenting cells (APCs). One year later, VSs were reported to also represent the primary mechanism of HIV-1 cell-to-cell transmission. HIV-1 transmission through VS was defined as “cytoskeleton-dependent, stable adhesive junctions through which the virus is transferred via directed transmission” (88).

Env binds to its receptor CD4 on the target cell, forming a stable cell-cell junction that is further stabilized by the interaction of integrins with their ligands (89), as illustrated in Figure 4. Simultaneously, lymphocyte function-associated antigen 1 (LFA-1), intercellular adhesion molecule 1 (ICAM-1), and ICAM-3 become co-enriched at the junction. Subsequently, GM1-rich lipid rafts accumulate at the site of infection towards the synaptic cleft, which is followed by cytoskeleton remodeling (90). The establishment of the VS triggers the recruitment of the Gag-polyprotein and other structural proteins to the contact site, HIV-1 assembles at the GM1-rich lipid rafts which results in directed and polarized budding inside the synaptic cleft (91).

Coreceptors CCR5 and CXCR4 appear to have a limited role in the formation of the VS. However, they are crucial for post-entry processes following the passage through the synapse (92).

There is ongoing debate about the pathways through which particles enter the target cell after crossing the synaptic cleft. Some studies have reported that immature particles are transferred and subsequently internalized via dynamin- and clathrin-mediated endosomal pathways (93, 94). However, these results have not been consistently reproduced, including by the Sattenau group, which initially described the VS in 2004 (92).

A significant contributing factor to the delayed description of HIV-1 cell-to-cell transmission via VS can be attributed to the need for advanced imaging techniques. Major breakthroughs in VS research have relied heavily on the use of fluorescence or electron microscopy. While scanning electron microscopy enabled visualization of budding particles at the contact zone (95), the identification of relevant receptors and cytoskeleton involvement where only accessible with emergence of immunofluorescence (IF) and confocal microscopy (88–90). In the absence of a replication-competent tagged HIV-1 derivative, studies were limited to static representations of transmission via the VS. Given that cell-to-cell is a dynamic process, these methods provided only a partial understanding of the entire process. The introduction of a fluorescently labeled HIV-1 derivative marked a significant advancement, as it allowed for the analysis of dynamic processes involved in conjugate formation and the transfer of fluorescently labeled Gag (96). Confocal microscopy revealed Gag polarization in the donor cell towards the contacted target cell, a finding supported by TEM that identified budding particles colocalizing with the Gag-accumulation sites. The formation of a synaptic button composed of condensated Gag was observed in 80% of conjugated cell pairs, with an average formation interval of 82 minutes. Combining confocal microscopy with electron tomography highlighted the essential role of secretory pathways in HIV-1 dissemination via VSs, including the hijacking of signaling mechanisms typically associated with immunological synapses (97). Imaging of HIV-1 cell-to-cell transmission also revealed that in addition to being the main mechanism of HIV-1 particle dissemination, infected donor T cells can establish multiple synapses with distinct target T cells simultaneously, resulting in the formation of polysynapses (98).

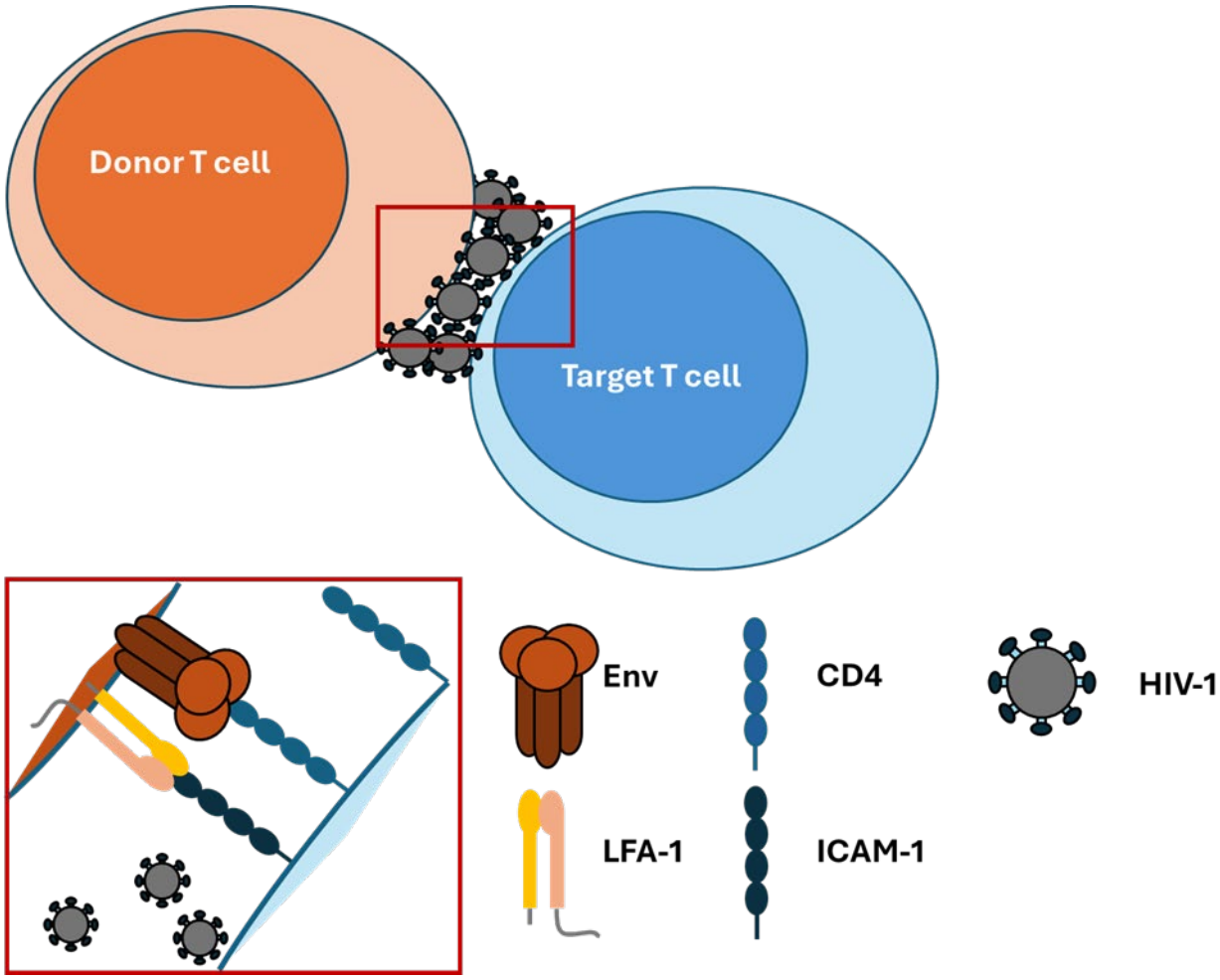

Figure 4 The HIV-1 virological synapse.
Upon contact formation between an infected donor T cell and an uninfected target T cell, a stable junction is formed through the binding of the CD4 receptor by viral Env. Co-enrichment of LFA-1 and ICAM-1 stabilizes the junction. HIV-1 particles bud into the synaptic cleft, and subsequently enter the target cell.

1.2.2 Efficiency of HIV-1 cell-to-cell transmission and relevance *in vivo*

Early studies on cell-associated HIV-1 transmission demonstrated a significantly higher efficiency of cell-to-cell transmission compared to cell-free transmission, with estimates ranging from 10 to 1000-fold (99). Directed budding towards the contact zone results in a localized high multiplicity of infection (MOI), which increases the probability of viral particles overcoming bottlenecks during both entry and post-entry pathways (100, 101). One example of how this has a beneficial impact on VS transmission is the restriction factor TRIM5α. It has been shown that TRIM5α can become saturated with a high number of incoming capsids, which impairs its ability to protect the cell from the influx of additional viral particles (102). Various approaches have been utilized to measure the relative contributions of cell-to-cell versus cell-free transmission. When contact formation between lymphocytes was disrupted by shaking the culture system, a substantial decrease in replication kinetics was observed, while virus release remained

unaffected (103). Trans well systems provide another method for distinguishing between cell-free and cell-to-cell transmission. This method also revealed a significant increase in transmission efficiency, as demonstrated in the aforementioned study. A fluorescent virus transfer assay was performed, resulting in an 18,000-fold increase in efficiency for cell-associated transfer between Jurkat T cells and primary CD4+ T cells, compared to cell-free transmission (104). According to a mathematical model, around 60% of viral infections *in vitro* were associated with cell-to-cell transmission. The model also predicted a reduction in virus generation time by a factor of 0.9 and an increase in viral fitness by a factor of 3.9 (105). The large discrepancies in estimated efficiency ranges are likely due to differences in experimental methodologies and the variability among cell types.

While the transfer of HIV-1 via VS is well documented *in vitro* in both immortalized T cell lines and primary CD4+ T lymphocytes, and is considered the primary mode of transmission, *in vivo* research is still limited to a small number of models. Murooka *et al*. demonstrated the systemic relevance of cell-associated transmission within the lymph nodes of humanized mice through multiphoton intravital microscopy (106). Additionally, HIV-1 spread between lymphocytes was shown to cluster within lymphoid tissues, where tissue-anchored infected cells form Env-dependent conjugates with target CD4+ T cells (101).

A deeper understanding has been gained regarding the impact of cell-to-cell transmission on drug resistance and neutralizing antibodies. In particular, nucleotide analog reverse-transcriptase inhibitors (NRTIs) have demonstrated limited efficacy in suppressing reverse transcription during cell-associated transmission. Prominent pharmaceutical agents, including AZT, tenofovir, and stavudine, have exhibited reduced effectiveness in impeding replication in cell-to-cell transmission (107). The insufficient inhibition of cell-to-cell transmission is likely caused by elevated MOI at the contact site, requiring higher drug doses and greater RT-mediated nucleotide excision activity (108). Combination therapies have been shown to successfully overcome these limitations and restore their inhibitory capacity (109) and are therefore the standard of care in antiretroviral treatment.

The loss of neutralization activity in patient-derived sera against cell-associated HIV-1 was observed before the discovery of broadly neutralizing antibodies (bNAbs) (80). Following the identification of bNAbs, it became evident that antibodies targeting the CD4 binding site were less effective at neutralizing cell-to-cell transmission (110). Furthermore the neutralization potency was shown to vary depending on the viral strain (111). The mechanisms driving resistance to bNAbs are still not fully understood. One proposed explanation is that VS may shield viral particles, obstructing antibody access (111). Similarly, high MOI might reduce neutralization

potency by overwhelming the available antibody pool. However, complete resistance solely due to antibody saturation is unlikely and is not supported by existing data (112, 113).

1.2.3 Other modes of HIV-1 cell-to-cell transmission

In addition to the previously described mechanism of HIV-1 transmission via VS, other cell-associated pathways between T cells further contribute to the complexity of viral transmission. One such mechanism involves the formation of nanotubes, membranous protrusions that connect two T cells. When these nanotubes are established between an infected and an uninfected T cell, HIV-1 particles can exploit these structures for direct transfer to the target cell (114). Nanotubes are classified as either closed-ended or open-ended, the latter known as tunneling nanotubes (TNTs) (92). TNT formation is primarily driven by F-actin, though several other proteins, including M-Sec, LST1, and Myo10, also contribute to their establishment (115). These nanotubes can range in length from 50 to 200 nm, with HIV-1 particles being transferred by "surfing" along these filamentous structures (114, 116). Additionally, HIV-1 Nef has been reported to stimulate TNT formation by interacting with the exocyst complex protein (117).

The formation of a stable cell-cell junction is a prerequisite for viral VS formation. This process is initiated by the binding of the viral Env protein to the CD4 receptor on the surface of target T cells. Env has fusogenic properties, meaning that it not only promotes VS formation but can also trigger cell-cell fusion. This fusion results in the formation of a multinucleated infected cell, a process referred to as syncytium formation (118, 119). Syncytium formation was initially regarded as a critical element in the pathogenesis of HIV-1 during the early days of AIDS research and even served as a classification criterion for certain HIV strains. However, *in vivo* detection was primarily observed in naturally fusogenic cells such as macrophages, leading to ongoing debate over its true impact on in-host transmission, with many researchers viewing it as an *in vitro* artifact (120). The significance of syncytia in the transmission of HIV-1 was reinforced by the identification of small syncytia in humanized mice (106). Given that numerous independent studies have identified VS formation as the primary route of productive cell-to-cell transmission, it can however be assumed that syncytia are, if relevant *in vivo*, only a minor contributor to HIV-1 transmission to prevent excessive fusion. Env is rapidly downregulated in the absence of the Gag polyprotein and is sequestered via its cytoplasmic tail by immature Gag in the donor cell, thereby reducing its fusogenic potential (121). Additionally, the EWI-2 protein, which belongs to the immunoglobulin superfamily (IgSF) and associates with tetraspanins and ezrin, has been identified as a syncytium formation inhibitor (122). The functional role of small T cell syncytia in

productive HIV-1 infection and viral spread remains unclear and continues to be a subject of debate in the field.

1.3 Labeling strategies for live microscopy of HIV-1

The advancement of microscopy and imaging techniques has been a significant driving force in the field of biomedical research. This is particularly true for microbiology and virology, disciplines that examine agents and processes at the micro- or nano-scale. Unlike bacteria, which can be observed with light microscopy, the structural analysis of entities initially described as "ultrafiltratable infectious protein particles" demanded the advent of electron microscopy. This technological breakthrough allowed Helmut and Ernst Ruska to capture the first images of viral particles in 1933 (123). Visualization of viral replication dynamics however posed significant challenges until the green fluorescent protein (GFP), discovered in the early 1960s in the jellyfish *Aequorea victoria* (124), provided new opportunities for tracking molecular and infectious processes. The ability to fuse GFP to proteins of interest enabled detailed analysis of replication dynamics, virus-host interactions, and achieved spatial resolution of individual particles in a dynamic environment. Nowadays, various fluorescent proteins (FPs), spanning from blue to far-red wavelengths, have emerged as an essential tool in modern infectious research (125). Nevertheless, labeling proteins in living systems remains complex, as the addition of large proteins can alter physiological interactions and properties, and expanding the viral genome can affect genome packaging. The following sections will discuss strategies for labeling HIV-1 particles with FPs and the self-labeling tag SNAP.

1.3.1 Fluorescent HIV-1 derivatives tagged with FPs

A key advantage of fluorescent live microscopy is its ability to continuously observe dynamic processes, which static imaging techniques like electron microscopy (EM) or immunofluorescence cannot achieve. This allows for the real-time monitoring of distinct protein-protein interactions and detailed tracking of various stages of the viral replication cycle. However, labeling HIV-1 with FPs presents a challenge because only a few locations within the viral genome are suitable for the insertion of large artificial sequences such as GFP. These insertions potentially result in substantially impacted protein folding kinetics of the fused HIV-1 protein of interest, ultimately affecting the viral ability to undergo a full replication cycle in cells. The first successful attempt to label viral particles was achieved by fusing GFP to the Vpr protein (126). This method utilized the interaction between VPR and the p6 domain of Gag, allowing for the incorporation of exogenously expressed Vpr-GFP into the viral particles. This allowed tracking of labeled HIV-1 within the cytoplasm and the observation of interactions with cytoskeletal components. While

this method enabled tracking of virions after their entry into the cell, visualization was restricted to the cytosol until the point of nuclear import (127). To enable tracking of all intracytoplasmic stages, a direct labeling approach was required. This was accomplished shortly after, by fusing enhanced GFP (eGFP) to the C-terminal end of the MA domain, resulting in the generation of an infectious HIV-1 derivative, NL4-3^{EGFP} (128). The insertion of eGFP into HIV-1 affected viral replication significantly, with full recovery only achievable through 50% wild-type complementation. To address this, Hübner *et al*. developed a GFP-tagged HIV-1 derivative, where GFP was inserted into the interdomain linker sequence between MA and CA, rather than being fused to a protein within Gag (104). For this derivative, known as HIV Gag-iGFP, the authors reported single-round infectivity comparable to wild-type (wt) HIV_{NL4-3} in HeLa MAGI indicator cells and rapid viral spread in the highly permissive T cell line MT4, without requiring a helper virus. However, the virus demonstrated markedly reduced spread in T cell lines other than MT4. HIV Gag-iGFP allowed for tracking of full-length, unprocessed Gag in most virus-producing cells. By employing HIV Gag-iGFP, the researchers successfully quantified cell-to-cell transmission through live cell imaging and flow cytometry, as summarized in 1.2.1 (94, 96, 129).

Beyond labeling Gag, various labeling strategies have been developed for different viral proteins to highlight distinct stages of viral infection. Fusing eGFP to IN allowed for the visualization of PICs in the nucleus, without altering the infectivity of the fluorescent virions. (130). To simultaneously image interactions between HIV-1 genomes and Gag during assembly, researchers used a combination of Gag labeled with mCherry and RNA tagged with stem loops that bind to the coat protein of bacteriophage MS2, which was fused with GFP (131). Labeling of Env was achieved by inserting GFP into the V4 and V5 loops, a region shown to tolerate fluorescent proteins (132). However, this insertion led to a significant reduction in infectivity. Wang *et al*. developed a dual-fluorescent HIV derivative by labeling Gag with mCherry and inserting super folder GFP (sfGFP) into the Env V4 loop (133). Although the resulting virus was non-infectious, it was still capable of forming VS and transferring fluorescent Gag and Env into target cells. Fluorescence recovery after photobleaching (FRAP) studies revealed that Env accumulation at the VS and its incorporation into new particles occurred via a process of continuous internalization and targeted secretion, rather than through irreversible interactions with the budding virus. Nevertheless, it was determined that this recycling process has a minimal impact on VS formation and the transfer of the virus across this structure. In summary, despite the development of various techniques for labeling Gag and other proteins on the HIV-1 virion, a tagged HIV-1 derivative that maintains full replication competence over multiple infection cycles has not yet been established.

However, direct labeling of Gag is the only method that facilitates tracking of virions from their entry into the cell until nuclear import and enables observation of Gag expression before plasma membrane assembly. To examine HIV-1 dissemination across multiple infection cycles with minimal effects on protein function, it is essential to develop a fully replication-competent, tagged HIV-1 derivative.

1.3.2 SNAP-tag and SNAP-tag labeling

Labeling of proteins of interest was not only achieved with FPs, but also with self-labeling enzyme derivatives such as SNAP-, CLIP-, or Halo-tag (134). Unlike FPs, self-labeling tags do not exhibit autofluorescence, thereby eliminating the issue of photostability, which is of particular importance for live imaging in living cells.

The SNAP-tag is derived from the human DNA repair protein O6-alkylguanine-DNA-alkyltransferase (AGT), which naturally dealkylates O6-alkylated guanine residues in damaged DNA (135). The reaction with O6-benzylguanine (BG) derivatives results in an irreversible transfer of the benzyl group to the active site cysteine of AGT. This reaction was used to label proteins by fusing AGT to the protein of interest and conjugating BG to fluorophores. Genetic engineering enhanced substrate specificity by reducing labeling of endogenous AGT (136). The labeling process is highly specific with minimal background interference, as fluorescence appears only upon binding of the SNAP-tag, resulting in increased fluorogenicity (137, 138). BG substrates can be conjugated to a variety of fluorophores, offering greater flexibility for fluorescence microscopy compared to FPs. A variant of SNAP, termed SNAPf, was developed by adding nine amino acid substitutions and a C-terminal deletion to the wild-type AGT sequence, resulting in a tenfold increase in reactivity toward BG substrates (136, 138).

In 2011, Eckhardt and colleagues observed improved replication kinetics in SNAP-tagged HIV-1 derivatives compared to variants with GFP inserted into Gag. They developed HIV-1^{SNAP} by fusing SNAP to the MA domain, and found that this did not substantially interfere with virus entry or infectivity (139). In contrast to HIV-1^{iGFP} the SNAP-tag was fused C-terminally to MA, without the PR cleavage site introduced by Hübner *et al.* in 2007 (140), since the aim at the time was to observe the viral MA protein and no functional benefits could be detected (141). The SNAP-tag offers several advantages over FPs (i) its smaller size leads to fewer potential negative impacts on the virus or target protein; (ii) the fluorophores linked to BG substrates have higher quantum yield and photostability, enhancing brightness and reducing photobleaching; (iii) the SNAP-tag supports a wider range of fluorophores, particularly in the far-red spectrum, offering greater versatility; (iv) it allows full control over the timing of fluorescence activation; (v) the variant SNAPf

enables rapid labeling, achieving 50% efficiency in just 12 seconds with TMR Star *in vitro* (138, 139, 142–144). Another advantage is its compatibility with super-resolution microscopy, as proteins can be labeled with organic fluorophores with higher photon yield compared to FPs, resulting in a brighter and more photostable signal (145).

1.4 Effect of CpG content in the HIV-1 genome on viral replication

Zinc-finger antiviral protein (ZAP) is a host antiviral factor that selectively binds to cytosine–guanine dinucleotide pairs (CpG) in RNA sequences, leading to their degradation and thereby reducing the accumulation of viral mRNA in the cytoplasm. Initially identified for its role in inhibiting murine leukemia virus (MLV) replication in rat cells, ZAP was later found to restrict a variety of other RNA viruses through similar mechanisms (146, 147). In 2011, Zhu *et al*. demonstrated that HIV-1 genomic RNA is also subjected to ZAP-induced RNA degradation. They showed that ZAP has an inhibitory effect on infection, when overexpressed in cells (148). Their findings indicated that ZAP predominantly affects multiply spliced viral mRNAs, with minimal impact on unspliced or singly spliced mRNAs. Further research by Takata *et al*. revealed that HIV-1 reduces CpG content in its genome to evade ZAP-mediated degradation, and artificial CpG enrichment was found to inhibit viral particle production (149). Ficarelli *et al*. later showed that inserting CpG-rich sequences into the HIV-1 genome enhances ZAP-mediated RNA degradation. It is noteworthy that the specific location of CpGs in the genome, rather than their overall abundance, determines ZAP sensitivity and antiviral efficacy (150). Given that FPs and self-labeling tags like SNAP naturally exhibit a high CpG content, their integration into the viral genome could increase vulnerability to ZAP. Roy *et al*. tested this hypothesis when inserting nano luciferase (nLuc) or near-infrared fluorescent protein (iRFP) into the HIV-1 genome upstream of Nef. By reducing the CpG content within those tags, they observed improved viral replication and reporter expression *in vitro* and *ex vivo* (132).

1.5 Aims and outline of this thesis

Previous research largely focused on HIV-1 derivatives labeled with GFP within the Gag region to explore cell-to-cell transmission dynamics via fluorescence microscopy (96, 94, 151). While this approach offered valuable insights into VS formation and productive infection, it also had notable drawbacks. Specifically, the approach mainly assessed the transfer of fluorescently labeled Gag and correlated these observations with the overall cell population. However, the cell-to-cell transmission observed in individual cell pairs at specific time points could not directly be linked to productive infection, as it was unclear whether the observed events were responsible for infection. This was due to the inability to distinguish between transferred and newly produced viral proteins in a fully infectious HIV-1 context.

In order to overcome the aforementioned limitations, the primary objective of this thesis was the establishment and characterization of a labeled, fully replication-competent HIV-1 derivative. Infectivity and replication kinetics needed to be assessed and compared to wild-type HIV-1_{NL4-3} (wt) as well as GFP-tagged derivatives, which were used for the majority of studies investigating the dynamics of cell-to-cell transmission, as described in 1.2.1. As the derivative must be able to retain the label in order to be employed in experiments investigating HIV-1 spread, the stability of the HIV-1 derivative needed to be verified by passaging the derivative over multiple rounds of infection.

The second aim was to develop a protocol for live detection of productive cell-to-cell transmission that allows clear discrimination between transferred and newly expressed viral components, thereby providing a substantial advantage over previously described systems. The imaging data generated from this protocol required quantitative, non-biased analysis to thoroughly assess the dynamics during VS formation and post-entry events. This quantification had to be performed automatically with sophisticated techniques for the segmentation and tracking of cells, as well as the registration of VS formation events, based on the previously established reporter HIV-1 derivative. This study presents a novel approach to examining HIV-1 cell-to-cell transmission and live cell observation of VS formation, that overcomes the limitations of previously described systems. This was achieved by establishing a pulse-chase-labeling protocol that allows the correlation of distinct contact events to productive infection.

2. Material and Methods

2.1 Materials

2.1.1 Laboratory equipment

Name	Company
Agarose gel electrophoresis system	Bio-Rad, Hercules, CA, USA
Bacterial Shaker Multitron Pro	Infors HT, Bottmingen, Switzerland
C1000 Touch Thermal Cycler	BioRad, Hercules, USA
Centrifuge 5417C	Eppendorf AG, Hamburg, Germany
Centrifuge Avanti J-26 XP with JA-10 rotor	Beckman Coulter, Brea, USA
CFX 96 Real Time PCR detector (for SGPERT)	BioRad, Hercules, USA
Electrophoresis power supply EPS 601	Amersham Biosciences, Little Chalfont,
Gel iX Imager (Agarose gel UV-imager)	INTAS Science Imaging, Göttingen, Germany
Ice Maker AF 103	Scotsman, Sprockhövel
Incubator C200	Labotect Labor-Technik-Göttingen
L8-70M Ultracentrifuge with SW28 and SW32 rotor	Beckman Coulter, Brea, USA
LiCor Odyssey Imager CLx	LiCor Bioscience, Lincoln, USA
Light Microscope ELWD 0.3 T1-SNCP	Nikon Instruments Inc., Melville, USA
Microbiological Cabinet	Envair, Emmendingen
Microwave for Agarose gels	Sharp, Cologne
NanoPhotometer	Implen, Munich
PCR FlexCycler	Analytik Jena, Jena
Plate Reader Inifinite M200 Pro	Tecan, Männedorf, Switzerland
SDS-PAGE electrophoresis chamber Mighty smal	Hoefer, Almstetten
Semi-Dry Blotter Fastblot B32	Whatman Biometra, Göttingen
Thermomixer, Eppendorf, Thermomixer comfort	Eppendorf, Hamburg
TL-100 Ultracentrifuge with TLA 45 rotor (Tabletop)	Beckman Coulter, Brea, USA
Vortex Genie 2	Scientific Industries, Bohemia, USA
Water Filtering System	Stakpure, Niederahr
Waterbath MP	Julabo, Seelbach
XS40025 Deltarange Weight Scale	Mettler Toledo, Gießen

2.1.2 Chemicals and consumables

Reagent	Reference
Ampicillin	Carl Roth, Karlsruhe, Germany
BD Cyto perm buffer	BD Biosciences
BD Cytofix/Cytoperm Fixation/Permeabilization Solution Kit	BD Biosciences
BioTracker 400 Blue Cytoplasmic Membrane Dye	Sigma Aldrich
Bromophenol blue	Chroma, Fürstenfeldbruck, Germany
BSA 100x	NEB, Ipswitch, USA
$CaCl_2$	Sigma-Aldrich, St. Louis, USA
CellVue Claret Far Red Fluorescent Cell Linker Mini Kit for General Membrane Labeling	Phanos Technologies
DNA ladder 1 kb Plus	Thermo Scientific, Waltham, USA
dNTP Set	Thermo Scientific, Waltham, USA
Dulbecco's Modified Eagle Medium (DMEM)	Invitrogen, Karlsruhe, Germany
EasySep Direct Hu CD4 Iso Kit	Stemcell technologies
Efavirenz (EFV)	Sigma-Aldrich
Enfuvirtide (T-20)	Roche; NIH AIDS Reagent Program
Fetal Calf Serum (FCS)	Biochrom, Berlin, Germany
Gel Loading Dye, Purple (6x) for DNA	New England Biolabs, Ipswich, USA
High Pure RNA Isolation kit	Roche, Basel, Switzerland
Hoechst33258	Merck
Interleukin (IL)-2	Sigma Aldrich
Kalium-hexacyanoferrat(III)	Sigma-Aldrich
Kanamycin	Carl Roth, Karlsruhe, Germany
LI-COR Blocking Buffer (TBS)	LI-COR Bioscience, Lincoln, USA
Midori Green	Nippon Genetics Europe GmbH, Dueren, Germany
Nitrocellulose membrane	Protran, Schleicher & Schull/Whatman, Dassel, Germany
NucleoBond PC 500, Maxi kit	Macherey Nagel
Nucleospin Gel and PCR Cleanup Kit	Macherey Nagel, Germany
PageRuler prestained	Thermo Scientific, Waltham, USA

Paraformaldehyde (PFA)	Electron Microscopy Sciences
Penicillin Streptomycin (PenStrep)	Thermo Scientific, Waltham, USA
PGEM-T vector system	Promega
Polybrene Infection/Transfection Reagent	Sigma Aldrich
Polyethylenimine (PEI)	Sigma-Aldrich, St. Louis, USA
Poly-L-lysin solution	Sigma Aldrich
Raltegravir (Ral)	AIDS Reagent Program, NIAID
RNaseOUT™ Recombinant Ribonuclease Inhibitor	Thermo Scientific, Waltham, USA
SNAP-Cell 647-SiR	New England Biolabs
SNAP-Cell TMR-Star	New England Biolabs
SPY555-BG	Spirochrome
Sucrose	AppliChem GmbH, Darmstadt, Germany
Superscript III RT	Thermo Scientific, Waltham, USA
TransActTM	Mitenyi Biotec
TritonX-100	Merck, Darmstadt, Germany
X-Gal 5-bromo-4-chloro-3 indolyl-b-D-galactopyranoside	Thermo Scientific, Waltham, USA
ZombieVioloet	Biolegend

2.1.3 Plasmids

name	**reference**	**description**
pNL4-3unc-p6opt, sfGFP on Gag	this thesis	NLC backbone with sfGFP C-terminal to p6 by uncoupling p6 from p6*
pNL4-3unc-p6opt, sfGFPopt on Gag	this thesis	NLC backbone with sfGFP(opt) C-terminal to p6 by uncoupling p6 from p6*
pNLC 4-3	Bohne *et al*. (152)	fully replication competent pNL4-3 backbone under the control of a synthetic CMV promotor

pNLC.isfGFP	this thesis	NLC backbone with sfGFP between MA and CA
pNLC.isfGFPopt	this thesis	NLC backbone with sfGFP(opt) between MA and CA
pNLC.iSNAP	Eckhardt *et al.* (139)	NLC backbone with SNAP between MA and CA
pNLC.iSNAPf	this thesis	NLC backbone with SNAPf between MA and CA
pNLC.iSNAPfopt	this thesis	NLC backbone with SNAPf(opt) between MA and CA
pNLC.iSNAPopt(PRD25N)	this thesis	PNLC.iSNAPf with a mutation in the protease at PR residue 25

2.1.4 Buffers, solutions, and media

name	**composition**
4x Resolving Buffer	1.5 M Tris (pH 8.8), 0.4 % SDS
Acrylamide Stock	30 % Acrylamide 0.15 % Bisacrylamide
Developing solution (Blue cell assay)	H_2O 3mM Potassium ferricyanide 3mM Potassium ferrocyanide 1mM $MgCl_2$ 0.2mg/ml X-Gal (in DMSO)
HBS 2X	H_2O 250 mM NaCl 250 mMHepes 1.5 mMNa_2HPO_4
Laemli SDS buffer	150 mM Tris HCl, pH 6.8 6 % w/v SDS 30 % Glycerin 0.06 % Bromophenol Blue 10 % β-Mercaptoethanol

Resolving Gel	17.5 ml Acrylamide Stock 7.5 ml 4x Resolving Buffer 5 ml H_2O
Running Buffer	1 g SDS 3.03 g Tris 14.4 g Glycine ddH_2O to 1000 ml
SG-PERT dilution buffer 1X (pH 8.0)	5 mMddH_2O $(NH_4)_2SO_4$ 20 mM KCl 20mM Tris-HCl
SG-PERT lysis buffer 2X (pH 7.4)	ddH_2O 50mM KCl 100mM Tris-HCl 40% Glycerol 0.25% Triton X-100
SG-PERT PCR reaction buffer 2X	SG-PERT dilution buffer 10mM $MgCl_2$ 0.2 mg/mlBSA 400µM dNTPs 1 pmolPrimer RT-Assay-fwd 1 pmolPrimer RT-Assay-rev 8ng MS2 RNA 1:10000SYBR Green 0.5 UGoTaq Hotstart Polymerase
Stacking Gel	15 ml Acrylamide Stock 30:0.8% 25 ml 4x Stacking Buffer 60 ml H_2O
TBS-T (10x) pH 7.5	175.32 g NaCl 121.14 g Tris 10 ml Tween dd H_2O 2000 ml
Virus resuspension buffer	PBS 1X 10mM Hepes (pH 7.5) 10 % FCS (v/v)

Western Blot blocking buffer	30 % LI-COR buffer (v/v) dd TBS-T
Western Blot Transfer Buffer 1	0.3 M Tris 20 % Methanol dd H_2O 1000 ml
Western Blot Transfer Buffer 2	0.025 M Tris 20 % Methanol dd H_2O 1000 ml

2.1.5 List of Antibodies

Reagent	Reference	Dilution
Donkey polyclonal Alexa Fluor (405, 488, 568 and 647) secondary antibodies	Thermo Fisher Scientific	1:1000
HIV-1 core antigen-FITC (KC57)	Beckman Coulter GmbH	1:100
HIV-1 core antigen-RD1 (KC57)	Beckman Coulter GmbH	1:100
rabbit IgG, IRDye 800CW conjugated	Li-COR Biosciences; RRID:AB_621848	1:10000
rabbit polyclonal anti-HIV-1 CA	In-house	1:1000
rabbit polyclonal anti-HIV-1 gp120	In-house	1:100
sheep IgG, IRDye 680RD conjugated	Li-COR Biosciences; RRID:AB_10954442	1:10000
sheep polyclonal anti-HIV-1 CA	Müller *et al. (153)*	1:5000

2.1.6 Cell lines

Name	reference	Description
C8166 T cells	Salahuddin *et al. (154)*	Human umbilical cord blood cells containing defective HTLV genome
Embryonic kidney 293 T cells (HEK293T)	Pear *et al.* (155)	human embryonic kidney cell line expressing large T antigen of SV40
HeLa TZM-bl	Wei *et al. (156)*	HeLa derived cell line expressing CD4, CXCR4 and CCR5; contains HIV-1 Tat-driven firefly luciferase and β-galactosidase gene
Human CD4+ T lymphoblast cells A3.01	Folks *et al.* (157)	Human T cell line

2.1.7 List of primers

Oligo name	sequence	length (bp)
SU6_msfl2b (+)	AAATCTCTAGCAGTGGCGCCCGAACAG	27
SU7_f2nst (+)	GCGGAGGCTAGAAGGAGAGAGATGG	25
SU8_pro5F (+)	AGAAATTGCAGGGCCCCTAGGAA	23
SU9_pro3F (+)	AGANCAGAGCCAACAGCCCCACCA	24
SU12_proRT (-)	TTTCCCCACTAACTTCTGTATGTCATTGACA	31
SU13_RT3474R (-)	GAATCTCTCTGTTTTCTGCCAGTTC	25
SU17_VIF-VPUoutR1 (-)	GGTACCCCATAATAGACTGTRACCCACAA	30
SU18_nefyn05 (-)	GTGTGTAGTTCTGCCAATCAGGGAA	25
SU19_UNINEF 7' (-)	GCACTCAAGGCAAGCTTTATTGAGGCTT	28
SU20_snapseq_fw1	ACAGCTACAACCATCCCTTC	20
SU21_snapseq_rev1	CCCTTGGTTCTCTCATCTGG	20
SU22_snapseq_rev2	TGATATGGCCTGATGTACCATTTG	24
SU23_Gag1	CCCGAACAGGGACTTGAAAG	20
SU24_Gag2	CAATAGCAGTCCTCTATTGTGTG	23
SU25_Gag3	GCCTGCACCGTATCATCTTC	20
SU26_Gag4	GTGAAGTTTGGAGAGGTCATC	21
SU27_Gag5	ACCCTATAGTGCAGAACCTC	20

SU28_Gag6	CTATTGCACCAGGCCAGATGAG	22
SU29_Gag7	AAACTCTAAGAGCCGAGCAAG	21
SU30_Gag8	GTGTTTCAATTGTGGCAAAGAAGG	24
SU31_Gag9	GGGAAGAGACAACAACTCCCTC	22
SU32_Pol1	CTGCGGACATAAAGCTATAGG	21
SU33_Pol2	CCATACAATACTCCAGTATTTGCC	24
SU34_Pol3	AGTATAAACAATGAGACACCAGGG	24
SU35_Pol4	CCATTCCTTTGGATGGGTTATG	22
SU36_Pol5	CCGGTACATGGAGTGTATTATGAC	24
SU37_Pol6	AAAGGAAACATGGGAAGCATGGTG	24
SU38_Pol7	ATTCATCTAGCTTTGCAGGATTCG	24
SU39_Pol8	TAGATGGAATAGATAAGGCCCAAG	24
SU40_Pol9	CAGGGCAAGAAACAGCATAC	20
SU41_Pol10	CTTAAGACAGCAGTACAAATGGC	23
SU42_Pol11	AGCAAAGATCATCAGGGATTATGG	24
SU43_env1	ATGAGAGTGAAGGAGAAGTATCAG	24
SU44_env2	AATGACATGGTAGAACAGATGC	22
SU45_env3	GCATAAGAGATAAGGTGCAGAAAG	24
SU46_env4	ACACATGGAATCAGGCCAGTAG	22
SU47_env5	GGGACCCAGAAATTGTAACGCAC	23
SU48_env6	TTCAGACCTGGAGGAGGCGATATG	24
SU49_env7	TATTGTCTGATATAGTGCAGCAGC	24
SU50_env8	AACATGACCTGGATGGAGTGGGAC	24
SU51_env9	ATTCACCATTATCGTTTCAGACCC	24
SU52_env10	AGCCCTCAAATATTGGTGGAATC	23
SU53_Nef1	AAACATGGAGCAATCACAAGTAGC	24
SU54_Nef2	ACTGACCTTTGGATGGTGCTAC	22

2.1.8 Software

Name	Reference	Purpose
Amira-Avizo Software 2019.3	Thermo Fisher Scientific	Visualization and rendering
Arivis Vision4D 4.0	Carl Zeiss Microscopy Software Center Rostock GmbH	Image analysis and visualization
BioRender	BioRender.com	Science illustrations
CFX Manager Software 3.1	Bio-Rad	Analysis of real-time PCR data
eC-CLEM (Icy plugin; v 1.0.1.5)	Paul-Gilloteaux *et al*. (158)	Correlation
FACS Diva Software	B&D, Becton Dickinson	Data acquisition
Fiji 1.53c	Schindelin *et al*. (159)	General image analysis
FlowJo V10.9.0	FlowJo LLC, Ashland, USA	Data processing
Icy 2.0.3.0	De Chaumont *et al*. (160)	Correlation, Spot detection
Image StudioTM Lite 5.0	Li-COR Biosciences	Immunoblot analysis
Microsoft Office	Microsoft	Data presentation
NIS Elements	Nikon Instruments	Data acquisition and processing
Notion	Notion Labs, Inc.	Experiment planning and notes
Prism v8.0.0	GraphPad Software Inc	Visualization and Plotting
SnapGene 2.3.2	Snapgene.com	Cloning and sequence verification
Tecan i-control 1.10	Tecan	Plate reader software
Volocity 6.3	Perkin Elmer	Data acquisition

2.2 Standard methods in molecular biology

2.2.1 SDS-Polyacrylamide Gel Electrophoresis (SDS-PAGE) and Western blotting

For SDS-PAGE analysis, transfected cells or purified viral particles were lysed in a 3x Laemmli buffer composed of 150 mM Tris-HCl, 30% glycerol, 0.06% bromophenol blue, 20% β-mercaptoethanol, and 6% SDS. The lysates were incubated for 10 minutes at 95°C. Subsequently, 5 to 10 µl of the lysate was loaded onto a 15% SDS-PAGE gel (acrylamide:bisacrylamide 200:1). Proteins were separated by electrophoresis at a current of 25 mA per gel for 60 minutes. Following electrophoresis, semi-dry blotting at 0.8 mA/cm^2 for 1 hour was used to transfer the proteins onto nitrocellulose membranes. The membranes were then blocked for 30 minutes at room temperature in a solution of 1:3 diluted LI-COR blocking buffer in Tris-buffered saline with Tween20 (TBS-T). After diluting the primary antibodies in the diluted blocking buffer to the required concentration, they were incubated with the membranes at 4°C overnight. Following the incubation step, the membranes were washed three times with TBS-T and incubated for 45 minutes with IRDye700/800-conjugated secondary antibodies at room temperature in the absence of light. Following three additional washes with TBS-T, protein detection was performed using a Li-COR Odyssey CLx infrared scanner. Images were analyzed using Image Studio Lite software version 5.0.

2.2.2 Transformation

DNA samples (5 µl for PCR products, 10 µl for ligation products, and 1 µg for purified plasmid DNA) were mixed with 50 µl of chemically competent E. coli strains Stbl2 or DH5α. The mixture was gently pipetted to ensure thorough mixing, followed by a 20-minute incubation on ice. Bacteria were subsequently subjected to heat shock at 42°C for 45 seconds. After heat shock, the samples were returned to ice for 5 minutes, followed by the addition of 300 µl Luria-Bertani (LB) medium. The bacterial suspension was incubated for 1 hour at 37°C with shaking at 350 rpm. Following incubation, the bacteria were spread onto selective agar plates containing LB medium with 1.5% bacteriological agar and either 100 µg/ml ampicillin or 50 µg/ml kanamycin. The plates were incubated at 37°C overnight, and single colonies were picked for plasmid DNA preparation or transferred to LB medium for large-scale plasmid DNA generation.

Dh5α: Gibco, genotype: F− 80dlacZM15 (lacZYA-argF) U169 recA1 endA1 hsdR17(rk-, mk+) phoA supE44 - thi-1 gyrA96 relA1 28 5.

Stbl2: Invitrogen, genotype: F- mcrA Δ(mcrBChsdRMSmrr) recA1 endA1 lon gyrA96 thi supE44 relA1 λ- Δ(lac-proAB).

2.2.3 Preparation of plasmid DNA

Individual colonies of transformed E. coli Stbl2 or Dh5α were selected and used to inoculate 1 ml LB medium with selective antibiotics (100 µg/ml ampicillin or 50 µg/ml kanamycin) for mini cultures or 400 ml LB medium for maxi cultures. The cultures were grown overnight at 37°C in a bacterial shaker. Plasmid DNA was then extracted using the NucleoSpin Plasmid kit (Macherey Nagel) for mini cultures or the NucleoBond PC500 (Macherey Nagel) kit for maxi cultures, following the manufacturer's instructions. Purified DNA was eluted in TE buffer, and its concentration determined by spectrophotometric analysis. Absorbance at 260 nm was measured to quantify DNA concentration, and the 260/280 nm ratio was calculated to assess the purity of the DNA sample. The concentration of all plasmid DNA stocks was adjusted to 1 µg/µl based on the spectrophotometric analysis. Commercial Sanger sequencing (Eurofins Genomics, GER; Seqlab, GER) was used to confirm plasmid sequences, employing the primers listed in 2.1.7.

2.2.4 Isolation of viral genes from supernatant of infected cells

For sequencing of viral genes of viral particles obtained from supernatants of infected cells, a protocol comprising of RNA isolation, reverse transcription, amplification, and sequencing was employed. This procedure, including the primers used, was conducted based on the "Protocol for Nearly Full-Length Sequencing of HIV-1 RNA from Plasma" as described by Nadai *et al.* (161).

2.2.4.1 RNA Extraction and Reverse Transcription

Viral RNA of particles obtained from supernatants of infected A3.01 T cells was extracted using the Viral RNA Mini Kit from QIAGEN. Supernatants were thawed from storage at -80°C, and 1 ml was transferred to 1.5 ml polypropylene centrifuge tubes for ultracentrifugation at 44,000 rpm for 1.5 hours. Particle lysis and RNA extraction were performed according to the manufacturer's instructions. The extracted RNA was either stored in 15 µl aliquots at -80°C or used immediately for reverse transcription. The isolated viral genomic RNA was reverse transcribed using the SuperScript™ III One-Step RT-PCR System from Invitrogen. A 15 µl RNA sample was mixed with Master Mix A and incubated at 65°C for 5 minutes for denaturation. After cooling the samples on ice for 2 minutes, Master Mix B was added, and they were incubated at 50°C for 1.5 hours, followed by an additional incubation at 55°C for 1 hour. The reaction was then heat-inactivated at 70°C for 15 minutes.

Master Mix A:		**Master Mix B:**	
10 mM dNTP	2 µl	5x First strand buffer	8 µl
10 µM OligodT	1 µl	0.1 M DTT	2 µl
Water	8 µl	40 U/µl RNaseOUT	2 µl
		200 U/µl Superscript	2 µl
		Water	1 µl
Total	11 µl	**Total**	14 µl

1 µl endoribonuclease RNase H was added and incubated for 20 min at 37 ºC finalizes cDNA synthesis and samples are stored at -80 ºC until PCR amplification.

2.2.4.2 Amplification of DNA by polymerase chain reaction (PCR)

PCR was utilized in this study to amplify small quantities of reverse-transcribed cDNA derived from isolated genomic RNA. The PCR process consisted of three primary reactions, repeated over 25 to 40 cycles. Initially, DNA denaturation occurred at temperatures ranging from 95°C to 98°C. This was followed by annealing of primers to the DNA at approximately 50°C. The final step elongated the complementary DNA strands at temperatures of 68°C to 72°C. Given the limited amounts of cDNA generated by the previous steps, a nested PCR approach was employed for DNA of genomic origin. In this approach, 2 µl of the initial amplified PCR product was used in a second reaction under the same conditions. The sequences of the forward and reverse primers used are listed in section 2.1.7.

A standard PCR reaction consisted of:

x µl	template plasmid (20 ng)
2.5 µl	10x ThermoPol buffer
0.5 µl	forward primer (10 µM)
0.5 µl	reverse primer (10 µM)
2.5 µl	dNTPs (10 mM)
2.5 µl	DMSO
0.1 µl	Taq DNA Polymerase
25-(8.6+x) µl	Ultra-pure nuclease-free Water

Temperature profile of a standard PCR reaction:

Denaturation	96 °C	1 min	
Denaturation	96 °C	30 s	35 x
Annealing	58 °C	30 s	
Elongation	68 °C	3 min	
Final Elongation	68 °C	10 min	
Hold	4 °C	∞	

PCR products were purified either directly or through a gel extraction procedure using the NucleoSpin Gel and PCR Clean-up kit from Macherey Nagel, following the manufacturer's instructions.

2.2.4.3 Cloning of viral cDNA into TA vector

Amplified cDNA was not directly sequenced but instead cloned into a pGEM-T vector system to obtain multiple variants of the same sequence. Cloning was conducted following the manufacturer's instructions, using a vector-to-insert ratio of 1:5. The ligation mixture was incubated overnight at 4°C and subsequently transformed into E. coli DH5α cells, as outlined in section 2.2.2.

Transformed bacteria were plated on preprocessed ampicillin-selective agar plates. Preprocessing involved incubating the plates with a mixture of 40 µl 100 mM isopropyl-β-D-thiogalactopyranoside (IPTG) and 120 µl of 20 mg/mL 5-bromo-4-chloro-3-indolyl-β-D-galactopyranoside (X-Gal), followed by drying for 30 minutes at room temperature. The plated bacteria were then incubated overnight at 37°C in a bacterial shaker. LacZ-positive bacteria, capable of utilizing the X-Gal substrate, convert it to 5-bromo-4-chloro-3-indoxyl, which is oxidized to indigo, resulting in visibly blue colonies. Successful cDNA insertion disrupts the LacZ gene, leading to the formation of white colonies that signify successful cloning. White colonies were selected, and the plasmid DNA was purified as specified in section 2.2.3.

Plasmid DNA of positive clones was sent for commercial sequencing using sequencing primers listed in 2.1.7 and published in (161).

2.2.5 Restriction enzyme digest and gel electrophoresis

Restriction endonucleases are enzymes that recognize and cleave specific short target sequences within a DNA sequence. These enzymes typically target a palindromic sequence of 6-8 base pairs, resulting in either sticky (overhangs) or blunt ends (no overhangs) following cleavage.

Digested or PCR-amplified DNA fragments were separated by gel electrophoresis in 1 % agarose gels containing 1:10000 Midori green. Due to the negative charge of nucleic acids, DNA molecules migrate towards the positively charged anode under an electric field. DNA samples, along with a 1 kb plus DNA ladder, were mixed with a 6X purple gel loading dye (NEB) and loaded onto the solidified gel. Gel electrophoresis was performed at 90 V for 30-45 minutes, depending on the expected fragment size. Visualization of DNA fragments was achieved by exposing the gel to 254 nm UV light, and images were captured using the Gel iX Imager.

2.3 Cell biological methods

2.3.1 Cultivation of mammalian cells

All cell lines were cultivated in an incubator with a humidified atmosphere at 37°C and 5% CO_2. Cells were passaged at an appropriate ratio every three to four days. Human embryonic kidney 293T (HEK293T) cells and HeLa-derived TZM-bl (JC53BL-13) cells were grown in Dulbecco's Modified Eagle's Medium (DMEM) supplemented with 10% fetal calf serum, 100 U/ml penicillin, and 100 µg/ml streptomycin. A3.01 T cells and primary CD4+ T cells were cultured in Roswell Park Memorial Institute Medium (RPMI) 1640 with 10% heat-inactivated fetal calf serum, 100 U/ml penicillin, and 100 µg/ml streptomycin.

2.3.2 Cell transfection using calcium phosphate or polyethylenimine (PEI)

Transfection of HEK293T cells was performed to produce viral particles. For small-scale production using PEI, 3×10^6 cells were seeded into 6-well plates the day before transfection. 2 µg of DNA was mixed with 6 µl of PEI (1 µg/ml) in 200 µl Opti-MEM and vortexed. The mixture was subsequently incubated for 20-30 minutes, and then gently added to the cells resulting in a final volume of 2 ml per well.

For large-scale particle production of viral stock solutions, calcium phosphate precipitation was used in 50 % confluent T175 flasks. 50-70 µg of DNA per flask was combined with 4.5 ml of 1X $CaCl_2$ to form precipitates. To buffer the solution, 4.5 ml of 2X HBS was added dropwise, and the transfection mixture was incubated for 20 minutes at room temperature before being carefully applied to the cells. Six hours post-transfection, the medium was replaced with standard DMEM for continued cell culture as described in 2.3.1.

Virus particle harvesting was performed 48 hours post transfection and is described in 2.4.1.

2.3.3 Flow cytometry

Flow cytometry was employed to quantify the percentage of infected A3.01 T cells and to assess reporter expression. Between 2 x 10^5 and 6 x 10^5 cells were seeded into 96-well V-bottom plates and centrifuged at 2000 rpm for 5 minutes. To exclude dead cells from the analysis, a fixable viability dye, Zombie Violet (diluted 1:1000 in PBS) was added to the infected cells and incubated for 15 minutes at room temperature in the absence of light. Subsequently, cells were centrifuged at 2000 rpm for 5 minutes and fixed using the BD Cytofix/Cytoperm Fixation/Permeabilization Solution Kit for 15 minutes at room temperature. After fixation, cells were washed with BD CytoPerm buffer and permeabilized with 0.5% Triton X-100 for 15 minutes. To detect HIV-1 infected cells KC57, an antibody binding to the CA protein was used. A3.01 cells infected with HIV-1 derivatives expressing SNAPf, SNAPf(opt), or wildtype were incubated with a FITC-conjugated KC57 antibody. In contrast, cells infected with HIV-1 derivatives expressing sfGFP or sfGFP(opt) were incubated with an RD1-conjugated KC57 antibody. Incubation was performed for 45 min at room temperature in a PBS solution with 2 % bovine serum albumin (BSA). Incubation was performed for 45 minutes at room temperature in PBS containing 2% BSA. Subsequently, cells were centrifuged at 2500 rpm for 5 minutes and washed twice with PBS. Flow cytometric analysis was performed immediately using a FACSVerse flow cytometer. The respective reporters were detected by measuring the emission of fluorescent sfGFP or the covalently bound SNAP-CellSiR647 to SNAPf. Analysis of Flowcytometry data was performed using FlowJo_v10.10.0.

2.3.4 Isolation of primary CD4+ cells

Primary CD4+ T cells were isolated from buffy coats of healthy blood donors, obtained through the Heidelberg University Hospital Blood Bank in line with local ethical regulations. The CD4+ T lymphocytes were isolated using the EasySep™ Direct Human T Cell Isolation Kit and magnet, following the manufacturer's instructions. Activation of the CD4+ T cells was achieved by adding 100 U/ml interleukin-2 (IL-2) and a 1:100 dilution of TransAct™ human to the RPMI culture medium, with IL-2 being continuously present throughout all infection and imaging assays.

2.4 Virological methods

2.4.1 Virus particle production

Viral particles were purified from transfected HEK293T cells 48 hours post-transfection. For small-scale production, 1.5 ml of supernatant was filtered through a 0.45 µm nitrocellulose filter. The filtered supernatant was then layered onto a 20 % sucrose cushion in polypropylene

centrifuge tubes ultracentrifuged for 45 minutes at 44,000 rpm and 4°C using a TL-100 Ultracentrifuge with a TLA 45 rotor. DMEM/sucrose solution was removed, and the pelleted particles resuspended in a PBS-based solution supplemented with 10 % FCS and 10 mM HEPES. Suspended particles were subsequently aliquoted and stored at -80°C, or if used within the next 3 days at -20 °C. For large-scale production, the same principles were applied, but centrifugation was performed for 1.5 hours at 28,000 rpm and 4°C using a L8-70M Ultracentrifuge with SW32 rotor. Aliquots of the large-scale virus stock were consistently stored at -80°C. Prior to use in experimental assays, the quantity and infectivity of virus stocks was assessed using the SG-Pert (2.4.2) and blue cell assay (2.4.3).

2.4.2 Measurement of RT activity by SG-Pert

The SG-PERT (SYBR Green based Product Enhanced Reverse Transcriptase) is a quantitative method to estimate the concentration of viral particles in purified stock solutions or supernatants of infected cells based on RT activity (162). 5 µl of virus-containing samples were lysed for 10 minutes in 2 x lysis buffer (50 mM KCl, 100 mM Tris-HCl p.H 7,4, 40 % Glycerol, 0.25 % Triton-X100) containing 2 U of Ribolock RNAse inhibitor at room temperature. Following lysis, the samples were diluted with 90 µl of PCR buffer (50mM $(NH_4)_2$ SO_4, 200mM KCl, 200mM Tris-HCl p.H. 8,0) and 10 µl of this diluted sample was mixed 1:1 with 2 x SG-PERT reaction mix (1 x PCR Buffer, 10 mM $MgCl_2$, 2 x BSA, 400 µM dATP, 400 µM dTTP, 400 µM dGTP, 400 µM dCTP, 1 pmol fwd Primer, 1 pmol rev Primer, 8 ng MS2 RNA, SYBR Green 1:10.000 diluted). Concurrently, a serial dilution of an in-house produced standard was prepared under identical conditions to serve as a reference for calculating RT units following the quantitative PCR reaction. Real-time PCR was conducted using the CFX Touch 96-well Real-Time PCR Detection System and analyzed with the CFX Manager software provided by Bio-Rad (v. The cycling conditions were as follows: 20 minutes at 42°C, 2 minutes at 95°C, followed by 40 cycles of 95°C for 5 seconds, 60°C for 5 seconds, 72°C for 15 seconds, and 80°C for 7 seconds.

2.4.3 TZM-bl based infectivity assays

The relative single-round infectivity was evaluated utilizing the HeLa-derived TZM-bl cell line, which expresses CD4, CXCR4, and CCR5 receptors, thereby facilitating HIV-1 particle binding and entry. Additionally, these cells were engineered to contain reporter genes for E. coli β-galactosidase and firefly luciferase, which are driven by HIV-1 long terminal repeats. To determine infectivity, 5 x 10^3 cells/well were seeded into 96-well plates one day prior to infection.

For the luciferase-based assay Steady Glo, viral particles were added in serial two-fold dilutions, while for the β-galactosidase-based blue cell assay, serial ten-fold dilutions were employed. For

the luciferase assay, the medium was removed 48 hours post-infection and replaced with 100 µl of Steady-Glo luciferase assay substrate per well. After a 10-minute incubation at room temperature, 80 µl of the reaction mixture was transferred to white 96-well plates. Luciferase activity was measured with an Infinite 200 PRO plate reader, utilizing Tecan i-Control software version 1.10. Relative light units (RLUs) were analyzed by linear regression in GraphPad Prism v8.0.0, plotting RLUs against the inoculated volume and values normalized to RT activity.

For the β-galactosidase-based blue cell assay, the supernatant was removed 48 hours post-infection, and cells were washed with 100 µl PBS per well. Cells were then fixed with 100 µl of 4 % paraformaldehyde (PFA) for 10 minutes at room temperature. Following fixation, the solution was replaced with a staining mixture consisting of 1.5M Potassium-ferri-cyanide, 1.5M Potassium-ferro-cyanide, 0.5 M $MgCl_2$ and 200 µg/ml X-Gal in PBS. After a 2-4 hours incubation at 37 °C, the supernatant was discarded, and the wells were rinsed with PBS. Blue cells, indicative of successful infection, were manually quantified using a light microscope. Infectious blue cell units (BCU) per ml were calculated and used as the primary measure for inoculation in subsequent infection experiments.

2.4.4 Calculation of TCID50 in C8166 cells

Multiple-round infectivity was quantified by calculating the 50 % tissue culture infectious dose (TCID50) in C8166 T cells through endpoint titration. To perform this assay, 4 x 10^4 cells per well were seeded into 96 well plates. Purified viral particles or particle-containing supernatants were diluted in RPMI and added to the wells in serial 10-fold dilutions to a final volume of 100 µl, with four replicates per sample. Syncytia formation, serving as the readout for infection, was manually assessed after one week of incubation at 37 °C.

The relative infectious unit titer (I.U./ml) was calculated using the Spearman-Kaerber formula (163, 164), where $x_{p=1}$ represents the highest dilution, at which the virus could still be detected, d is the log10 of the dilution factor, x_{min} the most dilute dilution and p_x is the proportion of virus-positive wells at a specific dilution. The final calculated titer was normalized to RT activity determined by SG-Pert to ensure accurate comparisons across samples. (2.4.2).

$$\log_{10} TCID_{50} = \left(x_{p=1} + \frac{1}{2}d - d \sum_{x_{p=1}}^{x_{min}} p_x \right) * 10$$

2.4.5 Spin inoculation of A3.01 T cells

To enhance the efficiency of A3.01 T cell infection, spin inoculation was employed, a technique known to significantly increase infection rates by facilitating viral binding through the application of centrifugal forces (165). A suspension of 4×10^6 A3.01 cells/ml in RPMI containing 4µg/ml polybrene was prepared, and viral particles added to an amount representing an MOI of 0.1 based on the BCU in TZM-bl cells (2.4.3). 50 µl of the suspension was seeded into a 96-well plate, resulting in a final cell number of 2×10^5 per well. The plates were then centrifuged for 1.5 hours at 2000 rpm and 37°C. Post-centrifugation, the cells were incubated in a cell culture incubator at 37°C with 5% CO2. Four hours after centrifugation150 µl RPMI was added to each well and cells were centrifuged at 1200 rpm for 5 minutes to remove residual polybrene. As a final step the cells were resuspended with 200 µl fresh RPMI and incubated for 18-24 hours.

2.4.6 Detection of reverse transcription transcripts by ddPCR

Digital droplet PCR (ddPCR) was employed to detect early RT products in A3.01 T cells infected with HIV-1, primarily to confirm the inhibitory effect of Efavirenz (EFV) in a corresponding imaging setup under same conditions (2.5.3). Initially, A3.01 T cells were infected as described in 2.4.5. and lysed in a buffer containing 10 mM Tris-HCl pH 9, 0.1% Triton X-100 and 400 µg/ml Proteinase K. The lysates were incubated overnight at 55°C, followed by a 10-minute incubation at 95°C to inactivate the Proteinase K. ddPCR reactions were then prepared in a final volume of 20 µl, consisting of 2x digital PCR supermix for probes, a primer-probe mix, and 2 µl of the corresponding diluted sample. Early HIV-1 RT products were detected using a set of primers and probes that anneal to the 5'LTR region of the HIV-1 genome. Droplet generation for ddPCR was subsequently performed according to the manufacturer's instructions. The prepared 20 µl samples were loaded into 8-well cartridges along with 70 µl of droplet generation oil, and approximately 40 µl of droplets were generated using a QX200 droplet generator. The droplets were then transferred to a ddPCR 96-well plate, which was sealed using a PX1 PCR Plate Sealer. For PCR amplification, an initial denaturation was conducted at 95°C for 10 minutes, followed by 40 cycles at 94°C for 30 seconds and 57°C for 1 minute, with a final extension at 98°C for 10 minutes. The reaction was subsequently cooled to 4°C for 30 minutes. The analysis for absolute quantification of the droplets was conducted using a QX600 Droplet Reader, with data processed through QX Manager Standard Edition software. Samples with fewer than 10,000 accepted droplets were excluded from analysis. The copy numbers of early HIV-1 RT products were normalized to the copy numbers of the housekeeping gene ribonuclease P protein subunit p30 (RPP30).

2.5 Imaging and image analysis

2.5.1 Immunofluorescence (IF) and SNAP-tag labeling

T cells infected with HIV-1 derivatives were fixed with 4% PFA for 15 minutes and subsequently permeabilized using 0.5% Triton-X100 for 15 minutes. Following permeabilization, primary antibodies diluted in PBS containing 0.5% BSA were incubated with the cells for 1.5 hours at room temperature, followed by three washes with PBS. Secondary antibodies, also diluted in PBS with 0.5% BSA, were then incubated with the cells for 45 minutes at room temperature in the dark. If nuclear staining was required, Hoechst 33258 was added at a 1:1000 dilution to the secondary antibody solution. The cells were washed three additional times and stored in PBS at 4°C until imaging.

For SNAP-tag labeling, BG-coupled dyes were used at a concentration of 600 nM. Dyes obtained from NEB (SNAP-Cell® TMR-Star, SNAP-Cell® 647-SiR) were added to cells infected with HIV-1$^{iSNAPf(opt)}$ and incubated for 30 minutes at 37°C. The cells were then washed three times with cell culture medium over a period of 30 minutes before being either imaged or fixed.

SNAP-tag labeling with Spy555-BG for live-cell applications was conducted following spin inoculation. Specifically, 600 nM of the dye was added at the time of media replacement, 4 hours post-spin inoculation. Infected A3.01 T cells were subsequently washed three times over a 30-minute period to remove any residual dye, following the same procedure used for commercial dyes. For labeling with SNAP23, a no-wash protocol was employed, where 600 nM of the BG-coupled, cell-permeable dye was directly added to the imaging medium prior to live microscopy.

2.5.2 Spinning disc confocal microscopy (SDCM)

All microscopy conducted in this study, with the exception of correlative imaging for CLEM (2.5.4) was acquired using SDCM. The majority of fixed samples were imaged using a Perkin Elmer UltraVIEW VoX 3D spinning disc confocal microscope equipped with a 60x oil immersion objective (numerical aperture [NA] 1.49). Live-cell imaging, as well as imaging of fixed cell-free particles, was carried out on an inverted Nikon Eclipse Ti2 microscope, which was equipped with a Yokogawa CSU-W1 spinning disc unit and a humidified incubation chamber for live imaging at 37 °C and 5 % CO_2. Fluorescence emission was captured using an Andor DU-888 X-11374 electron-multiplying charge-coupled device (EMCCD) camera with a Plan Fluor 40x Oil DIC H N2 objective (NA 1.3, refractive index 1.515).

2.5.3 Live cell imaging

The development of a protocol for live imaging of cell-to-cell transmission under continuous observation was a key objective of this study, with detailed information provided in the results section. For the standard experimental setup 3.84 x10^6 A3.01 T cells were spin inoculated at an MOI of 0.1 BCU. For live imaging experiments, SNAP-tag labeling was conducted by directly adding 600 nM of the Spy555-BG dye (Abs/Em: 555/580 nm) to the inoculated cells during the media change four hours post-centrifugation. Eighteen hours after spin inoculation, cells were washed three times in antibiotic-free RPMI to remove any unbound dye. Concurrently, the plasma membranes of 3.84x10^6 A3.01 T cells were labeled using the "CellVue® Claret Far Red Fluorescent Cell Linker Mini Kit for General Membrane Labeling," according to the manufacturer's instructions. Both cell populations were counted, adjusted to a density of 2.5 x 10^5/ml, and mixed in a 1:4 ratio of SNAP-tag-labeled donor cells to membrane-labeled target cells. Subsequently, 600 nM Snap23 was added to the cell suspension, and 400 µl of the mixture was seeded into chambered, glass-bottom 8-well µ-Slides, resulting in a final density of 1x10^5/well. The slides were pre-coated with a 0.1 % poly-L-lysine solution for 30 minutes at room temperature, followed by two washing steps with PBS. As a negative control, a mixture containing mock-infected A3.01 T cells was prepared under the same conditions. In certain experiments, specific inhibitors were added to block stages of the viral replication cycle: EFV was used at 20 µM, T20 (Enfuvirtide) at 100 µM, and Raltegravir (RAL) at 5 µM concentration.

All imaging was conducted in antibiotic-free RPMI to minimize background interference. Live imaging was performed using the CSU-W1 Spinning Disk microscope with an inverted Nikon Ti2, capturing images over 18-24 hours at a rate of 0.33 frames per second within a humidified chamber maintained at 37 °C and 5 % CO_2. Unless otherwise specified, the laser configurations were as follows:

Laser	**ExW: 488 nm**	**ExW: 561 nm**	**ExW: 640 nm**	**Brightfield**
Binning	1x1	1x1	1x1	1x1
Exposure	30 ms	10 ms	100 ms	90 ms
Multiplier	300	300	300	300
Readout Speed	20 MHz	20 MHz	20 MHz	20 MHz
Vertical Shift Speed	0.6 µs	0.6 µs	0.6 µs	0.6 µs
Laser power	3 %	3 %	2 %	-
DIA intensity	-	-	-	6.0

2.5.4 Correlative light and electron microscopy (CLEM)

Correlative light and electron microscopy (CLEM) approaches were conducted in collaboration with Dr. Charlotta Funaya, head of the Electron Microscopy core Facility of Heidelberg University Hospital. A3.01 T cells were spin inoculated and stained as described in 2.4.5 and 2.5.1. Instead of being seeded in chambered 8 Well µ-Slides, 2 x 10^5 cells were seeded onto gridded MatTek dishes. During subsequent steps, a few diagonal scratches were made in the cell layer. 90 minutes after seeding, the cells were fixed with 4% EM-grade PFA and 0.2 % Glutaraldehyde (GA) for 90 minutes. Following fixation, the cells were washed in PBS, and Hoechst 33258 was added at a 1:1000 dilution in PBS for 15 minutes. Using a Zeiss Cell Discoverer equipped with a Zeiss Axiocam 712 mono camera initial overview images were captured with a Plan-Apochromat 20×/0.7 air objective with a 1× magnification changer. Potential VS events were identified in the overview images based on contacting donor and target cells with Gag.SNAPf(opt) polarization towards the contact zone. For higher resolution allowing detailed correlation with electron microscopy (EM) sections, images were captured with a Plan-Apochromat 50×/1.2 water immersion objective with a 2× magnification changer.

Subsequent steps were performed by Dr. Funaya. Following fluorescence imaging, cells were dehydrated through a graded ethanol series ranging from 40 % to 100 % at room temperature, then embedded in Epon 812 and polymerized for 48 hours. The embedded cells were sectioned into 250 nm slices using a Leica EM UC7 ultramicrotome and counterstained with Uranyless for 5 minutes, and then with lead citrate for 3 minutes. The sections were imaged using a JEOL JEM-1400 transmission electron microscope (TEM) equipped with a 4K TemCam F416 camera (Tietz Video and Image Processing Systems GmbH) at 80 kV. Tomograms were acquired by placing the samples in a high-tilt tomography holder and imaged using a Tecnai F20 electron microscope at 200 kV. Imaging was performed at tilted angles over a ±60° range using an FEI Eagle 4K × 4K CCD camera at a magnification of 19,000× with a binning of 2 (pixel size 1.13 nm).

Fluorescence microscopy-identified contact events were relocated using the grid, and the electron microscopy and fluorescence images were correlated using the eC-CLEM plugin within Icy image analysis software.

2.5.5 Image processing and analysis

The live-cell imaging data acquired as described in Section 2.5.3 exhibited a low signal-to-noise ratio due to the minimized laser power and exposure times. To enhance these signals, the embedded artificial intelligence (AI) within the NIS-Elements software was employed (Nis.ai). The AI was trained using image pairs captured under conditions of high laser power/long exposure

time and low laser power/short exposure time. Following individual enhancement of each channel, the signals from each fluorescent channel were merged into a 4-channel imaging sequence and subsequently split into individual fields of view (FoV). Fixed samples and individual frames from live-cell imaging sequences were processed for visualization in Fiji by contrast adjustment, utilizing standard greyscale or fire lookup tables (LUT). Three-dimensional renderings of z-stacks were generated using the "3D-Viewer" plugin in Fiji.

Icy software was used for correlation of fluorescence images with EM thin sections (as detailed in Section 2.5.4) and for analyzing the labeling efficiency of BG-coupled SNAP dyes in cell-free HIV-1$^{iSNAPf(opt)}$ particles. Individual particles were segmented using the spot detector based on CA IF. The mean intensity for the respective fluorophore channel within the detected particle spots was measured, and these intensities subsequently plotted against the CA IF mean intensities. The threshold for SNAP-dye positive cells was determined based on the dye intensity in particles lacking a functional SNAP-tag.

2.5.6 Semi-automated analysis of HIV-1 cell-to-cell transmission

Live cell imaging data were analyzed using Arivis Vision4D version 4.0. The integrated analysis pipeline employed the Python-based algorithm Cellpose (Cellpose_2_0_segmenter_v6, model "cyto") to segment T cells. This algorithm, trained through machine learning, was designed to detect cells with high accuracy. Segmentation was filtered based on cell diameter (15 µm) and signal intensity (750 for brightfield images and 650 for membrane-labeled target cells). An additional filter based on cell area was applied, setting a minimum threshold of 50 µm^2. Subsequently, segmented cells were tracked using the integrated pipeline, with the maximum allowable distance between frames set to 5 µm, a maximum gap time of 4 frames, and the motion type configured as Brownian Motion (Centroid). Tracked segments within the far-red channel resembled the target cell population, based on their membrane labeling. To distinguish the donor cell population, brightfield segmentation was further filtered for intensity in the red channel using a Python script (racksFilterByFeatures_RevA(4_0)) provided by Arivis. Donor cells selected for analysis were identified within the initial 5 frames (corresponding to the first 15 minutes of image acquisition) to reduce total processing time. Since the segmentation originated in the segments tracked over the whole imaging period, this has no effect on assessment of donor cell dynamics over time. The intensity filter was set to 800, based on the mean intensity observed in mock-infected cells.

For the analysis of contact events between donor and target cells, an additional Python script (Kiss and Run_RevR(4_1_2)), developed in collaboration and provided by Arivis, was utilized. This

script assessed green intensity in each frame in relation to contact events, defined as overlaps between donor and target cell segments. A positive event, indicative of Gag.SNAPf expression and potential productive infection, was defined by the observation of target cells in contact with a donor cell, where the fluorescence intensity increased above a predefined threshold and remained elevated for at least 40 consecutive frames. From the tracking data, metrics such as contact duration, contact frequency and mobility were extracted.

3. Results

3.1 Establishment of a replication competent labeled HIV-1 derivative

Fluorescent labeling approaches play a crucial role in visualizing viruses and tracking dynamic processes during the viral replication cycle. To this date, several approaches to label viral proteins with fluorogenic tags to track dynamic infection processes have emerged. One of the major drawbacks of altering viral sequences by fusing FPs to the protein of interest is interference with maturation of the protein and thus replication of the virus. Direct labeling of the main structural protein Gag in HIV-1 is especially challenging since the tight lattice structure restricts insertion of FPs to a very limited selection of positions. Incorporation of GFP between the MA and CA domain has been achieved either as C-terminal fusion protein with MA (128), or as internal domain between MA and CA flanked by two functional PR cleavage sites, resulting in a free tag after maturation and partially replication-competent HIV-1 derivatives (140). This position was shown to also be compatible with other FPs such as mCherry (166) and self-labeling tags e.g., CLIP-tag (167) and SNAP-tag (139). While approaches employing FPs enabled major breakthroughs in understanding the dynamics of the HIV-1 replication cycle, they exhibited only partial functionality, with significantly reduced replication capacity and indications for defects in particle assembly (128, 104) . Accordingly, the first objective of this project aimed to develop a tagged HIV-1 derivative that overcomes the aforementioned restrictions and is capable of undergoing multiple rounds of infection while retaining native molecular infection and stable expression of the fluorescent label.

3.1.1 Generation of tagged HIV-1 derivatives

FPs are subject to constant improvement and evolution in order to generate advanced versions with improved quantum yield, brightness, and chromophore maturation. One example is super folder GFP (sfGFP), an improved version of GFP, which exhibits considerably reduced maturation time in living cells (wt GFP t_{50} = 36.1, sfGFP t_{50} = 13.6 at 37 ºC (168)) and substantially enhanced capacity for protein folding when fused to a protein of interest (169). As impacted assembly appeared to be one of the major drawbacks in existing approaches of Gag labeling, sfGFP was determined as a promising alternative to result in improved characteristics compared to approaches utilizing GFP or eGFP when incorporated between the MA and CA domain. Furthermore, Gag labeling with SNAP-tag has been identified to result in a HIV-1 derivative with significantly improved replication compared to approaches utilizing FPs in the same context (139). A new variant of SNAP, referred to as SNAPf, has been reported to exhibit increased reactivity towards BG substrates by a factor of ten *in vitro* (138). Reduced time for labeling of SNAPf could increase the time resolution of the acquired imaging sequences and would thereby be beneficial for tracking expression of viral proteins in real-time.

For these reasons, I selected sfGFP and SNAPf as labels for direct Gag labeling, in order to generate a tagged HIV-1 derivative with improved replication kinetics. According to previous approaches, both labels were genetically incorporated into the wildtype proviral plasmid pNLC4-3 between MA and CA as internal domains (isfGFP and iSNAPf), flanked by two cleavage sites for PR, as schematically depicted in Figure 5 A, left site. This allows the processing by the viral PR and therefore the cleavage and release of the tag upon viral maturation. Additionally, sfGFP was fused to the C-terminus of p6. As frameshifting of the overlapping Gag and Pol ORF is essential for virus propagation, modification of the C-terminus of Gag is challenging and has not yet been implemented as a potential labeling strategy for HIV-1. By employing an HIV-1 derivative in the context of HIV-$1_{NL4\text{-}3unc}$ (170), where the overlapping gag and pol ORF are genetically uncoupled, C-terminal Gag labeling can be accomplished without affecting the production and processing of Pol (Figure 5 A, right site).

Takata et al. demonstrated that CpG-rich regions within the HIV-1 genome can elicit an antiviral response due to their recognition by the ZAP protein (149). It was therefore hypothesized that the introduction of CpG-rich sequences such as sfGFP and SNAPf could result in an increased ZAP-mediated RNA degradation. To test this hypothesis, the CpG content of sfGFP and SNAPf was reduced by introducing silent mutations, resulting in the generation of SNAPf(opt) and sfGFP(opt) as depicted in Figure 5 B.

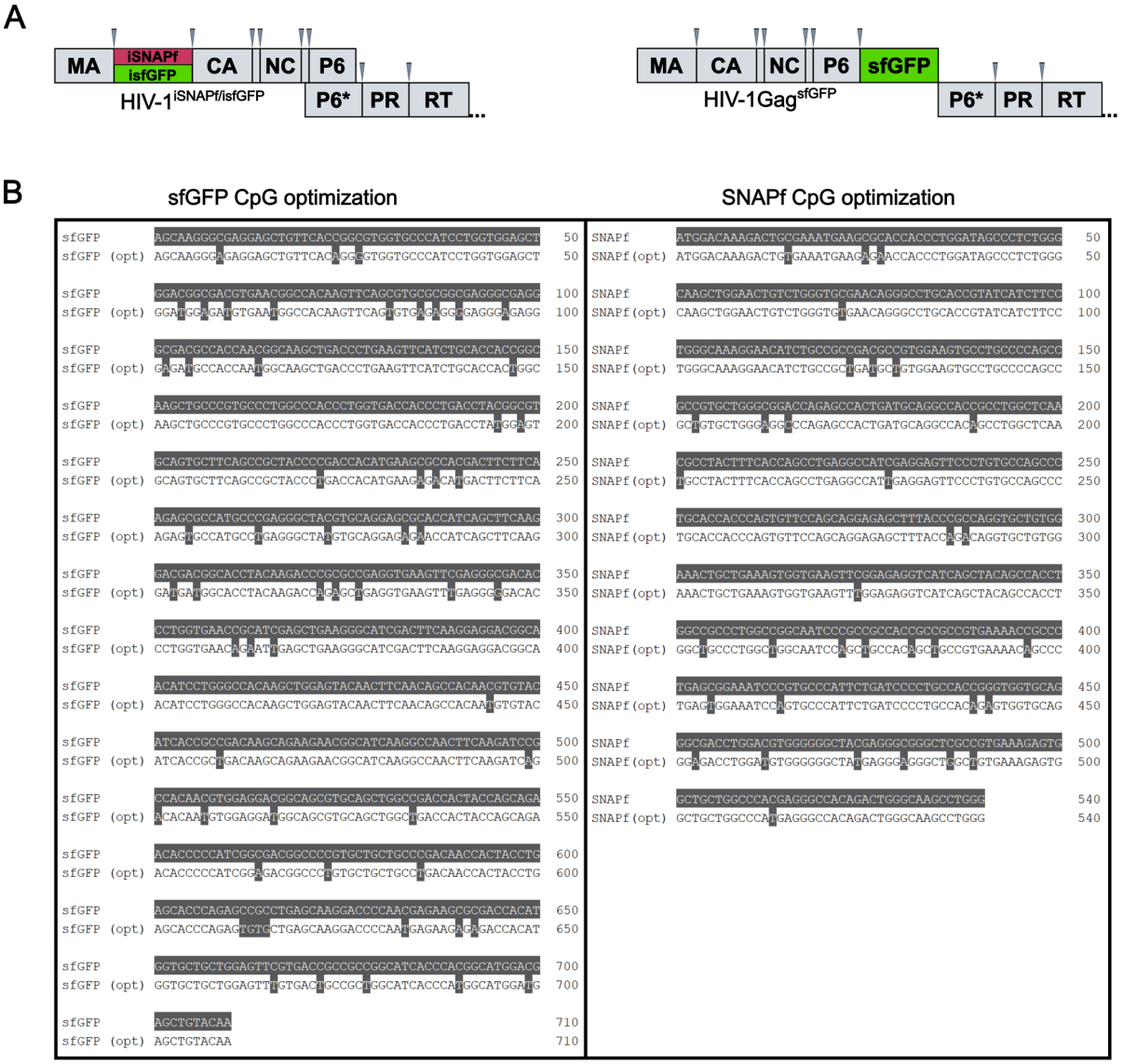

Figure 5 Schematic representation of HIV-1 derivatives and CpG optimization.
(A) Schematic representation of the HIV-1 Gag and the initial region of the Pol ORF, illustrating the insertion of iSNAPf (magenta) and sfGFP (green) between the CA and MA domain, or the placement of sfGFP (green) at the C-terminal end of Gag with uncoupled Gag and Pol ORFs. (B) sfGFP and SNAPf were modified through the introduction of silent mutations to reduce the density of CpG base pairs, resulting in the generation of SNAPf(opt) and sfGFP(opt).

3.1.2 SNAP-tag labeling of HIV-1$^{iSNAPf(opt)}$

In contrast to FPs, the SNAP-tag is not inherently fluorescent. Labeling is achieved by a self-labeling reaction, where the BG of a ligand forms a covalent bond with the SNAP-tag, resulting in the release of guanine and the activation of the functional group coupled to the BG. The BG functional group can be linked to a variety of fluorophores, providing labeling flexibility for microscopy. Since the BG-linked fluorophore dyes available for microscopy are in principle fluorogenic, SNAP-tag labeling can achieve a relatively high degree of specificity with low background signals. The version utilized in HIV-1$^{iSNAPf(opt)}$, SNAPf, represents an advanced iteration of the original tag with increased reactivity towards BG substrates (138).

In order to evaluate the labeling efficiency of several commercially available SNAP-reactive dyes in the context of HIV-1^{iSNAPf}, I infected A3.01 T cells with HIV-1$^{iSNAPf(opt)}$ and labeled Gag.SNAPf(opt) with 600nM of the respective dye 24 hours post infection. IF staining against CA allowed the identification of infected cells independent of labeled Gag.SNAPf(opt). As illustrated by the exemplary images and the quantification of signal intensities shown in Figure 6 A and B most CA positive cells were also stained with SNAP-Cell647SiR, and SPY555-BG, while infected cells stained for SNAP-Cell TMR Star exhibited a weaker signal compared to the other two dyes.
The efficiency of the labeling process was evaluated using HIV-1$^{iSNAPf(opt)}$ particles derived from transfected HEK293T cells. Virions were concentrated from the tissue culture supernatant, stained with BG-conjugated fluorophores, adhered to glass slides and counterstained against CA by IF and images recorded by spinning disc confocal microscopy. CA signals were subsequently segmented using the spot detector plugin in the image analysis software Icy. Mean intensity of the respective BG-conjugated fluorophore within the CA segments was measured and plotted against the CA signal (Figure 6 C-E). The TMRStar dye demonstrated the lowest labeling efficiency, with 99.56 % registered particles exhibiting a signal above the established threshold, based on background signal in wt labeled particles. For particles labeled with SNAPCellSir647 and SPY555-BG, a 100% correlation was observed, indicating that all particles detected by CA IF were also labeled with the respective SNAP dye. Spy555-BG displayed somewhat higher intensities relative to the CA signal than SNAPCellSir647, rendering it the most favorable dye of the tested panel.

In conclusion, I could demonstrate that Gag.SNAPf(opt) is expressed in HIV-1$^{iSNAPf(opt)}$-infected A3.01 cells and colocalizes with CA. Albeit TMR Star exhibited a lower labeling efficiency and lower signal intensities, all three evaluated commercially available SNAP dyes were shown to efficiently label the SNAPf-tag and can therefore be used to detect Gag.SNAPf(opt) in subsequent experiments.

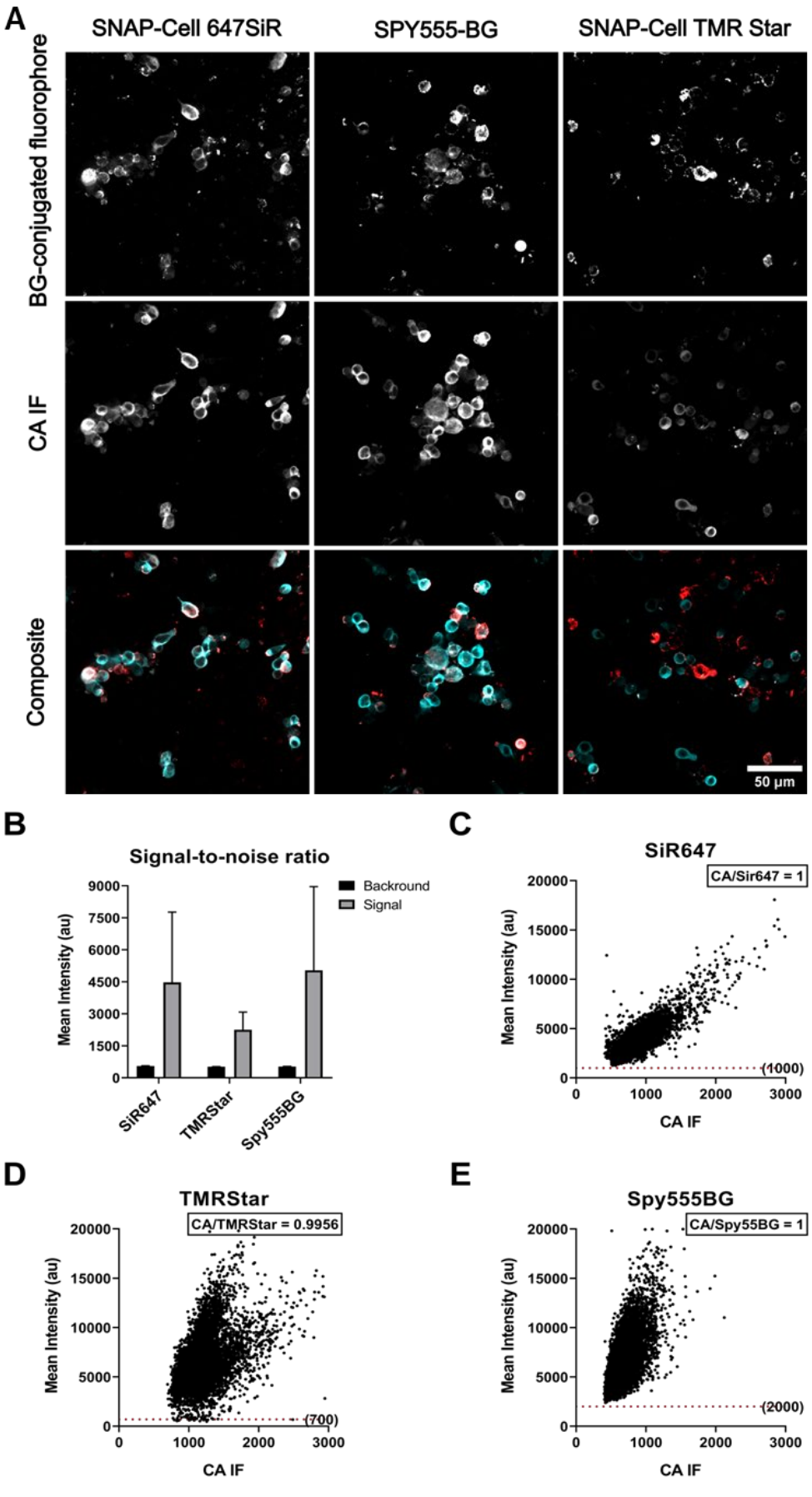
A
SNAP-Cell 647SiR
SPY555-BG
SNAP-Cell TMR Star
BG-conjugated fluorophore
CA IF
Composite
50 µm
B
Signal-to-noise ratio
Backround
Signal
Mean Intensity (au)
9000
7500
6000
4500
3000
1500
0
SiR647
TMRStar
Spy555BG
C
SiR647
CA/Sir647 = 1
Mean Intensity (au)
20000
15000
10000
5000
0
(1000)
0
1000
2000
3000
CA IF
D
TMRStar
CA/TMRStar = 0.9956
Mean Intensity (au)
20000
15000
10000
5000
0
(700)
0
1000
2000
3000
CA IF
E
Spy555BG
CA/Spy55BG = 1
Mean Intensity (au)
20000
15000
10000
5000
0
(2000)
0
1000
2000
3000
CA IF

Previous page: Figure 6 Gag.SNAPf(opt) labeling efficiency using commercially available SNAP dyes. *(A) Exemplary images for HIV-1$^{iSNAPf(opt)}$ infected cells stained with different SNAP reactive dyes. A3.01 T cells were infected with HIV-1$^{iSNAPf(opt)}$ and 24 hours later, Gag.SNAPf(opt) labeled with 600 nM of the respective SNAP-reactive dye (red). The labeling procedure was conducted for a period of 30 minutes, followed by three washes over the course of 30 minutes. Subsequently, the cells were fixed with 4% PFA, permeabilized with Triton X-100, and stained with polyclonal sheep anti-CA serum to detect CA and Gag.SNAPf(opt)(cyan). Images were acquired using a Perkin Elmer Ultra VIEW VoX 3D spinning disc confocal microscope with a 40x immersion oil objective. (B) Mean signal and background intensities for five images per condition of the imaging from panel A were measured. Fluorophore signal was measured in Gag.SNAPf(opt) expressing cells and background intensities outside of Gag.SNAPf(opt) positive cells. (C-E) 5 x 10^{11} pU RT of purified HIV-1$^{iSNAPf(opt)}$ particles were seeded in PEI-coated 15-well ibidi imaging dishes. Gag.SNAPf(opt) was labeled with 600 nM SNAP dye, and the samples incubated for 30 minutes. Following a 30-minute washing with RPMI particles were fixed and IF counterstaining against CA conducted. Five fields of view (FoV) per sample were acquired at 60x magnification using an inverted Nikon Ti2 spinning disc confocal microscope. The spot detector in Icy imaging analysis software was employed to detect CA signals based on mean signal intensity. The fluorophore signal was measured in the CA spots, and the intensity was plotted against the CA signal.*

3.1.3 Infectivity of SNAP-tagged HIV-1 derivatives is increased compared to sfGFP-tagged HIV-1 derivatives

To characterize the panel of tagged HIV-1 derivatives regarding incorporation and proteolytic processing of Gag, I produced viral particles by transfecting the respective proviral plasmids (pNLC4-3, pNLC.iSNAP, pNLC.iSNAPf, pNLC.iSNAPfopt, pNLC.iSNAPfoptPR-, pNLC.isfGFP, pNLC.isfGFPopt, and pNL4-3unc.Gag-sfGFPopt) into HEK293T cells. Particles concentrated from the tissue culture supernatant were normalized for RT activity and analyzed by western blot to evaluate whether incorporation and proteolytic processing of Gag was impaired by the insertion of the tag.

Staining for CA revealed the presence of a band at approximately 24 kDa for all variants except the PR- control, in accordance with the known size of mature CA. In addition, CA positive bands with apparent molecular masses of 55 kDa were observed for the wt (HIV-1$_{NL4-3}$), representing the Gag precurser. For tagged HIV-1 derivatives Gag was increased by the size of the molecular masses of SNAP (19.4 kDa) and sfGFP (26.8 kDa), respectively. The ratio of Gag to CA was roughly comparable for all variants, indicating that Gag processing was not impaired for the tagged variants. To investigate whether the same number of Env and Gag were incorporated into viral particles during assembly, antiserum against the gp120 subunit of the Env glycoprotein was applied. The relative gp120 levels of the tagged variants were similar to that of the wt control, indicating unaltered incorporation of Env. Staining with antiserum against GFP and SNAP revealed bands according to the molecular masses of SNAP and sfGFP and confirmed the shifted Gag bands to comprise the respective tag.

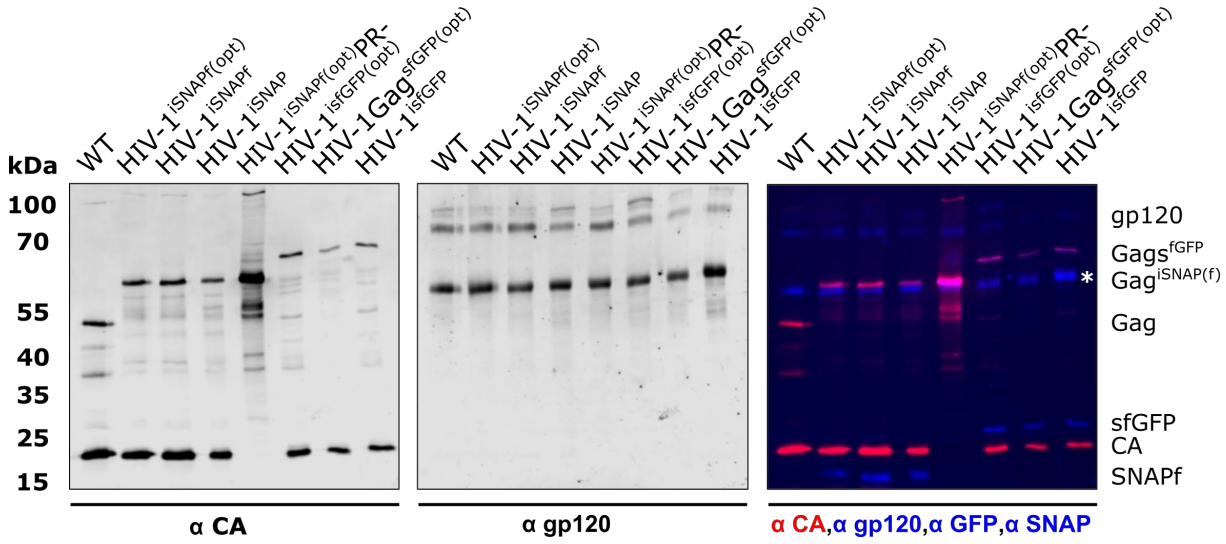

Figure 7 Detection of Gag and Env proteins of wildtype and tagged HIV-1 derivatives.
Particles concentrated from transfected HEK293T cells normalized for RT activity (1 x 10^{11} pU RT) and separated by SDS-PAGE followed by western blot analysis. Detection of proteins was performed using polyclonal sheep antiserum against CA, polyclonal rabbit antiserum against gp120, and polyclonal rabbit serum corresponding to the specific tag. IRDye 680RD-conjugated secondary antibodies were employed for the detection of CA, while IRDye 800CW-conjugated secondary antibodies were utilized for the detection of Env, as well as tag detection. Positions of the molecular mass standards are indicated to the left, positions observed for HIV-1 proteins are indicated to the right. The band marked by an asterisk in the α g120 immunoblot represents nonspecific reactivity against serum albumin remains from the tissue culture medium.

Following the conformation of normal Gag processing by the viral PR and and efficient incorporation of Gag into viral particles for all characterized viruses by western blot analysis, the infectivity of the HIV-1 derivative panel had to be assessed. HEK293T cells were transfected with proviral plasmids of the wt and tagged derivatives in order to obtain virus containing supernatants. 24 hours post-transfection supernatants were harvested and titrated on the HeLa-derived reporter cell line TZM-bl to assess single-round infectivity, and on C8166 T cells to evaluate virus spread over multiple rounds of infection. Infectivity data obtained were normalized for virus input based on RT activity determined for the supernatants.

On TZM-bl cells, HIV-1$^{iSNAPf(opt)}$ exhibited the highest relative infectivity of the panel analyzed, with a median of 91% relative to wt infectivity, which represents a non-significant difference (p=0.064) (Figure 8 A, dark blue). The same derivative without CpG optimized SNAPf-tag showed a slightly lower median infectivity (70% of wt, turquoise). However, since two outlier values drastically increased the dispersion with a maximum of 242% and minimum of 12% relative to wt infectivity, these data need to be interpreted with caution. Since both outliers were statistically significant (z = 1.7 for the max value and z = 0.95 for the min value with a critical z value of 1.715, based on Grubbs' outlier test (171)), they were still included in the analysis. It is important to mention that the spread in values was the result of high variability in the measured RT activity values (between

4.1 x 10^7 and 5.8 x 10^8 pURT/µl), which led to increased variability after normalization. With a median relative wt infectivity of 62%, the derivative expressing the original SNAP-tag showed the lowest single round infectivity of the SNAP-expressing derivatives (Figure 8 A light blue), with a significant difference to wt (p=0.004). Differences in infectivity between HIV-$1^{iSNAPf(opt)}$ and the non-codon-optimized SNAPf variant were not statistically significant (p = 0.926). When compared to the original SNAP-tag, a significant difference could be observed (p = 0.019).

Consistent with previous studies (139), GFP-expressing derivatives exhibited significantly lower relative infectivity in TZM-bl cells compared to wt HIV-1, with median infectivity ranging from 31% for HIV-$1^{isfGFP(opt)}$ (p=0.004) to 41% for HIV-1Gag^{sfGFP} (p=0.014) (Figure 8 A green outlines). For HIV-1$Gag^{sfGFP(opt)}$ one outlier (z=1.75 with critical value of z= 1.715 based on Grubbs' outlier test) with a relative infectivity of 96% was excluded from the analysis. Similar to the SNAP-tag derivatives, codon optimization of sfGFP did not provide any significant advantage.

Spread over multiple rounds of infection in C8166 cells was evaluated ten days post infection by assessing infected wells based on the appearance of syncytia and calculation of the TCID50 value according to Spearman-Kaerber (172). Results are shown in Figure 8 B and normalized to the virus input based on RT units measured by the SG-PERT assay. SNAP-tag-expressing derivatives (blue) yielded the highest viral titers, non-significant differences to wt (p = 0.384, 0.375, and 0.367, respectively). Similar to the observations for single round infectivity, sfGFP-expressing derivatives (green) showed lower titers compared to both wt and SNAP-tag-expressing HIV-1, however these differences were not statistically significant, with adjusted p-values ranging from 0.367 to 0.368 for the sfGFP-tagged derivatives when compared to wt. CpG optimization did not result in a clear replicative advantage for either tag, though sfGFP-expressing derivatives displayed marginally higher infectivity, but the dispersion of calculated titers was also higher for non-codon-optimized constructs.

In conclusion, comparative infectivity analysis of tagged HIV-1 derivatives in both TZM-bl and C8166 cells showed that SNAP-tag expressing derivatives exhibited higher overall infectivity compared to sfGFP-expressing derivatives. Of all tested derivatives, HIV-$1^{iSNAPf(opt)}$ exhibited the highest infectivity, comparable to that of the wt HIV-1_{NL4-3}. Codon optimization did not impact viral titers in C8166 cells; however, the relative infectivity of SNAPf increased from 70% to 90% in TZM-bl cells.

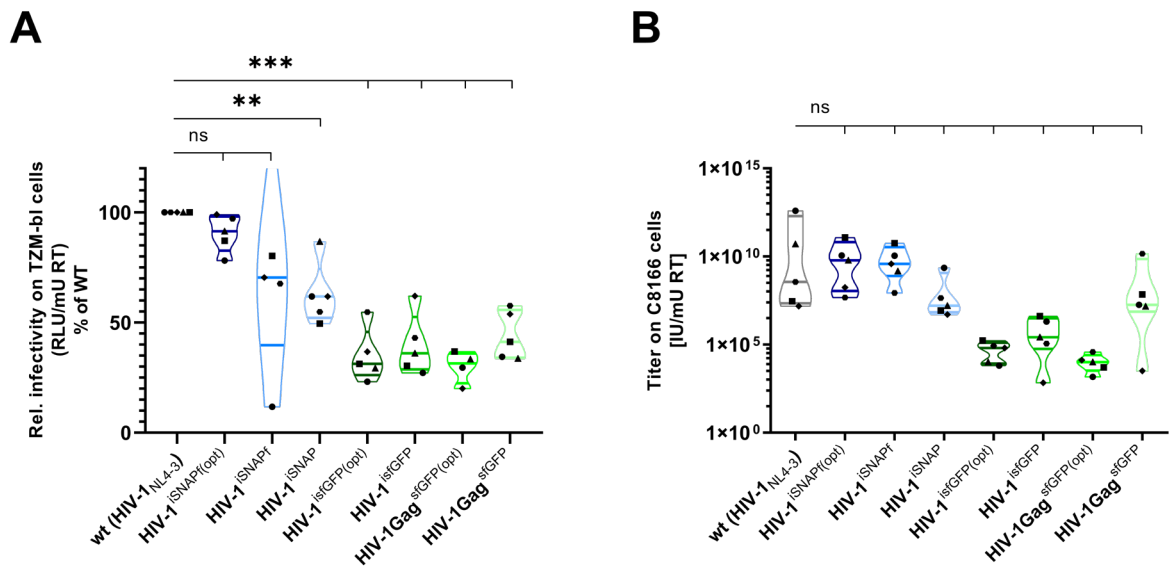

Figure 8 Infectivity of tagged HIV-1 derivatives.
The infectivity of the virus particles present in the supernatant of transfected HEK293T cells was determined by titration on TZM-bl reporter cells (A) and C8166 T cells (B) as described in materials and methods. Titers were normalized to the respective RT-activity, which was measured by SG-PERT. The figure depicts data from five independent experiments. The data for the tagged derivatives on TZM-bl cells were normalized to the value obtained for the wt virus in the same experiment. RLU, relative light units. n=5; Significance determined by a two-tailed paired t-test. The shape of the data points refers to the experiment replicate.

3.1.4 SNAPf-tagged HIV-1 derivatives show improved replication kinetics over sfGFP-tag variants

A major drawback of current methods for direct Gag labeling is their significantly reduced replication capacity. Without the presence of a helper virus, existing approaches only allow for a single round of infection under wt conditions, or require highly permissive cell lines such as MT4 for efficient viral spread (140). In order to gain a more comprehensive understanding of the replication capacity of HIV-1$^{iSNAPf(opt)}$ and the sfGFP-tagged derivatives, I performed replication kinetics in A3.01 T cells with the panel of labeled HIV-1 constructs. This cell line was selected as all experiments for subsequent cell-to-cell transmission assays were conducted in A3.01 T cells, so they represent the most relevant cells for this project.

Concentrated particles from transfected HEK293 T cells were quantified by the SG-Pert assay, and an RT concentration of 1.5 x 10^6 pU was used to inoculate A3.01 T cells. Subsequently, RT activity of released viral particles in the supernatant of infected cells was monitored over time. The experiments were performed with four replicates per derivative, utilizing viral particles derived from four independently generated viral stocks.

As shown in Figure 9, I identified reduced infectivity among all constructs compared to wt during the time-course experiment. The wt constructs showed an increase in RT activity at day two, reaching peak levels between days six and eight (grey line), while SNAPf-tagged constructs displayed a slight delay, peaking on day ten (blue lines). In contrast, RT activity was first detected at day ten for sfGFP-expressing derivatives, but reached peak levels already at day twelve, suggestive of a breakthrough infection (green lines). By this point, all analyzed derivatives exhibited similar RT activity levels. CpG optimization did not provide any noticeable benefit in either derivative, as replication kinetics were nearly identical between codon-optimized and non-optimized SNAPf and sfGFP-tagged constructs. These results indicated that a reduction in CpG content of artificially inserted Gag sequences did not result in improved viral spread in culture.

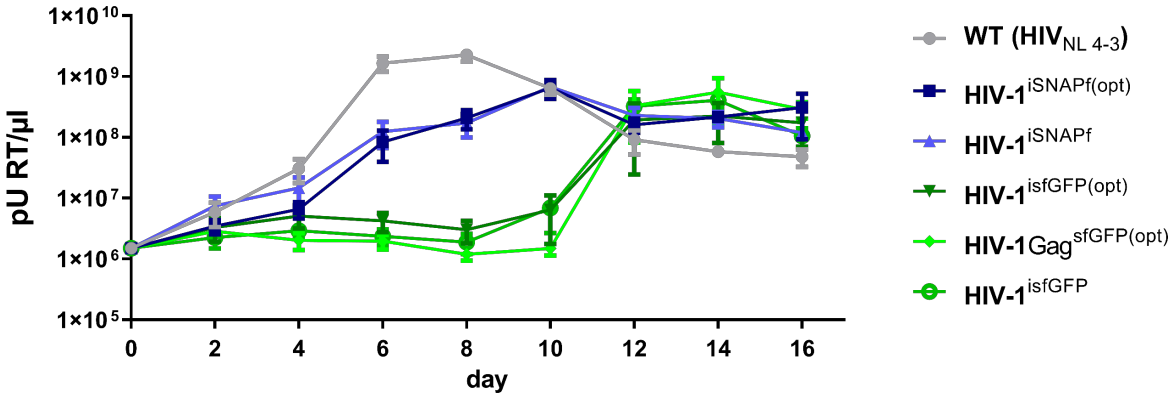

Figure 9 Replication kinetics of tagged HIV-1 derivatives in A3.01 T cells.
Proviral plasmids for each derivative were transfected into HEK293T cells, and particles were concentrated by ultracentrifugation through a sucrose cushion 48 hours later. RT activity was measured by SG-Pert, and 1.5 x 10^6 pU/µl RT used to inoculate A3.01 T cells. RT activity in the supernatant was monitored over 16 days. Samples were taken every two days and cells split every four days to maintain cell viability. Four independently produced virus particle stocks were used for each plasmid and replication kinetics performed in parallel.

To assess the stability of SNAPf and sfGFP insertions into Gag over the time-course experiment, I used fluorescence microscopy to examine the infected cells and performed western blot analysis on the viral particles harvested on day sixteen. I labeled SNAPf in HIV-1$^{iSNAPf(opt)}$ and HIV-1^{iSNAPf}-infected A3.01 T cells with SNAP-Cell 647SiR, followed by fixation and permeabilization of infected cells. To detect infected cells independently of the reporter, I counterstained against the CA protein by IF. The results are presented in Figure 10 A. With the exception of HIV-1Gag$^{sfGFP(opt)}$, the proportion of infected cells was similar in all cases based on CA IF. Visual inspection indicated that the vast majority of CA-positive cells infected with SNAPf-expressing derivatives also exhibited a signal for labeled Gag.SNAPf. In contrast, for cells infected with sfGFP-expressing derivatives, a substantial proportion of CA-positive cells did not show a GFP signal. These results

suggest that sfGFP may have been partially lost after 16 days, whereas SNAPf remained detectable.

To directly evaluate reporter stability in the viral particles, the particles were concentrated using sucrose cushion ultracentrifugation. Equal amounts of virus, based on RT activity, were then loaded onto an SDS-PAGE gel and analyzed by semi-dry western blotting. Antibodies against the reporter and CA were used to determine the CA-reporter ratio. For SNAPf-expressing derivatives, SNAPf was detected at levels comparable to CA in all replicates, regardless of CpG optimization (Figure 10 B). Conversely, sfGFP-expressing derivatives yielded more heterogeneous results. In at least one of the four replicates, sfGFP was either not detected or only faintly visible, while CA was detected at similar levels for all constructs. Staining for GFP revealed intermediate products of uncleaved Gag.sfGFP, suggesting a partial loss of the tag and notable impairment in processing by the viral PR.

In summary, the data revealed a notable reduction in particle spread for sfGFP-expressing derivatives, indicating that replication within cells was impaired and delayed. In contrast, the insertion of SNAPf showed only minor effects on replication compared to the wt virus, with stable tag integration maintained throughout several rounds of infection in A3.01 T cells. Significant differences related to reduced CpG codons were not observed under the tested conditions.

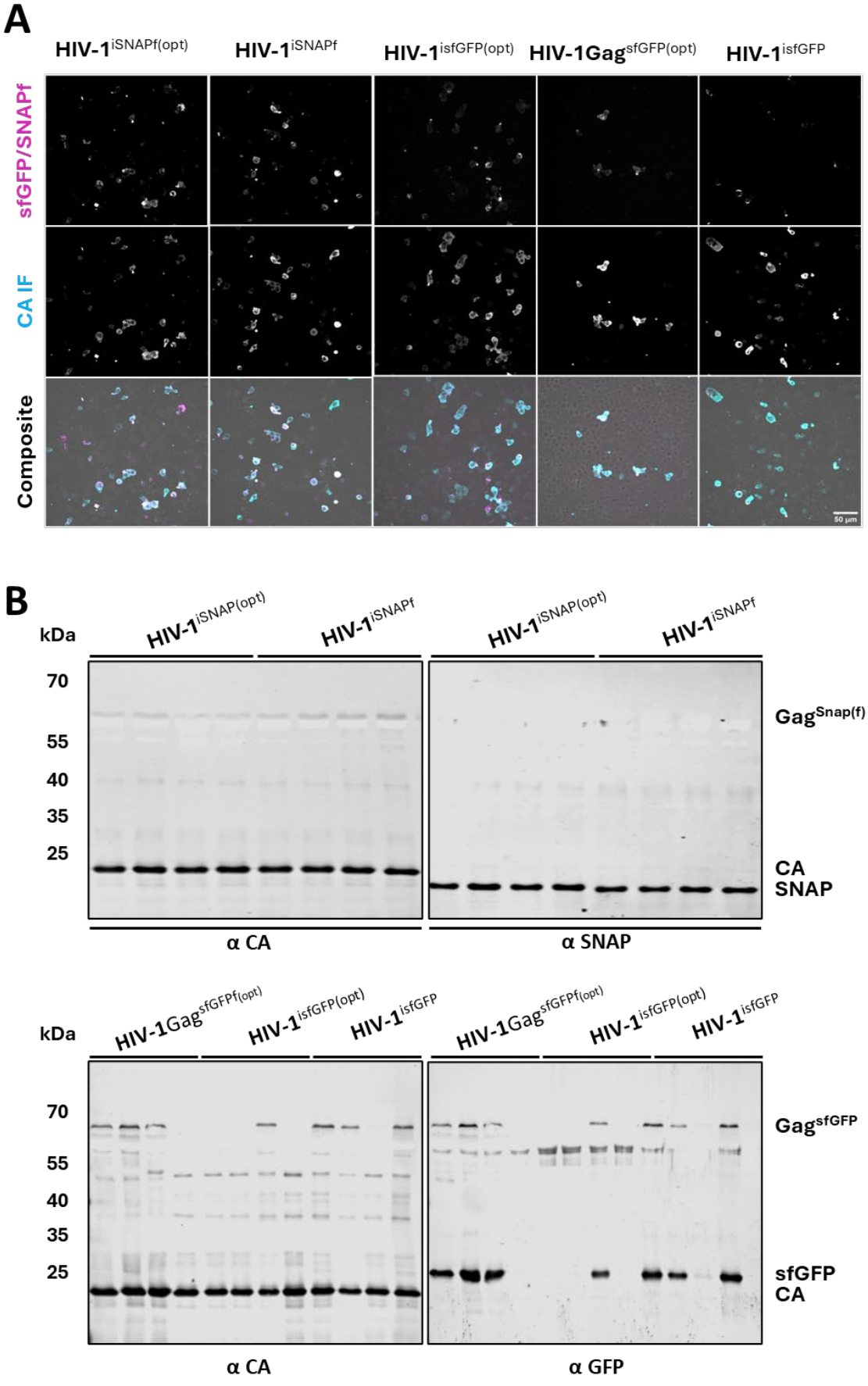
A
HIV-1iSNAPf(opt)
HIV-1iSNAPf
HIV-1isfGFP(opt)
HIV-1Gagsf GFP(opt)
HIV-1isfGFP
sfGFP/SNAPf
CA IF
Composite
50 µm
B
kDa
HIV-1iSNAP(opt)
HIV-1iSNAPf
HIV-1iSNAP(opt)
HIV-1iSNAPf
70
55
40
35
25
Gagsnap(f)
CA
SNAP
α CA
α SNAP
kDa
HIV-1Gagsf GFPf(opt)
HIV-1isfGFP(opt)
HIV-1isfGFP
HIV-1Gagsf GFPf(opt)
HIV-1isfGFP(opt)
HIV-1isfGFP
70
55
40
35
25
GagsfGFP
sfGFP
CA
α CA
α GFP

Previous page: Figure 10 Reporter stability within tagged HIV-1 derivatives 16 days post infection. *(A) A3.01 T cells in which the panel of tagged HIV-1 derivatives replicated continuously for 16 days were fixed with 4% PFA and permeabilized with 0.5% Triton X-100. Subsequently a polyclonal rabbit antiserum against CA was used to detect infected cells by IF. The SNAP and SNAPf-tags were labeled with 600nM SNAP-Cell 647SiR, as described in section 2.5.1. The acquisition of images was conducted using a Nikon Ti inverted spinning disc microscope at 40x magnification. (B) The supernatant particles from A3.01 T cells infected with the panel of tagged HIV-1 derivatives were concentrated by sucrose cushion ultracentrifugation. Equal amounts of virions, based on RT activity, were loaded onto an SDS-PAGE gel and subjected to semi-dry western blotting. The visualization of proteins was conducted using polyclonal sheep antiserum against CA and polyclonal rabbit serum against the respective tag. IRDye 680RD-conjugated secondary antibodies were employed for the detection of CA, while IRDye 800CW-conjugated secondary antibodies were utilized for the detection of sfGFP and SNAPf.*

3.1.5 SNAPf(opt) remains stable within Gag over several rounds of infection in A3.01 T cells.

In addition to the reduced infectivity caused by tag insertion, a key limitation of current methods for direct Gag labeling is the short-term stability of the tag integration over multiple infection cycles. As the previously described replication kinetic hinted to improved tag stability in the case of HIV-1$^{iSNAPf(opt)}$, I performed a passaging experiment to assess the long-term stability of the SNAPf(opt)-tag in Gag. I monitored continuous HIV-1$^{iSNAPf(opt)}$ replication over 90 days and evaluated reporter expression through flow cytometry and western blot analysis.

For initial infection, A3.01 T cells were spin-inoculated with the panel of CpG-optimized HIV-1 derivatives and wt at an MOI of 0.1 blue cell units (BCU) per cell. Three days later, flow cytometry analysis was used to assess the percentage of infected cells via indirect immunolabeling of CA, while reporter expression was evaluated by direct detection of sfGFP or SNAPf labeling using SNAPCellSir647. Every three days, the proportion of cells expressing CA and the reporter was measured by flow cytometry, and fresh A3.01 T cells were introduced to maintain a five % infection rate, ensuring continuous viral spread. The ratio of p24 expression to reporter expression provided a measure of the percentage of cells infected with an HIV-1 derivative that retained a functionally active tag within viral particles.

For the derivatives expressing the sfGFP(opt)-tag, I observed a progressive reduction in GFP signal after three passages, in line with the previous observations described in 3.1.4. Upon the sixth passage, cells positive for both sfGFP(opt) and CA had almost completely disappeared, suggesting a partial deletion of sfGFP, or a reversion to the wt HIV-1$_{NL4-3}$ (Figure 11). In contrast, viruses expressing the SNAPf(opt)-tag consistently retained the reporter for eighteen passages (Figure 12). Following a notable drop in overall infection, the HIV-1$^{iSNAPf(opt)}$1 replicate exhibited a gradual loss of the SNAPf(opt)-tag. However, the other SNAPf(opt)-expressing replicate maintained stable tag insertion throughout the experiment, persisting for 30 passages over the 90-day period.

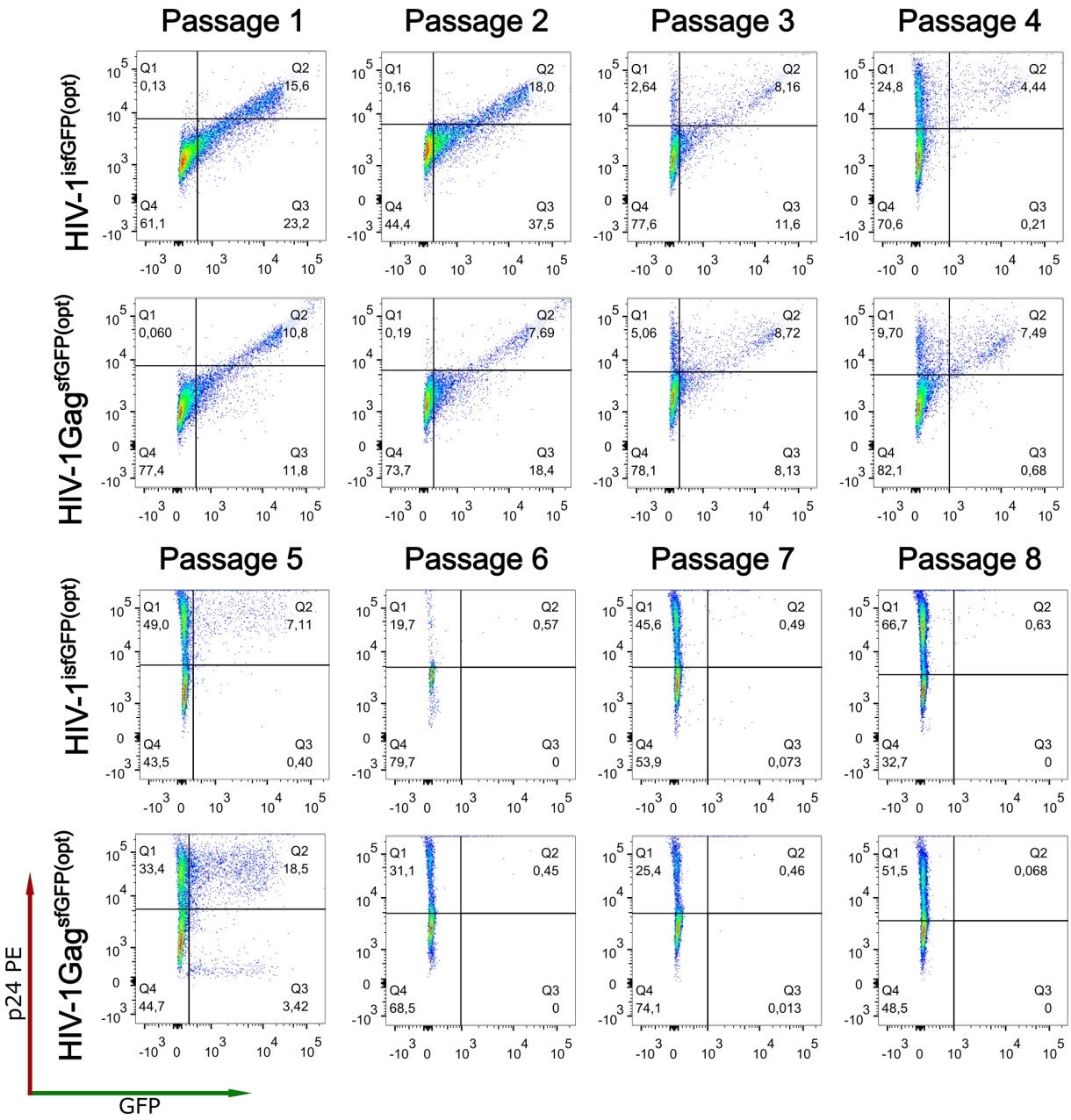

Figure 11 Reporter and p24 expression in sfGFP(opt)-tagged HIV-1 derivatives over time.
The reporter-expressing derivatives were passaged in A3.01 T cells for a period of 90 days. Three days post-infection, the infected cells were fixed using the BD Cytofix/Cytoperm Fixation/Permeabilization Solution Kit, followed by a washing step using the BD Cytoperm buffer and permeabilization with 0.5% Triton X-100. The percentage of infected cells was determined by flow cytometry using RD1-conjugated αCA antibodies. Every three days, CA and reporter expression were analyzed by flow cytometry and fresh A3.01 T cells were added to maintain 5% infection. The Q2 quadrant represents double positive cells. The y-axis represents CA expression, while the x-axis represents sfGFP-expression. The measurements were conducted using a BD FACSVerse Cytometer, and the analysis was performed using FlowJo (V10.9.0). Gates were set for each passage individually based on Mock cells stained with the RD1-conjugated αCA antibody.

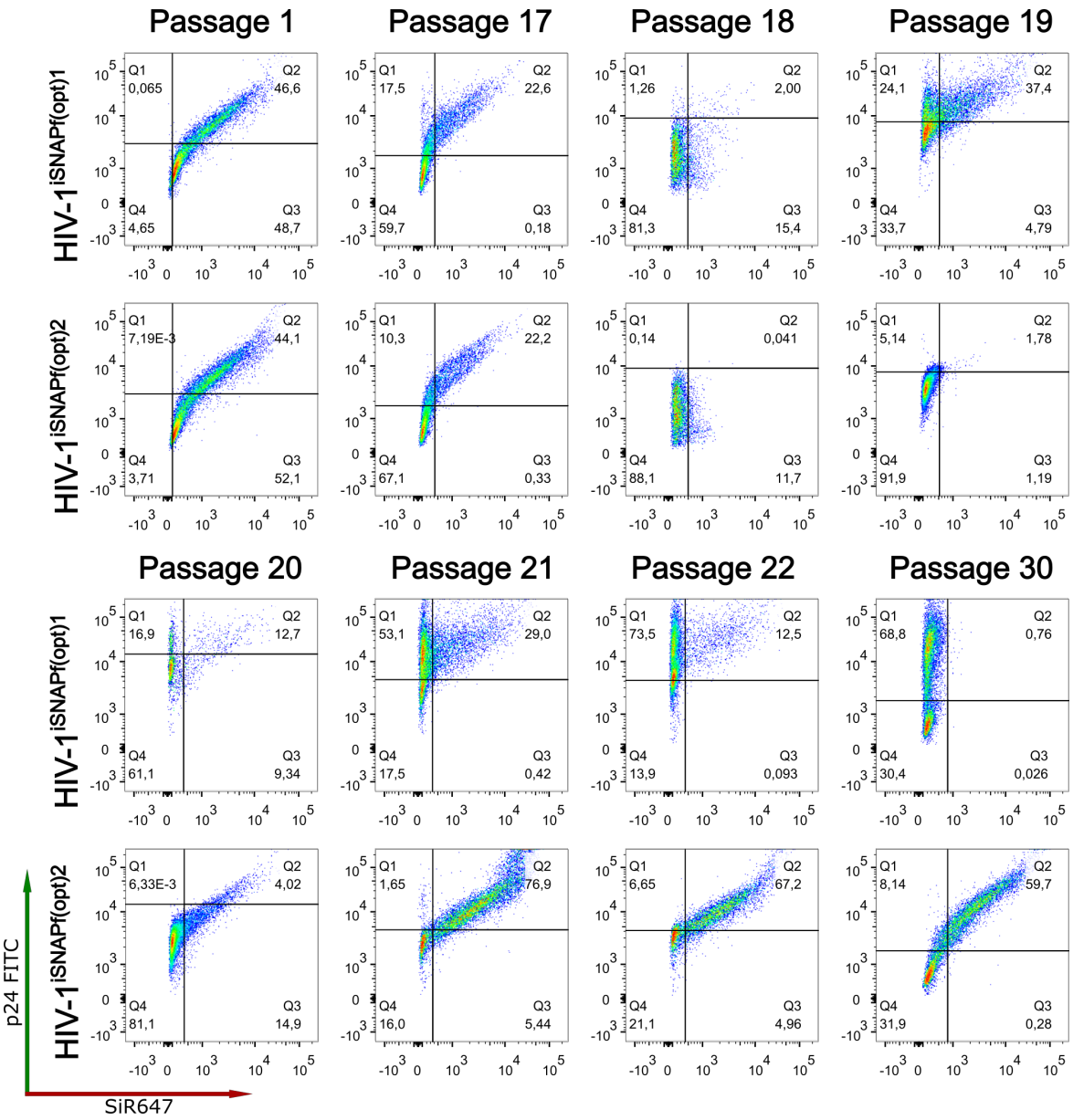

Figure 12 Reporter and p24 expression in SNAPf(opt)-tagged HIV-1 derivatives over time.
The reporter-expressing derivatives were passaged in A3.01 T cells for a period of 90 days. Three days post-infection, the infected cells were fixed using the BD Cytofix/Cytoperm Fixation/Permeabilization Solution Kit, followed by a washing step using the BD Cytoperm buffer and permeabilization with 0.5% Triton X-100. The percentage of infected cells was determined by flow cytometry using FITC-conjugated αCA antibodies. Gag.SNAPf(opt) expression quantified through labeling with SNAP-Cell 647SiR.Every three days, CA and reporter expression were analyzed by flow cytometry and fresh A3.01 T cells were added to maintain 5% infection. The Q2 quadrant represents double positive cells. The y-axis represents CA expression, while the x-axis represents SNAPf(opt)-expression. The measurements were conducted using a BD FACSVerse Cytometer, and the analysis was performed using FlowJo (V10.9.0). Gates were set for each passage individually based on Mock cells stained with the FITC-conjugated αCA antibody and SNAP-Cell 647SiR.

The ratio of p24- to reporter-expressing A3.01 T cells was plotted to illustrate the rapid decline of sfGFP(opt) (green lines, point of loss indicated by grey box) compared to SNAPf(opt) (blue lines) in the tested panel of HIV-1 derivatives (Figure 13 A). This depiction further highlighted that HIV-1$^{iSNAPf(opt)}$ demonstrated substantially greater tag stability than sfGFP(opt)-expressing derivatives, irrespective of the reporter position within Gag.

To assess reporter stability at the viral particle level, I harvested HIV-1$^{iSNAPf(opt)}$ particles from the supernatant of infected cells at the critical time point where reporter loss was observed in one of the derivatives (passage 19), as well as on subsequent passages until the end of the experiment at day 90. The particles were concentrated using sucrose cushion ultracentrifugation, and subsequently loaded onto an SDS-PAGE gel and analyzed by semi-dry western blotting. Antibodies against the reporter and CA were employed to quantify the CA-SNAPf(opt) ratio and detect potential intermediate products.

Staining for CA and SNAPf(opt), and comparison with the input virus, confirmed the progressive loss of the SNAPf(opt)-tag in HIV-1$^{iSNAPf(opt)}$ replicate 1, as previously observed by flow cytometry (Figure 13 B). In contrast, the second replicate retained SNAPf(opt) until the experiment concluded at day 30. Comparing the intermediate products of Gag.SNAPf processing between passage 0 and passage 30 revealed no detectable differences, suggesting that Gag processing remained intact throughout the 90 days of continuous viral spread.

To conclude this chapter, I achieved the first objective of this thesis: the development of a fully replication-competent HIV-1 derivative with stable reporter expression across multiple infection cycles. I showed that HIV-1$^{iSNAPf(opt)}$ had infectivity nearly as high as the wt virus in TZM-bl and C8166 assays, substantially outperforming sfGFP-expressing HIV-1 derivatives, regardless of whether sfGFP was placed between MA and CA or at the C-terminus of Gag. Additionally, I observed that the replication kinetics of HIV-1$^{iSNAPf(opt)}$ were only slightly stunted compared to HIV-1$_{NL4-3}$ in A3.01 T cells cells but reached similar plaetaus after ten days. Long-term passaging in A3.01 T cells confirmed that SNAPf(opt) remained stably integrated into Gag for at least eighteen passages in this experiment. This stability provides a notable advantage over existing models for studying Gag trafficking *in vitro* and establishes HIV-1$^{iSNAPf(opt)}$ as a valuable tool for investigating the HIV-1 replication cycle using fluorescence microscopy and flow cytometry.

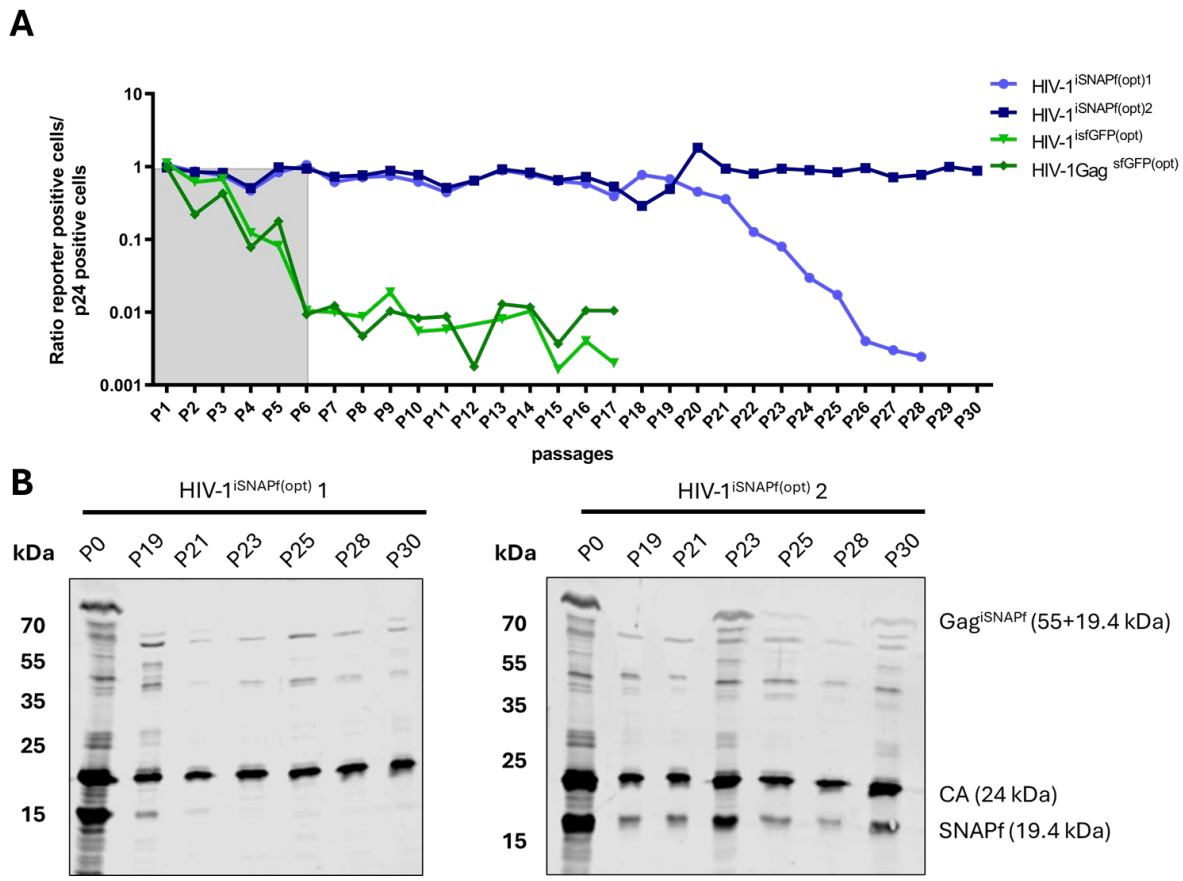

Figure 13 Passaging of HIV-1 derivatives in A3.01 cells.

(A) The panel of reporter-expressing HIV-1 derivatives was passaged in A3.01 T cells for a period of 90 days. The cultures were evaluated by flow cytometry at three-day intervals and adjusted to a 5% infected cell concentration by the addition of fresh cells. Flow cytometry was employed to quantify the infected cells, utilizing FITC-coupled αCA antibodies for SNAPf(opt)-expressing derivatives (blue) and RD1-conjugated αCA antibodies for sfGFP-expressing viruses (green). The ratio of cells positive for SNAPf-tag or sfGFP and CA was determined to yield the proportion of infected cells still carrying a functional reporter. The grey box indicates the point of sfGFP loss. (B) The supernatant particles from A3.01 T cells infected with the panel of tagged HIV-1 derivatives were concentrated by sucrose cushion ultracentrifugation. Viral samples were loaded onto an SDS-PAGE gel and subjected to semi-dry western blotting. The visualization of proteins was conducted using polyclonal sheep antiserum against CA and polyclonal rabbit serum against SNAP-tag. IRDye 680RD-conjugated secondary antibodies were employed for the detection of CA, while IRDye 800CW-conjugated secondary antibodies were utilized for the detection of SNAPf.

3.2 HIV-1$^{iSNAPf(opt)}$ particles show normal morphology in context of the virological synapse

The structural properties of VSs can be visualized using electron microscopy. This has been accomplished for both wt (88) and tagged HIV-1 (96, 151). Nevertheless, despite the detection and colocalization of mature HIV-1^{iGFP} particles with the GFP signal, elevated levels of Gag at the plasma membrane suggested the possibility of delayed particle assembly and release, which could explain the impaired replication competence of those viruses (128). To ascertain whether this phenomenon could also be observed in the case of HIV 1$^{iSNAPf(opt)}$, a correlative light and electron microscopy (CLEM) approach was conducted in collaboration with Dr. Charlotta Funaya from the electron microscopy facility of Heidelberg University. I spin inoculated A3.01 T cells with either HIV-1$^{iSNAPf(opt)}$ or HIV-1$^{isfGFP(opt)}$. Eighteen hours post-infection, the respective infected cell populations were mixed with membrane-labeled uninfected A3.01 T cells to facilitate the clear discrimination of donor and target cells. Subsequently, the samples were fixed, and fluorescence microscopy images were acquired using a Zeiss Cell Discoverer 7. Following fluorescent imaging, the cells were embedded in Epon and sectioned into 250 nm thin slices by Dr. Charlotta Funaya. Fluorescently labeled Gag.SNAPf (red) was successfully detected and correlated with viral particles visible in the EM counterpart (Figure 14 A). At the contact site, multiple viral particles could be observed in the thin section (see orange box). The depicted example of an HIV-1$^{iSNAPf(opt)}$ induced VS did not display the characteristic pocket between the donor and target cell, and Gag.SNAPf appeared to be located more on the side of the cell. However, electron tomography confirmed that this is mainly caused by the z-resolution, with particles present within a synaptic pocket. Furthermore, electron tomography of the section revealed the presence of budding sites at the donor cell site, with mature particles situated within the synaptic cleft (Figure 14 B). The observed VSs in HIV 1$^{iSNAPf(opt)}$ infected A3.01 cells exhibited a morphology consistent with that described for wt HIV-1 (88). More examples for correlated cell pairs can be seen in the appendix (Supplementary Figure 1 A-C).

Additionally, the HIV 1$^{isfGFP(opt)}$ induced VS was correlated using the same approach to enable a comparison of particles from both HIV 1 derivatives (Figure 14 C). Mature particles could be observed in the contact zone, correlating with the sfGFP signal acquired by pre-embedding fluorescence microscopy. Neither the HIV-1$^{iSNAPf(opt)}$ nor the HIV-1^{isfGFP} induced VS exhibited any significant abnormalities in the assembly of Gag towards the synaptic cleft.

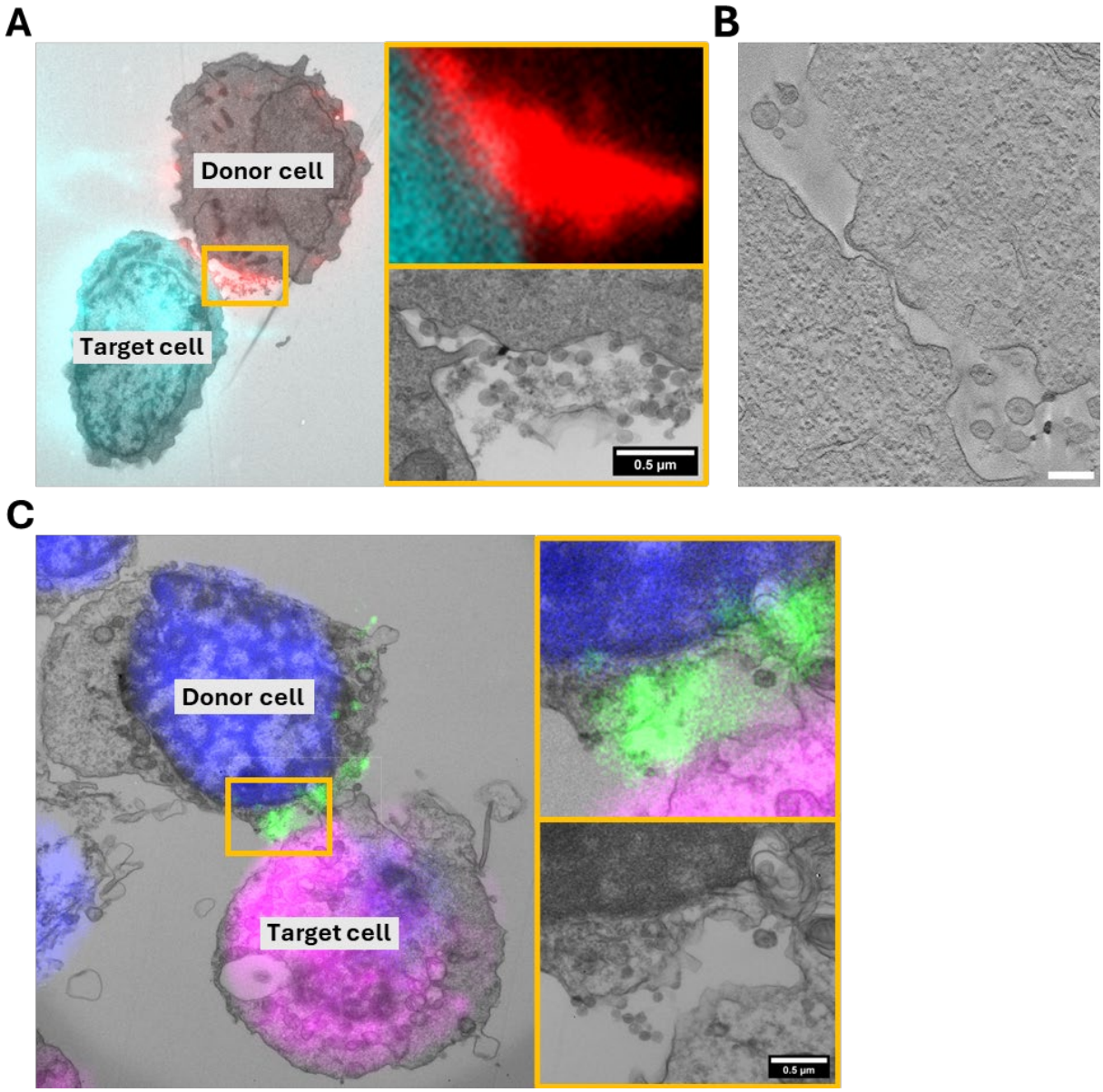

Figure 14 CLEM analysis of the HIV-1$^{iSNAPf(opt)}$ VS and comparison with HIV-1$^{isfGFP(opt)}$

A3.01 T cells were infected with either HIV-1$^{iSNAPf(opt)}$ (A) or HIV-1$^{isfGFP(opt)}$ (C). At 18 hours post-infection, Gag.SNAPf(opt) was labeled using 600 nM SPY555-BG, washed, and mixed with membrane-labeled uninfected A3.01 cells (target cells) at a ratio of 1:4 and seeded onto gridded MatTek dishes. Subsequently, the cells were fixed for an additional 90 minutes with 4% PFA and 0.2% GA, washed, and stained with Hoechst 33258. Subsequently, Dr. Funaya proceeded to dehydrate the cells, embed them in Epon, and section them. The resulting sections were imaged using a JEOL JEM-1400 transmission electron microscope and a Tecnai F20 electron microscope. Contact events identified by fluorescence were relocated using the grid, and EM and fluorescence images were correlated using the eC-CLEM plugin in Icy software. (A) Correlation of a HIV-1$^{iSNAPf(opt}$) infected donor cell with an uninfected target cell. In panel B, Gag.SNAPf(opt) is pseudo-colored in red, while the membrane of the target cell is represented in cyan. Panel C depicts a tomographic slice of the synaptic cleft of the cell pair shown in panel A. Panel D illustrates the correlation of an HIV-1$^{isfGFP(opt)}$ infected donor cell with an uninfected target cell. In this case, Gag.SNAPf(opt) is pseudo-colored in green, the membrane of the target cell is represented in magenta, and the nucleus is shown in blue.

3.3 Development of a microscopy assay for live detection of productive cell-to-cell transmission

One of the central aims of this study was to develop a live microscopy setup for imaging cell-to-cell transmission through VSs using the fully replication-competent HIV-1 derivative HIV-1$^{iSNAPf(opt)}$. Previous studies have mainly utilized HIV-1 derivatives tagged with GFP within the Gag region between the MA and CA domains for live imaging of cell-to-cell transmission (96, 94). Although this approach provided insight into the quantitative and morphological aspects of VS formation and productive infection, it also had some limitations. The majority of studies involving this derivative have primarily focused on the transfer of fluorescently labeled Gag and/or Env, to subsequently correlate these observations to the overall cell population. The observed cell-to-cell transmission at the level of individual cell pairs at a given time point is matched to the total number of productively infected target cells. It is not possible to conclude whether the observed event is the definitive cause of productive infection, as there is no clear differentiation between transferred and newly produced viral proteins.

The objective of the second part of this project was to establish a protocol for the live detection of productive cell-to-cell transmission. In particular, the main aim includes the differentiation between transferred and newly expressed viral components, thereby offering a significant advantage over existing systems.
To fully assess the dynamics occurring during VS formation and post-entry events, it was furthermore essential to analyze the imaging data in a quantitative and non-biased manner. This quantification should be performed automatically with specialized, advanced techniques for the segmentation and tracking of cells, as well as the registration of VS formation events.

The following chapters will present a novel pulse-chase-labeling approach for the time-resolved resolution of cell-to-cell transmission, with correlation of contact events between donor and target T cells to productive infection.

3.3.1 Visualization of cell-to-cell transmission using HIV-1$^{iSNAPf(opt)}$

In order to ascertain the infection capacity of HIV-1$^{iSNAPf(opt)}$ in primary CD4+ T cells and compare it to infection in the T cell line A3.01, I infected A3.01 or primary CD4+ T cells with HIV-1$^{iSNAPf(opt)}$ and labeled Gag.SNAPf(opt) using SNAPCellSir647 72 hours post infection. Using an MOI of 0.1 based on the blue cell assay (BCU), 52.7 % of A3.01 T cells and 29.4 % of CD4+ T cells were productively infected (Figure 15 A). To validate the use of HIV-1$^{iSNAPf(opt)}$ for visualizing cell-to-cell transmission between T cells, I first aimed at establishing optimal imaging conditions. A3.01 T cells were

infected with an MOI of 0.1 BCU and Gag.SNAPf(opt) labeled with SNAPCellSir647 24 h post infection. A second target cell population was labeled with a fluorescent membrane dye and mixed with the infected donor cell population to a ratio of 1:3. The mixed cell suspension was then seeded into glass-bottomed imaging dishes, and 20 minutes later images acquired by spinning disc confocal microscopy. Figure 15 B shows an exemplary image in which Gag.SNAPf(opt) is pseudo colored in red and the membrane label of target cells is shown in blue. Under these conditions multiple interactions between donor and target cells could be observed, with and without Gag.SNAPf(opt) polarization towards membrane labeled target cells. Additionally, no obvious uptake of membrane dye by donor cells was visible, rendering the tested setup suitable for imaging of transmission events between both populations.

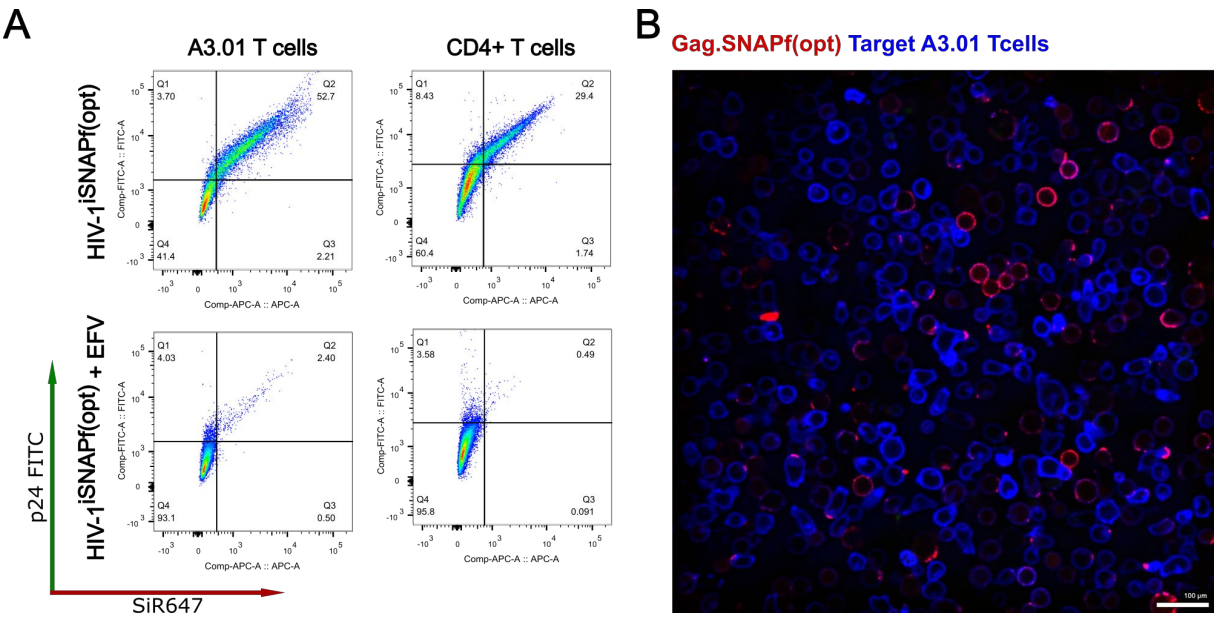

Figure 15 Infection capacity of HIV-1$^{iSNAPf(opt)}$ in T cells and imaging of a labeled mixed donor-target cell population.

(A) A3.01 or primary CD4+ T cells were infected with HIV-1$^{iSNAPf(opt)}$ at an MOI of 0.1 BCU/cell. 72 h post-infection, the proportion of infected cells was quantified through flow cytometry on a FACSVerse system and subsequently analyzed using FlowJo. A negative control was employed in where the NNRTI EFV was added at point of infection with a concentration of 20 µM. (B) Uninfected A3.01 target cells were membrane labeled using CellVue® Claret lipid dye. Infected A3.01 donor T cells and membrane-labeled A3.01 target cells were mixed in a 1:3 ratio. The cell mixture was then transferred to a glass-bottomed imaging dishes, and images acquired 20 min later after settling of cells using an inverted Nikon Ti2 confocal spinning disc microscope with a 60x oil objective under BSL3 conditions. Scale bar is 100 µm.

In order to optimize imaging conditions for time-resolved live-imaging, I examined different coating options for the glass-bottomed imaging slides. T cells are suspension cells and, as such, not adherent to the imaging surface. This markedly enhances the dynamic and motile properties of the cells. Although cells need to maintain mobility for interactions that facilitate VS formation and cell-to-cell transmission, surfaces that are less restrictive make it increasingly difficult to track individual cells for later analysis. To evaluate the optimal balance between restriction and mobility for trackable cell-to-cell transmission, three distinct conditions were tested. These included a control without any coating, a coating with poly-L-lysine, and a coating with PEI. A time course spanning 120 minutes was employed, with cells fixed at 30, 60, 90, and 120 minutes. Subsequently, I conducted IF staining against Env, as polarization of Env towards the synaptic contact zone has been documented as a characteristic of VS (91). Figure 16 A depicts an exemplary image of a contact zone with weak Gag.SNAPf(opt) and strong Env polarization at the assembly sites towards the contact zone with a target cell. I manually quantified the number of cell contacts between donor and target cells and assessed Gag.SNAPf(opt) and Env polarization at the contact site, as a measure of VSs. In the absence of coating, the majority of cells were lost from the coverslip during the fixation process, so only VS on poly-L-lysine and PEI-coated dishes could be analyzed. While there was no substantial difference between the two conditions, a trend towards an increased number of VSs and earlier VS formation was observed on poly-L-Lysin-coated imaging slides (Figure 16 B). The earlier detection of VS may be attributed to the enhanced mobility of cells on the less restrictive surface, which facilitates rapid migration towards each other. In light of these findings, subsequent experiments were conducted exclusively on poly-L-lysine-coated imaging slides.

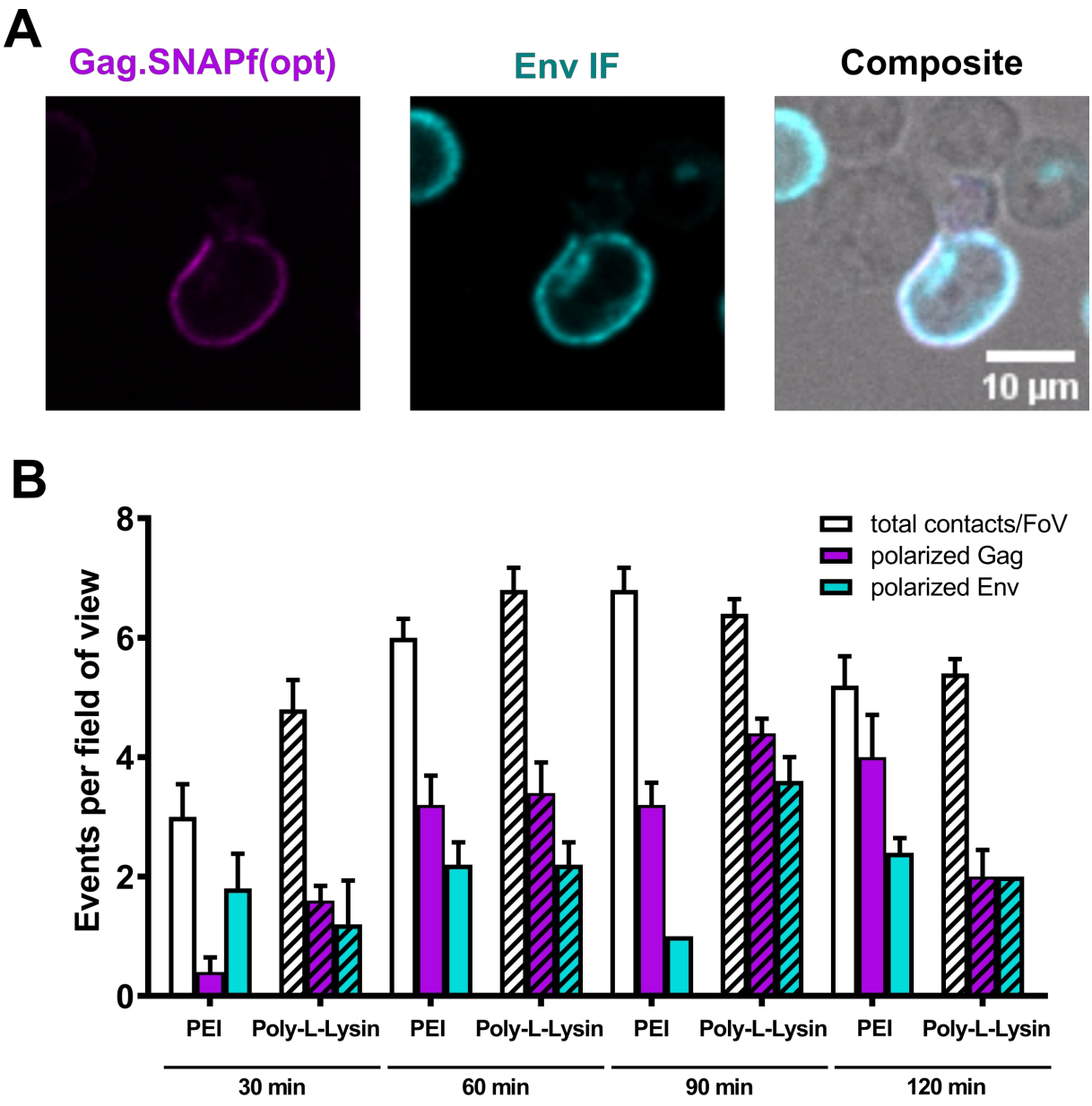

Figure 16 Determination of the optimal coating for live detection of VS-formation.
A3.01 T cells were infected with 0.1 BCU/cell and, 24 hours later, Gag.SNAPf(opt) labeled using SNAPCellSir647. The cells were then combined with a fresh target cell population at a ratio of 1:4. Ibidi 8-well glass bottom dishes were coated with 200 µl of PEI (1 mg/ml) or poly-l-lysine (0.1% (w/v)) for 30 minutes and subsequently rinsed twice with PBS. 1 x 10^5 per well (1 cell per 10 μm^2) was seeded into the precoated dishes and cells were fixed at 30, 60, 90, and 120 minutes post seeding. Subsequently, immunofluorescence staining against Env was conducted using a polyclonal antiserum. Five fields of view per condition were imaged on an inverted Nikon Ti2 confocal spinning disc microscope with a 60x oil objective for the quantification of cells in contact with each other, as well as for the assessment of Gag.SNAPf(opt) and Env polarization in those contacts.

Another crucial element to be considered was cell viability. The relatively small volume of 400 µl per imaging well, combined with constant illumination over prolonged imaging sessions of up to 24 hours, induced cell apoptosis and phototoxicity based on visibly impaired cell shape in the DIC channel. In an effort to decrease cell mortality, the laser power and exposure time were minimized. To recover sufficient signal for subsequent image analysis and visualization, software-supported enhancement was employed using an artificial intelligence (AI) algorithm, "NIS.ai enhance", released by Nikon. This algorithm is specifically designed to restore details in low-signal images. I trained the AI to enhance the signal of images with minimal laser power and exposure time based on a complementary image of the same FoV with high laser power and exposure time, with high signal-to-noise ratio. To ensure that the algorithm did not produce artifacts, the raw image of the Gag.SNAPf(opt) signal acquired at 2% laser power and 30 ms exposure time was compared with the AI-generated enhanced counterpart. Figure 17 depicts an example of the low signal-to-noise image and the enhanced version of the same FoV. The application of AI enhancement resulted in a substantial improvement in the signal-to-noise ratio without introducing artifacts. By limiting the illumination intensity, I was able to reduce phototoxicity to a level that permitted continuous live imaging for up to 24 hours.

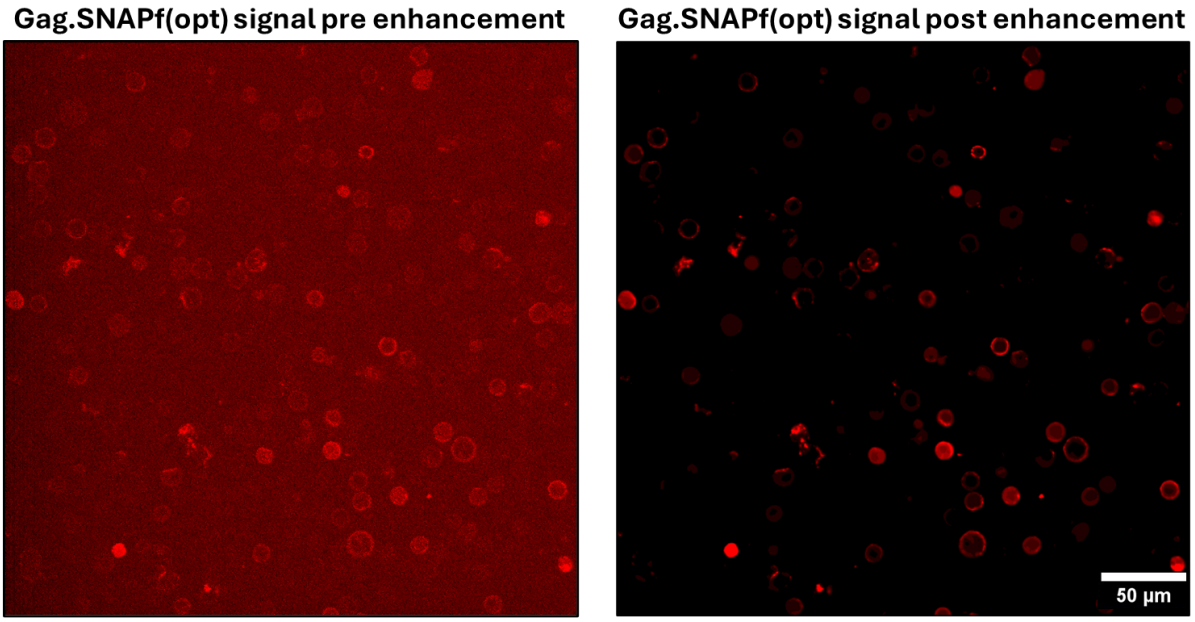

Figure 17 Software enhanced Gag.SNAPf(opt) signal using NIS-Elements NIS.ai.
A3.01 cells were infected with HIV-1$^{iSNAPf(opt)}$ and Gag.SNAPf(opt) labeled with 600nM MaP555 18 h post infection as described previously. 1x 10^5 cells were seeded on poly-l-lysine-coated dishes and immediately imaged on an inverted Nikon Ti2 confocal spinning disc microscope with a 40x oil objective. The image was acquired with 2% laser power and 30 ms exposure time, which corresponded to the lowest settings at which a signal could be detected. The NIS-Elements AI "Enhance.ai" employs a training algorithm based on image pairs acquired with high laser power with prolonged exposure time and low laser power with short exposure time, which have been iterated over 1,000 times and on multiple image pairs.

Utilizing the optimized imaging conditions, I conducted a live imaging experiment to observe the dynamics of cell-to-cell transmission of HIV-1$^{iSNAPf(opt)}$ particles between donor and target A3.01 T cells. Gag.SNAPf(opt) in HIV-1$^{iSNAPf(opt)}$ infected A3.01 T cells was labeled with SNAPCellSir647 18 hours post infection and donor cells mixed with a membrane-labeled target cell population. Subsequently, the cells were seeded into poly-l-lysine-coated imaging dishes and imaged for 20 hours at a framerate of 0.33 per minute. Figure 18 A shows an exemplary FoV in which contact zones between donor cells with labeled Gag.SNAPf(opt) (magenta) and membrane-labeled target cells (green) were detected after 20 hours of imaging. The visualization of multiple contact zones between donor and target cells was achieved. As illustrated in panel A1, Gag.SNAPf(opt) polarizes at the contact zone, forming a synaptic button with the green target cell. Panel A2 illustrates the formation of a poly synapse by a donor cell, which establishes a contact zone with a labeled and a non-labeled target A3.01 T cell. Frames from live cell imaging of the cell-pair highlighted in Panel A1 (Figure 18 B) demonstrated that at time point 0 hours, Gag.SNAPf(opt) polarization towards the unstained cell was already established, whereas polarization in the direction of the newly added green target cells proceeded over several hours.

The system was employed to conduct a preliminary quantitative analysis, which consisted of manually assessing the contacts between the donor and target cells (Figure 18 C). The image depicts a donor cell in contact with four membrane-labeled target cells exhibiting varying degrees of Gag.SNAPf(opt) polarization. The graph on the right represents the manual quantification over a period of five hours, with dark grey indicating a contact and light grey indicating no contact. Over the course of imaging, a fifth cell was contacted that was not yet visible at the beginning of the imaging session and is represented with light grey for the first seven frames. Contacted cell 2 was visibly apoptotic after approximately one hour and therefore excluded upon that time point, which is highlighted by white color in the graph.

In summary, I established and optimized imaging conditions for live observation of VS formation and donor-target cell interactions using HIV-1$^{iSNAPf(opt)}$. I was able to observe VS with the defining features of Gag.SNAPf(opt) as well as Env polarization and improved cell viability to support prolonged imaging over 24 hours at a frame rate of 0.33 frames per minute. Cell mobility on poly-L-lysin-coated imaging dishes allowed manual quantification of contact events between productively infected donor A3.01 T cells and membrane-tagged target A3.01 T cells.

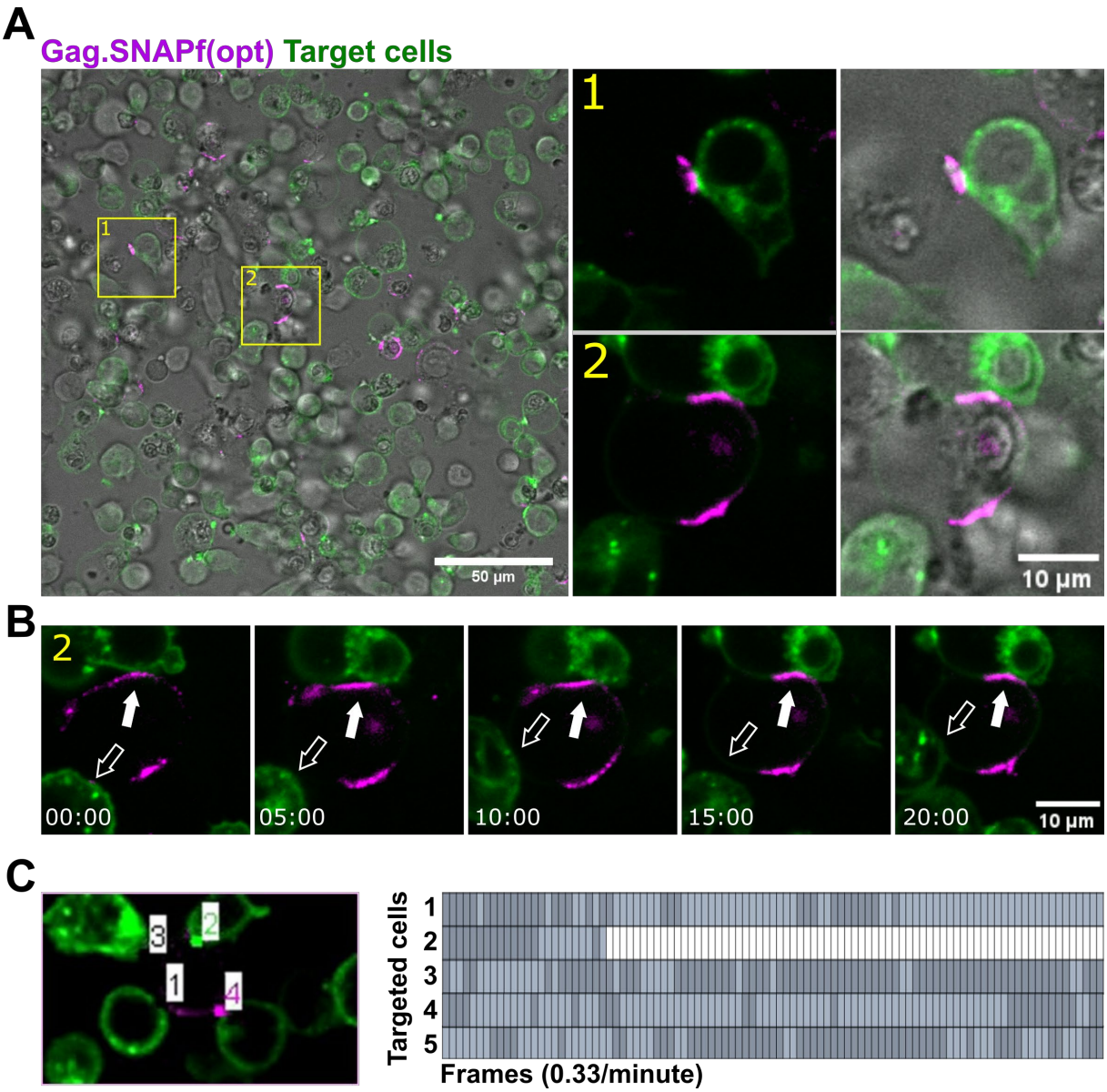

Figure 18 Detection of VS Synapse formation with HIV-1$^{iSNAPf(opt)}$.
A3.01 cells were infected with HIV-1$^{iSNAPf(opt)}$ and Gag.SNAPf(opt) labeled with 600nM SNAPCellSir647 18 h post infection, as previously described. Subsequently, uninfected target cells were membrane-labeled with CellVue® Claret lipid dye. Infected donor cells and membrane-labeled target cells were mixed in a 1:4 ratio. 1 × 10^5 cells were seeded on poly-l-lysine-coated dishes and immediately imaged on an inverted Nikon Ti2 confocal spinning disc microscope with a 40x oil objective at a rate of 0.33 frames per second. (A) Planar view of cells after 20 hours of live imaging with Gag.SNAPf(opt) pseudo colored in magenta and membrane labeling of target cells in green. The figures highlight cell pairs with varying degrees of Gag.SNAPf(opt) polarization towards the target cell. (B) Frames from live cell imaging of the cell-pair highlighted in Panel A1. Polarized contact is highlighted with a white arrow, non-polarized contact with a hollow arrow. (C) Manual analysis of image series was conducted to assess contact events. The image depicts a donor cell exhibiting varying degrees of Gag.SNAPf(opt) polarization towards four membrane-labeled target cells. The graph on the right quantifies these interactions over a five-hour period. Dark gray represents cell contact, while light gray indicates a lack of contact. A fifth cell, initially undetectable, is represented in light gray for the initial seven frames. Cell 2 displayed apoptotic characteristics after approximately one hour, and therefore excluded from analysis at that time point, marked in white on the graph.

3.3.2 Pulse chase labeling of productive HIV-1 infection

To achieve real-time detection of productive cell-to-cell transmission alongside the ability to distinguish between transferred and newly expressed viral components, the system described in the previous section required further development. The incorporation of the SNAPf(opt)-tag, as opposed to GFP, in labeling HIV-1 derivatives not only preserves full replication competence but also addresses the issue of differentiating between transferred and newly synthesized Gag. The self-labeling SNAP-tag allows the specific labeling of Gag with a variety of stable and highly fluorescent chemical dyes at a designated time point. Because the fluorescent BG-substrate is covalently bound to SNAP, it supports pulse-chase approaches. By removal of the BG-coupled dye at a certain time or by consecutive addition of different fluorescent substrates, proteins synthesized in a given timepoint can be tracked over time. Accordingly, in context of this approach, the use of HIV-1$^{iSNAPf(opt)}$ enabled the observation and discrimination of consecutive rounds of infection. To visualize cell-to-cell transmission, a novel approach was employed: pulse-chase labeling of HIV-1 infection in a mixed population of infected donor and uninfected target T cells. A schematic overview of the workflow developed is presented in Figure 19 A. The workflow encompasses the infection of A3.01 T cells with HIV-1$^{iSNAPf(opt)}$ to produce a donor cell population, followed by staining with the cell-permeable BG-dye 1. Unbound dye is removed through washing, so a dye with a different fluorophore can be used in a subsequent round of infection to detect newly expressed Gag.SNAPf(opt) in target cells.

Figure 19 B shows a representative example of an experiment of this nature. Twenty-four hours after the spin inoculation of A3.01 T cells with HIV-1$^{iSNAPf(opt)}$, Gag.SNAPf(opt) was labeled using TMRStar (orange). Following the removal of unbound dye, live imaging was conducted for a period of 24 hours to observe the formation of VSs and transfer of fluorescent material. A VS was defined as a visible contact between two cells, with polarization of Gag.SNAPf(opt) towards the contact zone, including a visible synaptic button. A3.01 T cells that had been involved in VS formation during live imaging were subsequently analyzed for newly expressed Gag.SNAPf(opt), by labeling with SNAPCellSir647. A donor cell that maintained a contact that fulfilled all of the initial criteria for a VS with a previously uninfected target cell could be identified in the example illustrated in Figure 19 B. The previously uninfected cell contained newly expressed Gag.SNAPf(opt) (magenta) and the donor cell also showed evidence of continued Gag expression. A three-dimensional rendering of both cells revealed the synaptic button, which appeared to be primarily composed of Gag.SNAPf(opt) expressed subsequent to the initial labeling. Furthermore, a singular spot of TMRStar-labeled viral material was detectable in the target cell that had been transferred through the VS, indicated by the white arrow.

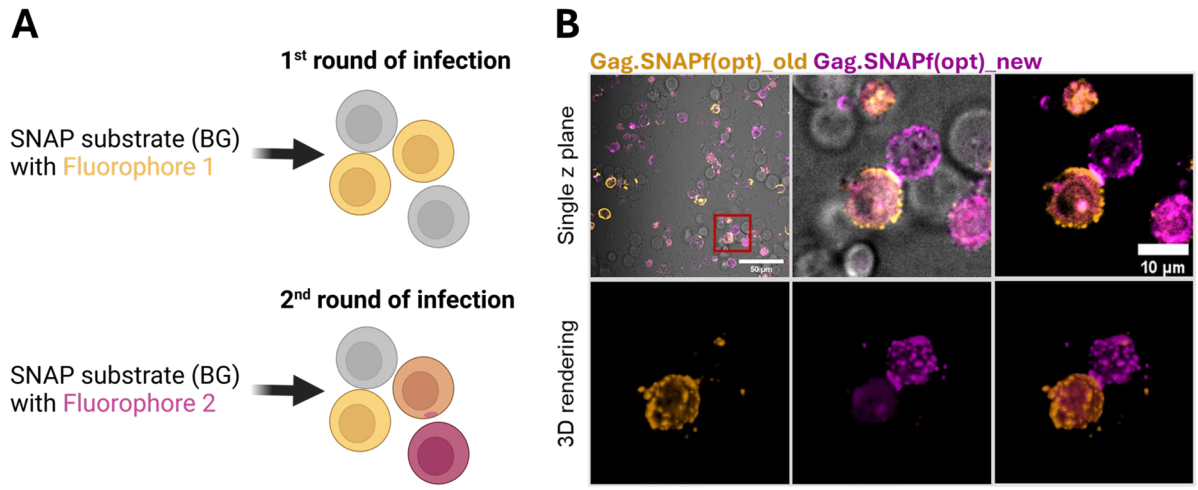

Figure 19 Pulse-chase-labeling of HIV-1$^{iSNAPf(opt)}$ in context of cell-to-cell transmission.
(A) Schematic overview of the pulse chase labeling approach, alongside an exemplary depiction of the experiment. (B) A3.01 T cells were infected with HIV-1$^{iSNAPf(opt)}$ with an MOI of 0.1 BCU/cell, and 24 hours later, Gag.SNAPf(opt) was labeled with the cell-permeable BG-coupled dye SNAPCellTMRStar (orange). Following a washing step to remove unbound dye, 1 × 10^5 cells were seeded on poly-l-lysine-coated dishes and immediately imaged on an inverted Nikon Ti2 confocal spinning disc microscope with a 40x oil objective at a rate of 0.33 frames per second. Following imaging, SNAPCellSir647 was utilized to detect newly expressed Gag.SNAPf(opt) (magenta). The image depicts the planar view of two cells in contact at the end of the imaging period, as well as a 3D rendering created with the 3D-Viewer plugin in Fiji imaging software. The white arrow indicates transferred Gag.SNAPf(opt) into the target cell.

Although this approach enabled the differentiation between distinct stages of infection, the full time-course following a contact event and subsequent productive infection remained uncertain. This was caused by the time-consuming process of adding a second dye and subsequent washing to reduce background interference. Furthermore, exchanging the medium under BSL-3 conditions necessitates the use of a safety hood, rendering this procedure impossible without first removing the imaging dish from the microscope. This introduces unwanted movement within the cells, as well as the challenge of accurately relocating the precise positions for subsequent imaging.

I therefore wanted to establish a pulse chase staining procedure that could be implemented without washing steps. The signal-to-noise ratio of a variety of commercially available dyes was assessed, but none proved suitable for imaging without washing away unbound dye. To address this issue, a novel highly fluorogenic dye, SNAP23 (173), was kindly provided by the group of Kai Johnson at the Max Planck Institute for Medical Research in Heidelberg. The development of fluorogenic probes that are sufficiently advanced to permit wash-free SNAP-tag labeling is a challenging and continually evolving process. SNAP23, a member of the rhodamine derivative class, is an ideal candidate due to its high photostability, cell permeability, and spirocyclization equilibrium, which ultimately leads to high fluorogenicity. Lardon *et al*. demonstrated that it

exhibits high fluorescence signal upon binding of SNAP, high cell permeability, and low background by adjusting the equilibrium between the non-fluorescent, cell-permeable spirolactone and the fluorescent zwitterion (173). I thus decided to explore whether SNAP23 could be used as the dye used for pulse-chase experiments.

To ascertain the feasibility of wash-free labeling of Gag.SNAPf(opt), I added 600nM of SNAP23 to the imaging medium of HIV-1$^{iSNAPf(opt)}$ infected A3.01 T cells. Live imaging of the labeled cells revealed an exceptionally low background and a gradual expression of Gag.SNAPf over time (Figure 20 A). As illustrated in the presented example, productive cell-to-cell transmission could be observed. The target cell was initially contacted at the beginning of the imaging series and subsequently served as a donor cell 16 hours later, undergoing a full round of infection (Figure 20 A). The combination of the pulse-chase labeling approach with this novel, highly fluorogenic dye thus allow for continuous observation of the second round of infection, enabling the direct correlation of distinct contact and VS events to productive infection. In the context of cell-to-cell transmission, this approach allows the differentiation between transferred and newly expressed viral material, as well as the determination of whether the event was productive or abortive based on the presence of an increasing amount of newly expressed Gag.SNAPf(opt), as plotted in Figure 20 B.

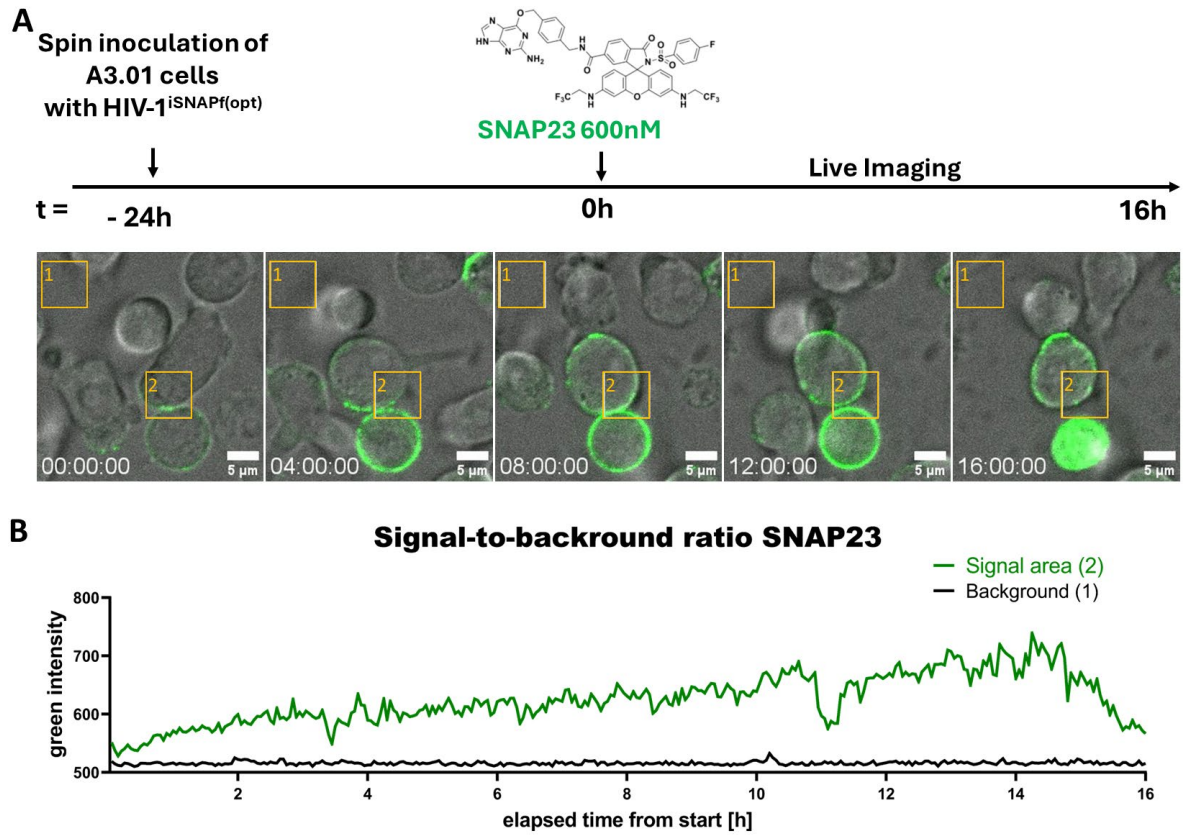

Figure 20 Continuous expression and observation of Gag.SNAPf(opt) labeled with SNAP23.
(A) A3.01 T cells were infected with HIV-1$^{iSNAPf(opt)}$ with an MOI of 0.1 BCU/cell, and 24 hours later, Gag.SNAPf(opt) was labeled with 600 nM of the novel, cell-permeable and highly fluorogenic dye SNAP23 (green). 1 × 10^5 cells were seeded on poly-l-lysine-coated dishes without washing steps to remove unbound dye. Imaging was conducted on an inverted Nikon Ti2 confocal spinning disc microscope with a 40x oil objective at a rate of 0.33 frames per second for 16 hours. (B) The mean signal intensity in the indicated orange boxes, representing both the background area and the contact area between the initially infected donor cell and a target cell, is plotted over time.

3.4 Live detection of productive infection in target cells under continuous observation

Based on the findings described above, I developed a protocol for the real-time analysis of cell-to-cell transmission events in T cells. A3.01 T cells were spin-inoculated with HIV-1$^{iSNAPf(opt)}$, and 18 hours post-infection, Gag.SNAPf(opt) was labeled using SPY555-BG to identify the donor cell population. To ensure that only uninfected target cells are used for subsequent analysis, I labeled the membrane of a second, fresh A3.01 T cell population using CellVue Claret, a commercially available lipid dye for general membrane labeling, as established in section 3.3.1.

The two cell populations were combined in a 1:4 ratio, and live cell imaging was performed for 18 to 24 hours at a frame rate of 0.33 frames per minute. The imaging medium included the novel, highly fluorogenic dye SNAP23 for live detection of newly expressed Gag.SNAPf(opt). A productively infected target cell was defined as a membrane-labeled target cell exhibiting an increasing signal of the green-emitting SNAP23 subsequent to contact with a donor cell containing SPY555-BG-labeled Gag.SNAPf(opt). Figure 21 A provides a schematic overview of the established protocol.

Figure 21 B shows representative timelapse images of a pulse-chase labeled cell-to-cell transmission event. At 1:18 hours, the blue target cell (with a white asterisk) forms a contact with the magenta donor cell. The cell establishes continuous contact with the indicated target cell and other target cells with Gag.SNAPf(opt) polarization, forming a polysynapse. Contacts to multiple target cells were simultaneously observed for a large portion of donor cells. About 17 hours after initial contact, a green signal appeared in the target cell, which increased over time. At 22:33 hours into the imaging series newly expressed Gag.SNAPf(opt) was observed across the entire cell membrane of the donor cell, hinting to productive infection within the target cell following the cell-cell contact to the donor cell earlier.

Figure 22 depicts additional exemplary individual events from independent experiments, each demonstrating the onset of Gag.SNAPf(opt) expression after stable contact with a target cell. The examples are ordered by the duration between contact formation and the appearance of the SNAP23-labeled Gag.SNAPf(opt).

In summary, this approach effectively resolved the challenges faced with previous methods using GFP-tagged HIV-1 derivatives, as it allowed for the continuous observation and clear distinction between transferred and newly synthesized Gag.SNAPf(opt) in target cells.

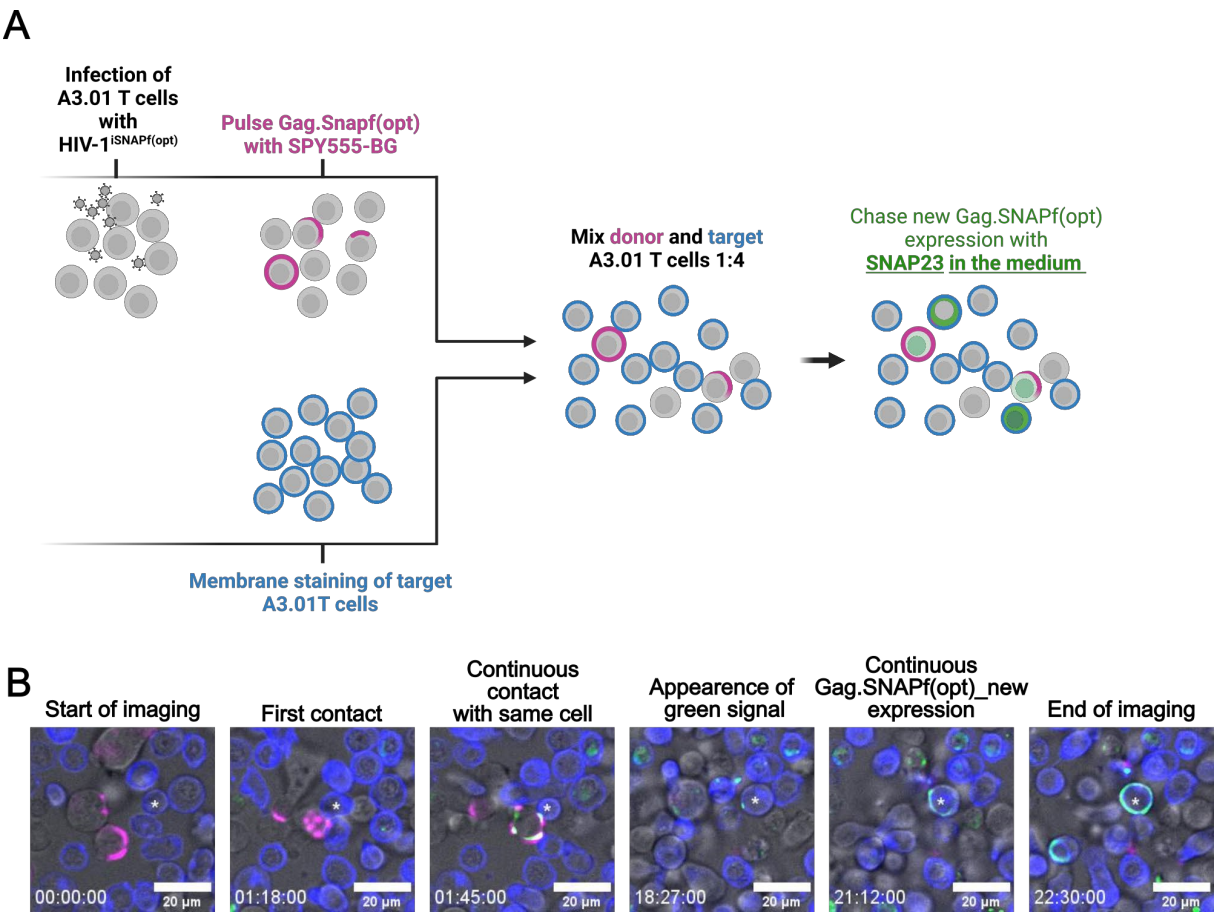

Figure 21 A protocol for live detection of productive cell-to-cell transmission.
(A) A schematic representation of the established protocol. A3.01 T cells were infected with HIV-1$^{iSNAPf(opt)}$, and 18 hours post-infection, Gag.SNAPf(opt) was labeled using SPY555-BG. The membrane of a second A.301 population was stained using CellVue® Claret lipid dye, and both populations were mixed in a 1:4 ratio. Live cell spinning disc microscopy with 0.33 frames/s was performed while having SNAP23 present in the medium. (B) Image sequence of a productive VS transmission event. Gag.SNAPf(opt) (magenta) polarized towards a blue target cell (white Asterix) and maintained continuous contact. Approximately 17 hours later, the cells were no longer in contact, and a green signal resembling newly expressed Gag.SNAPf(opt) began to appear and increase over time.

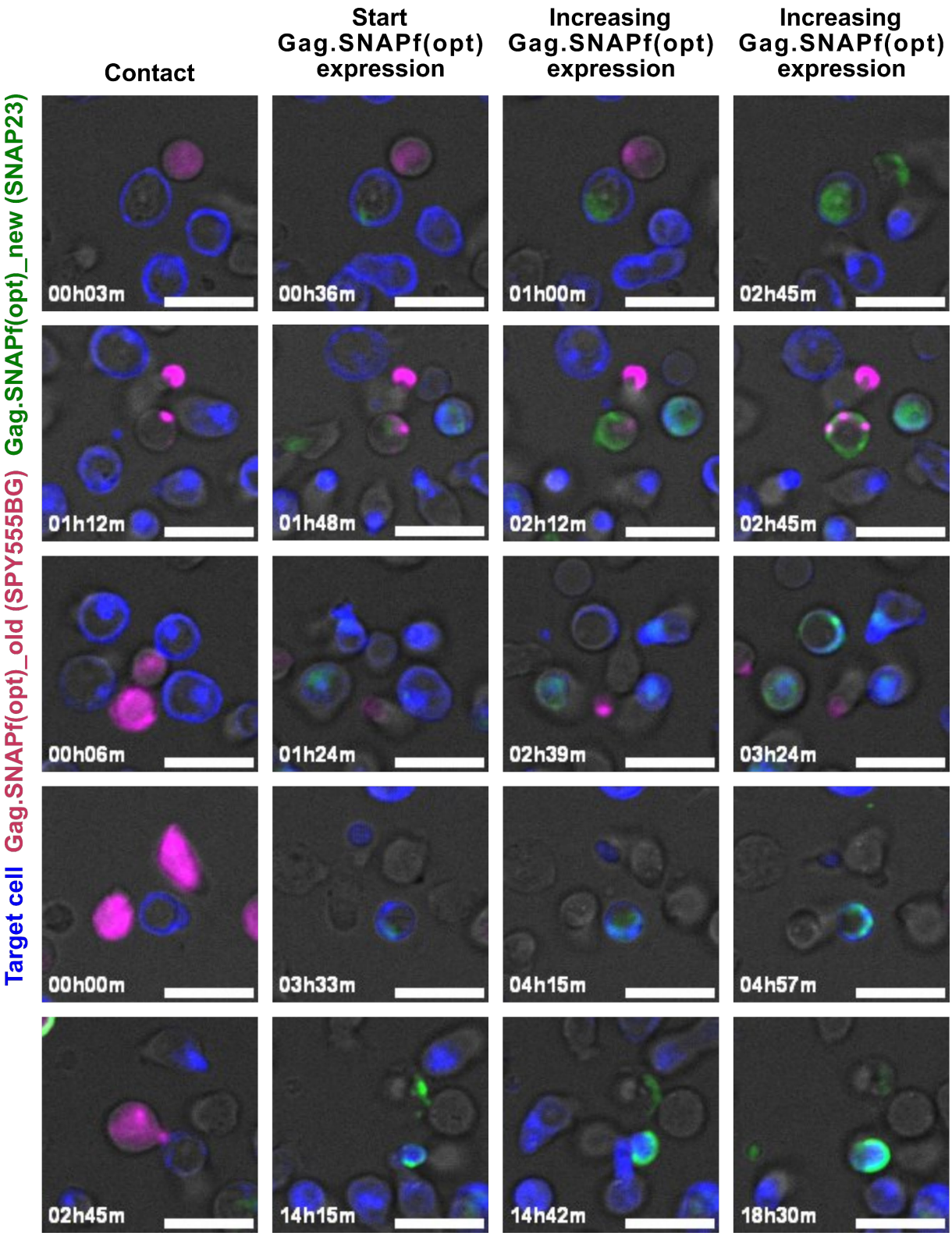

Figure 22 Examples for live detection of new Gag.SNAPf(opt) expression in target cells after contact with productively infected donor cells.

A3.01 T cells were infected with HIV-1$^{iSNAPf(opt)}$, and 18 hours post-infection, Gag.SNAPf(opt) was labeled using SPY555-BG. The membrane of a second A.301 population was stained using CellVue® Claret lipid dye, and both populations were mixed in a 1:4 ratio. Live cell spinning disc microscopy with 0.33 frames/s was performed while having SNAP23 present in the medium. Scale bar represents 20 µm.

3.4.1 Semi-automated analysis workflow for quantification of productive contact events

Although it was feasible to manually quantify contact events and productive infection for the initial cell-to-cell transmission imaging data (see section 3.3), an automated system was essential for unbiased analysis of statistically significant numbers of events within the established system described in section 3.5. The dynamic nature of moving cells and tracking productive infection through increasing SNAP23 intensity rendered manual analysis extremely time-consuming and susceptible to bias, thereby affecting the validity of the results. Initially I implemented cell segmentation using Ilastik (174). However, tracking and the detection of potential contacts between donor and target cells remained challenging. The dynamic migration of cells and the gradual redistribution of plasma membrane label to intracellular structures such as the ER and mitochondria presented challenges for reliable detection and tracking of donor and target cells by the algorithm. Better results were achieved using Vision4D software by Arivis, which provided effective tracking. Nevertheless, detection of contacts was not reliably accomplished. Arivis provides custom analysis scripts, including one called "kiss and run," which is designed to detect cell attachment and detachment. In close collaboration with the company, a semi-automated workflow for quantifying VS formation and productive infection, tailored to the established experimental conditions, was developed.

The workflow was initiated with the registration and segmentation of cells using the DIC channel, followed by the identification of donor and target cells based on staining. Donor cells were segmented using the DIC channel and filtered by signal of the SPY555-BG dye, representing Gag.SNAPf(opt) from the initial spin inoculation. Target cells were segmented based on lipid membrane staining in the far-red channel. The segmentation was conducted using the Python-based Cellpose algorithm (Cellpose_2_0_segmenter_v6, model "cyto"), with filtering based on cell diameter (≥15 µm), signal intensity (750 for all cells in brightfield, 650 for membrane-labeled target cells), and area (≥ 50 μm^2). Segmented donor and target cells were both tracked over time, and contacts were identified as overlapping bounding boxes of segments with a minimal overlap volume. All contacts that occurred during the imaging process were recorded, and the median green intensity in target cells was monitored over time. The appearance of SNAP23 fluorescence in target cells following a contact with donor cells was considered establishment of a productive infection. The system permitted comprehensive examination of contact events and their correlation with productive infection. A schematic representation of the aforementioned workflow is provided in Figure 23 A and B. To enhance the specificity of productive infection analysis, supplementary filters were introduced. To prevent the occurrence of false positives resulting from the simultaneous transfer of new and old Gag.SNAPf(opt) or cell fusion, cells that

became immediately triple-positive (i.e., positive for old Gag.SNAPf(opt), new Gag.SNAPf(opt), and a membrane label) after donor-target cell interaction were excluded. A crucial feature for the exclusion of false positive events was the alteration in SNAP23 fluorescence over time. Productively infected cells were classified based on gradual and sustained increase in SNAP23 fluorescence indicative of new Gag.SNAPf(opt) expression. To enhance robustness of the analysis, cells classified as productively infected target cells were required to sustain a signal above the threshold for a minimum of two hours. Figure 23 C illustrates the median SNAP23 fluorescence intensity trace for a legitimate event (black line) in comparison to traces of various false-positive events.

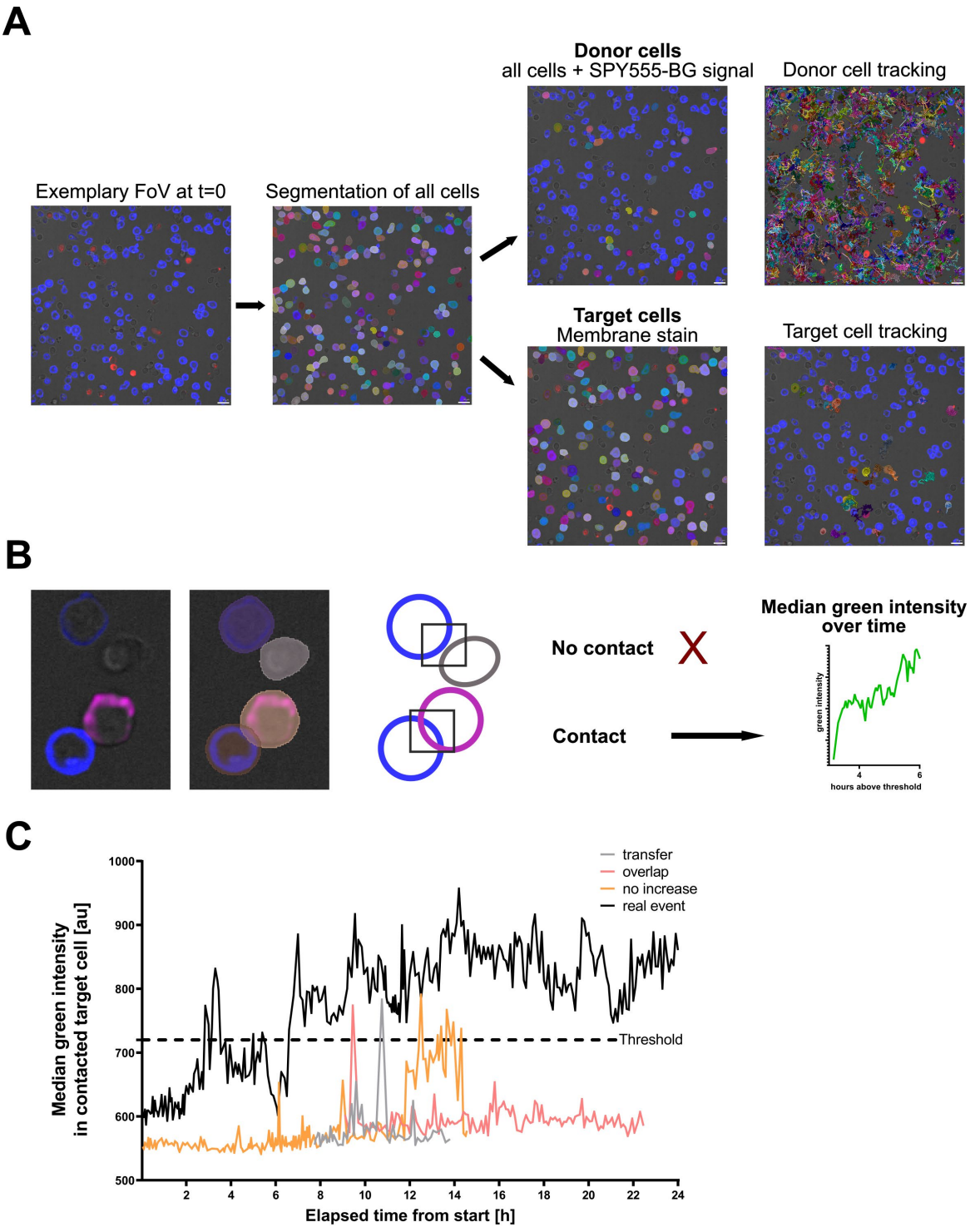

Figure 23 Semi-automated analysis pipeline for automated detection of productive cell-to-cell transmission.

(A) Using the integrated analysis pipeline in Vision4D by Arivis, cells are identified and segmented based on the DIC channel. Subsequently, the donor and target cells are delineated based on their respective staining. Donor cells are distinguished by a DIC cell segment exhibiting a red signal, while the target cell population is identified based on its lipid membrane stain. Subsequently, cells are tracked, and contacts are determined as an overlap of the bounding boxes of two segments and a minimal volume of the overlap. (B) An example of what would be considered a real contact or not. (C) The median green intensity in contacted target cells was plotted over time. While a real productive event displayed an increasing signal and remained above the threshold (black line), false positive events surpassed the threshold only for a brief time in a spike pattern.

3.4.2 A single contact is sufficient for onset of new Gag.SNAPf(opt) expression, independent of contact duration

I conducted multiple independent experiments in accordance with the established protocol detailed in the previous section, utilizing independently generated viral stocks and different lots of SNAP dyes, with the exception of non-commercially synthesized SNAP23. The imaging sequences were subjected to analysis via the previously established semi-automated analysis pipeline and subsequently verified manually to ensure that only those events representing true new Gag.SNAPf(opt) expression were considered.

The extracted data demonstrated a correlation between contact time and the outcome of new Gag.SNAPf(opt) expression but indicated no strict requirement for a minimal total contact time or a minimal duration of individual contacts for subsequent Gag.SNAPf(opt) expression. However, not all target cells that had been involved in contacts for a prolonged total time were found to express new Gag.SNAPf(opt) (Figure 24 A). I also analyzed the average duration of individual contact events for a given target cell (Figure 24 B). The minimal average duration determined was approximately three minutes, which is close to the time resolution of the setup, with a frame rate of 0.33 per second. The frequency of such short events may be caused by the seeding density of $1x10^5/cm^2$, chosen to promote sufficient contacts between donor and target cells, which also facilitated random short-term encounters. While the population of cells that was found to produce new Gag.SNAPf(opt) included cells that underwent mainly short-term events, the proportion of cells that underwent longer lasting individual contacts was substantially higher than for the cells that did not proceed to productive Gag.SNAPf expression. The likelihood of new Gag.SNAPf(opt) expression also increased when target cells formed multiple consecutive contacts donor cells, as indicated by the substantial proportion of Gag.SNAPf negative cells that underwent only a single contact (Figure 24 C). Target cells expressing new Gag.SNAPf(opt), however, showed a broader range of total contacts with individual donor cells.

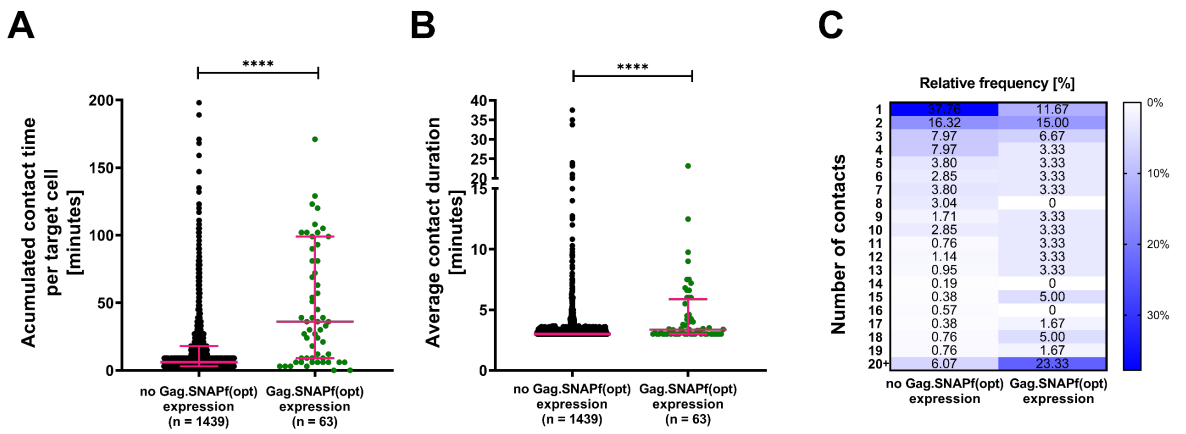

Figure 24 One contact can be sufficient for productive infection, independent of contact duration. *A3.01 T cells were infected with HIV-1$^{iSNAPf(opt)}$, which was prepared from transfected HEK293T cells. At 18 hours post-infection, Gag.SNAPf(opt) was labeled using 600 nM SPY555-BG, washed, and mixed with membrane-labeled uninfected A3.01 cells (target cells) at a ratio of 1:4 in imaging medium containing SNAP23. Live cell SDCM was conducted at a rate of 0.33 frames per second to observe cell-cell contacts and new Gag.SNAPf(opt) expression in target cells. The data were analyzed using Vision4D, a software program developed by Arivis. This analysis included the segmentation of the donor and target cell populations, as well as the tracking and detailed examination of contact patterns. (A) The total duration of contact between a given target cell and a donor cell during the observation period was classified according to the outcome observed in the target cell. The data points represent the individual target cells. The median value and standard deviation are indicated for each data set. Statistics were calculated with an unpaired non-parametric t-test (Mann-Whitney test). (B) The average duration of a contact between a donor and a target cell in the context of subsequent Gag.SNAPf(opt) expression is presented. Each data point represents an individual target cell. The median value and standard deviation are indicated. Statistics were calculated with an unpaired non-parametric t-test (Mann-Whitney test). (C) The relative frequency (also illustrated by color scale) of the number of contact events with a donor cell that a given target cell underwent during the observation period is shown. Contact numbers exceeding 20 are accumulated into one column.*

3.4.3 Observed transmission phenomena beside cell-to-cell transmission

The primary objective of this study was to visualize productive infection following VS HIV-1 transmission. It should be noted, however, that other modes of cell-to-cell transmission could also be identified and visualized. One illustrative example is the phenomenon of cell fusion. It is well established that cells expressing the HIV-1 Env glycoprotein can fuse with cells carrying receptor and co-receptor, forming multinucleated syncytia in tissue culture (118, 119). However, the *in vivo* relevance of syncytia formation remains controversial. The implementation of the filter mentioned in section 3.4.1 to exclude fusion events revealed that about 5% of the observed events initially classified as productive transmission event resulted in syncytia formation, which is consistent with the results of other research groups. (118). A representative time lapse series showing the formation of a syncytium is presented in Figure 25. The donor cell (red D) formed a contact with a target cell (yellow T) and at 04:12 hours, cells began to fuse. The fusion process

was completed approximately 20 minutes later, resulting in the formation of a syncytium. The syncytium remained mobile and started to interact with a new target cell approximately six hours after fusion was completed, indicating that the syncytium did not represent a dead-end event in this case.

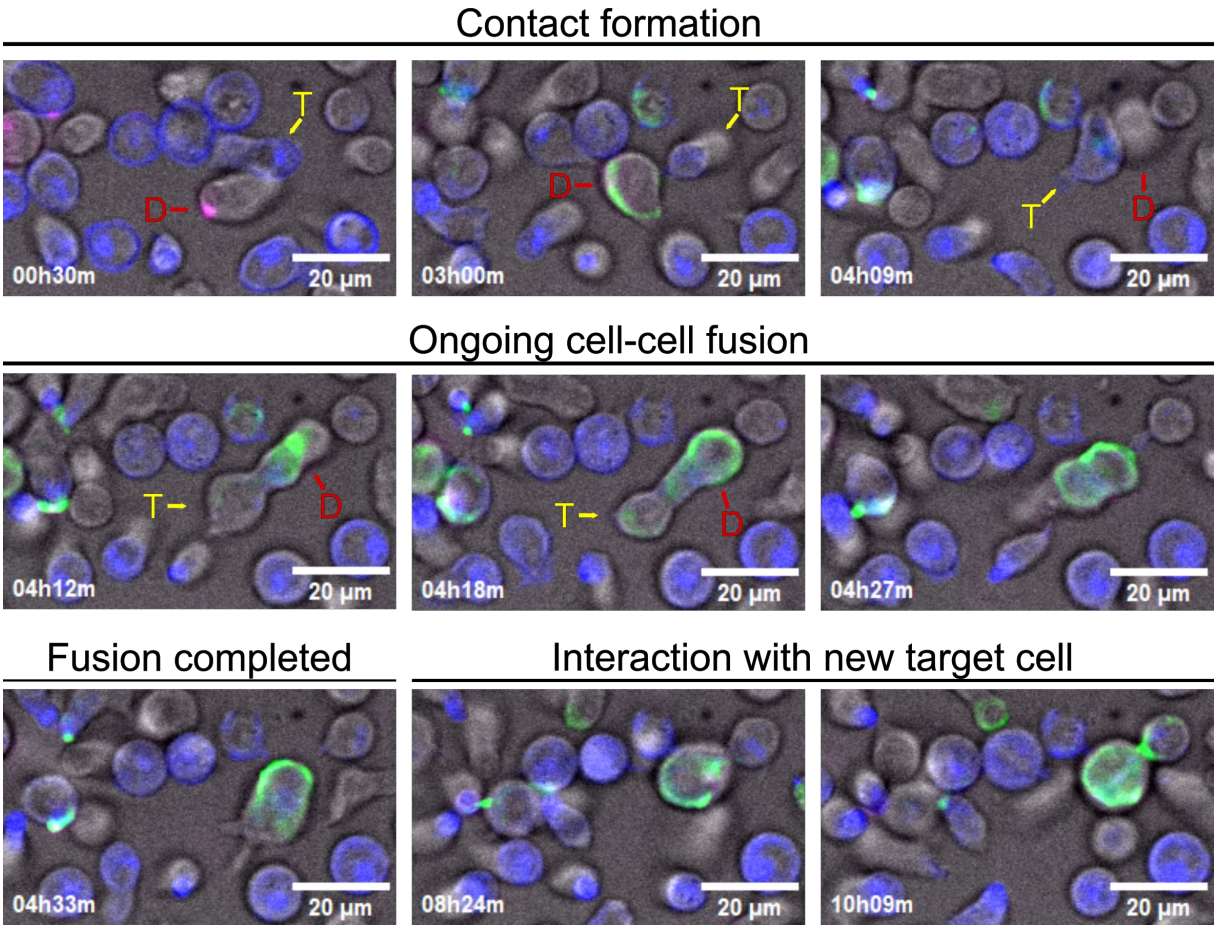

Figure 25 Syncytium formation of HIV-1$^{iSNAPf(opt)}$ infected donor cells and target cells.
A3.01 T cells were infected with HIV-1$^{iSNAPf(opt)}$, which was prepared from transfected HEK293T cells. At 18 hours post-infection, Gag.SNAPf(opt) was labeled using 600 nM SPY555-BG, washed, and mixed with membrane-labeled uninfected A3.01 cells (target cells) at a ratio of 1:4 in imaging medium containing SNAP23. Live cell SDCM was conducted at a rate of 0.33 frames per second to observe cell-cell contacts and new Gag.SNAPf(opt) expression in target cells. The infected donor cell is highlighted by a red arrow and "D", the target cell by a yellow arrow and "T".

3.4.4 The average time for productive target cell infection is faster than reported time for reverse transcription and integration

The primary advantage of my system in comparison to previously published approaches on the visualization of cell-to-cell transmission is the ability to distinguish between transferred and newly expressed Gag.SNAPf(opt). Consequently, one of the most intriguing aspects to investigate was not only the correlation between contacts and productive infection, but also the time frame within which targeted cells began to express newly synthesized viral components. Based on statistical analysis with inhibitors, the time required for reverse transcription and integration *in vivo* was estimated to be 11.4 hours in CD4+ T cells, with 4.6 hours for reverse transcription and 6.8 hours for integration (175). In tissue culture, the estimated duration for a full intracellular cycle of HIV-1 infection in CD4+ T cells is approximately 24 hours, as reported in the same study. P24 expression can be detected between nine and twelve hours post-infection (176), thus Gag.SNAPf(opt) expression in the present system was anticipated to occur within that time range. However, while this phenomenon was observed in a subset of target cells, the majority of cells exhibited expression of new Gag.SNAPf(opt) within a period of less than two hours following initial contact with donor cells (Figure 26 A; see also Figure 22). The total proportion of target cells expressing Gag.SNAPf(opt) after interacting with productively infected donor cells was 4.32 %.

Based on the published results mentioned above, it appears unlikely that Gag.SNAPf(opt) detected so early upon cell contact represents the result of productive HIV-1 infection. I therefore addressed potential alternative explanations for my observation. A recent publication reported direct translation of HIV-1 Gag from the genomic RNA of incoming viral particles (177). If reverse transcription-independent Gag.SNAPf(opt) expression had caused the observed early expression events in my system, such events should also be detectable in the presence of an RT-inhibitor. I therefore performed experiments in the presence and absence of the NNRTI EFV. To validate the inhibitory effect of EFV in my system, early viral reverse transcription products (based on LTR5U) were identified by digital droplet PCR (ddPCR) at 0, 6, and 24 hours post spin inoculation under identical conditions as those employed for the microscopy setup. The ddPCR was conducted by Dr. Samara Martín Alonso. The copy number detected at the start of the experiment represents viral cDNA contributed from the productively infected donor cells. In the absence of EFV, the number of copies per cell increased, whereas no increase was observed in the presence of the drug (Figure 26 A). These findings confirmed that EFV is an effective inhibitor of reverse transcription and replication under my experimental conditions.

To further ascertain the role of reverse transcription in the observed Gag.SNAPf(opt) expression, imaging experiments were then conducted in the absence or presence of EFV, added at time of donor and target cell mixing. As a control, experiments were also performed in the presence of the fusion inhibitor T-20, which inhibits uptake of viral RNA into the cells (Figure 26 C). In the presence of T-20, I detected two cells (0.4% of all registered target cells that formed a contact with a productively infected donor cell in this experiment) displaying increased SNAP23 fluorescence intensity following contact with a donor cell. However, both of these cells died shortly after fluorescence was detected, suggesting that it may represent autofluorescence caused by apoptosis. In contrast, early expression events could still be detected in 1.8% of all registered target cells contacted by donor T cells in the absence of reverse transcription when reverse transcriptase was inhibited. Without inhibitor the proportion for detected new Gag.SNAPf(opt) expression in contacted target cells was substantially lower, however this could be attributed to the lower sample size for the in parallel experiment, as the previous experiments displayed in Figure 26 A, showed a five times higher proportion of Gag.SNAPf(opt) expressing target cells.

In conclusion, I developed a protocol for the real-time detection of productive cell-to-cell transmission. This was accomplished by employing pulse-chase labeling of a replication-competent SNAPf-tagged HIV-1 derivative, which allowed me to distinguish between different infection stages and linking contact events to productive infection. Furthermore, I established a semi-automated workflow for analyzing and quantifying the data obtained. I found that target cells displaying new Gag.SNAPf(opt) expression after interacting with donor cells typically formed longer contacts than those without a transmission event. Notably, even brief contact events could result in new Gag.SNAPf(opt) expression, with a single contact being sufficient for productive infection. When assessing the timing of new Gag.SNAPf(opt) expression, I noted a substantial cluster of cells that showed early onset of expression. Experiments performed in the presence of the NNRTI EFV suggested that these events were independent of reverse transcription.

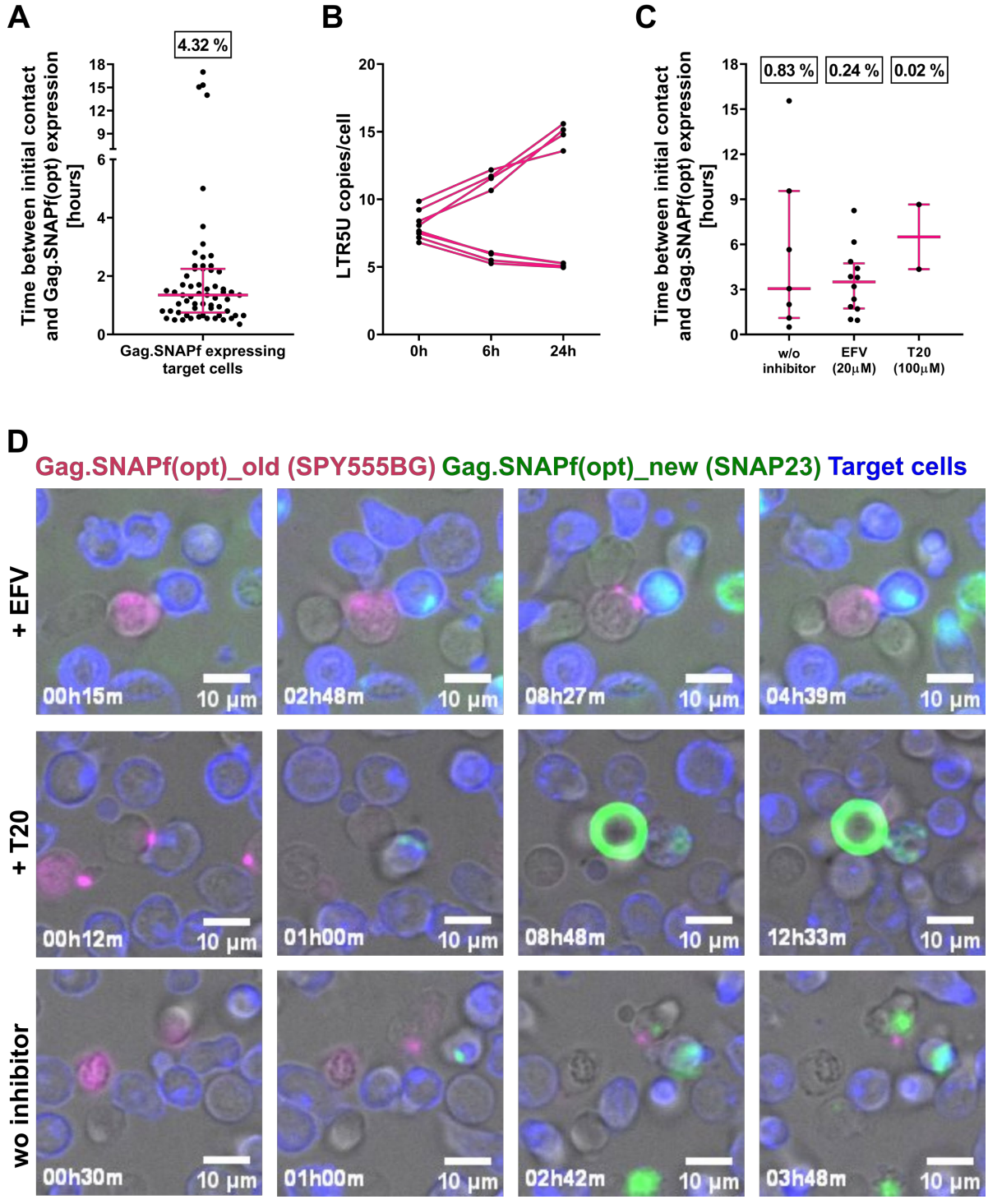

Figure 26 Onset of Gag.SNAPf expression after VS formation.

A3.01 T cells were infected with HIV-1$^{iSNAPf(opt)}$, which was prepared from transfected HEK293T cells. At 18 hours post-infection, Gag.SNAPf(opt) was labeled using 600 nM SPY555-BG, washed, and mixed with membrane-labeled uninfected A3.01 cells (target cells) at a ratio of 1:4 in imaging medium containing SNAP23. Live cell SDCM was conducted at a rate of 0.33 frames per second to observe cell-cell contacts and new Gag.SNAPf(opt) expression in target cells. The data were analyzed using Vision4D, a software program developed by Arivis. This analysis included the segmentation of the donor and target cell populations, as well as the tracking and detailed examination of contact patterns. (A) The interval between the initial detection of contact between a donor-target cell pair and the initiation of Gag.SNAPf expression within the target cell. Percentage indicates the number of cells that formed contact with a target cell and

subsequently expressed new Gag.SNAPf(opt). (B) The inhibitory effect of EFV in the imaging setup was verified by ddPCR. The presence of early viral RT products (based on LTR5U) was detected by ddPCR at 0, 6, and 24 hours post spin inoculation, in the presence or absence of EFV at a concentration of 20 µM. (C) Imaging of cell-to-cell transmission was conducted in the presence of the NNRTI EFV (20 µM) or the fusion inhibitor T-20 (100 µM) at time of mixing donor and target cell populations. The percentages indicated above represent the proportion of all registered target cells expressing Gag.SNAPf(opt) following a contact event. Percentage indicates the number of cells that formed contact with a target cell and subsequently expressed new Gag.SNAPf(opt). (D) The figure below shows an exemplary image sequence of a target cell expressing Gag.SNAPf after contact with an infected donor cell in the presence of EFV. The images were derived from the same experiment displayed in Panel C.

3.4.5 Conclusion

In conclusion, the characterization of reporter-carrying HIV-1 derivatives revealed a clear advantage of the SNAPf-tag over sfGFP when inserted into Gag, particularly regarding replication competence and stability. Reducing the CpG content of the tags did not result in a notable enhancement of replication kinetics. A novel approach for real-time detection of productive cell-to-cell transmission was developed using pulse-chase labeling with a fully replication-competent HIV-1 derivative, the previously characterized HIV-1$^{iSNAPf(opt)}$. This approach enabled the distinction between different infection rounds and linked contact events to productive infection. Furthermore, a semi-automated system for the quantitative analysis of the extensive datasets resulting in the pulse-labeling approach has been established. The extracted data indicated that a single contact can be sufficient for productive expression of new Gag.SNAPf(opt), irrespective of contact duration. The most striking result was the observation of early onset of Gag.SNAPf(opt) expression with increasing intensity in the contacted target cells. As this result is not compatible with the established time range required for the HIV-1 replication cycle, further investigation and more data sets are required to elucidate the underlying mechanism responsible for this phenomenon.

4. Discussion

In this dissertation, a novel method for visualizing HIV-1 cell-to-cell transmission was developed, employing pulse-chase labeling to differentiate between viral transfer and productive infection. Additionally, I developed and characterized HIV-1$^{iSNAPf(opt)}$, a fully replication-competent HIV-1 derivative with a SNAPf(opt)-tag inserted between the MA and CA domain. This represents a major advancement, as earlier approaches for visualization of cell-to-cell transmission depended on HIV^{iGFP}, a derivative with severely impaired replication kinetics and robust infectivity limited to a single round of infection (140). I could show that the replication kinetics of HIV-1$^{iSNAPf(opt)}$ closely resembled those of the wt virus and the insertion of the SNAPf(opt)-tag remained remarkably stable over weeks of passaging in A3.01 T cells.

The impact of codon optimization within sfGFP and SNAPf inserted into Gag was investigated, prompted by findings that higher CpG dinucleotide frequencies lead to RNA degradation via the ZAP pathway in HIV-1 (149). Results indicated that codon-optimized derivatives did not show notable improvements in replication kinetics or infectivity in A3.01 T cells or in reporter cell lines. HIV-1$^{iSNAPf(opt)}$ exhibited a near-wildtype level of infectivity and remarkable stable integration of SNAPf(opt) into Gag, as evidenced by the detection of tag expression via flow cytometry and western blot following prolonged passaging in A3.01 T cells. Additionally, I developed a real-time method for detecting productive cell-to-cell transmission of HIV-1. This approach involved labeling Gag.SNAPf in donor cells using a cell-permeable BG-conjugated SNAP dye, followed by continuous monitoring of Gag.SNAPf expression in target cells upon contact with the novel highly fluorogenic SNAP dye “SNAP23”. A semi-automated analysis pipeline, created in collaboration with the company Arivis, was applied to quantitatively analyze the factors involved in VS dynamics. This pipeline also enabled the establishment of a correlation between cell-to-cell transmission and Gag.SNAPf(opt) expression in target cells that had come into contact with virus producing cells.

The results of the quantitative analyses indicated that a single contact was sufficient to induce new Gag expression in the target cell, irrespective of the duration of the contact. Furthermore, Gag.SNAPf expression in target cells was observed as early as 30 minutes after VS formation, indicating the potential for direct translation of incoming genomic RNA.

In conclusion, pulse-chase labeling of HIV-1 infection and cell-to-cell transmission provides a versatile tool for studying the various stages of the HIV-1 replication cycle. In the context of VS, this is the first time that distinct contact events have been directly linked to new Gag.SNAPf(opt) expression in target cells. However, it remains unclear which percentage of observed

Gag.SNAPf(opt) expression actually resulted in productive infection and which part led to the direct translation of incoming viral Gag.SNAPf(opt), which was subsequently identified as productive infection.

4.1 Effect of CpG optimization of reporter proteins in HIV-1 Gag

The host antiviral factor ZAP binds selectively to CpG dinucleotides in RNA sequences, thereby reducing the accumulation of mRNA in the cytoplasm and inhibiting the replication of RNA viruses (146, 147). ZAP binds to the viral RNA at specific response elements (ZRE) and facilitates the recruitment of cellular decay factors, such as deadenylase PARN, de-capping enzyme Dcp1, and the 3'–5' exosome complex (178). Takata *et al*. demonstrated that HIV-1 exhibits CG suppression in its genome to evade RNA degradation by ZAP. Furthermore, artificial enrichment of CG dinucleotide content was found to inhibit particle production (149). Subsequently, Ficarelli and colleagues demonstrated that the insertion of CpG-rich sequences into the HIV-1 genome is associated with the capacity of ZAP to target and degrade viral RNA. Notably, it was not the overall abundance of CpGs, but rather the specific region within the genome where they were introduced that was identified as the primary determinant of ZAP sensitivity and antiviral activity (150). The initial hypothesis of this thesis, derived from the findings mentioned above, was that introducing CpG-rich sequences into the HIV-1 genome, through fluorescent proteins like sfGFP or self-labeling tags like SNAP, could produce similar effects. A similar hypothesis was proposed by Roy *et al*. during the course of my work (179). Utilizing HIV-1 derivatives where nLuc or iRFP were integrated into the HIV-1 genome upstream of Nef, they exhibited enhanced viral replication *in vitro* and reporter expression *in* and *ex vivo* through the removal of CpG dinucleotides (179). The results of my experiments indicated that codon optimization with a reduced number of CpGs did not result in a significant effect on either single-round or multiple-round infectivity when compared to the respective parental derivatives (Figure 8). Furthermore, no notable disparity in particle yield was observed in infected A3.01 T cells over a 16-day period for HIV-1 derivatives with sfGFP or SNAPf inserted between MA and CA in Gag (Figure 9). In light of the region-dependent specificity identified by Ficarelli *et al*., it is plausible that the absence of a significant effect in my experiments is attributed to the lower detrimental impact of CpG abundance within Gag compared to other regions of the HIV-1 genome. This hypothesis aligns with a recent publication that suggests the 700 bases at the 5' end of the env ORF predominantly determine ZAP sensitivity (180). Several different cofactors have been identified to be involved in ZAP-mediated RNA virus restriction (181). One example is RIG-I, for which ZAP has been demonstrated to be the dominant regulator in human cells, including HEK293T cells and HeLa cells (182). Given that ZAP has been

demonstrated to influence antiviral responses in HeLa cells, it was anticipated that a notable effect would be observed in the HeLa-derived cell line TZM-bl. However, this does not appear to be the case for HIV-1$^{iSNAPf(opt)}$ and HIV-1$^{isfGFP(opt)}$. Studies investigating the replication kinetics of CpG dinucleotide-reduced CXCR4-tropic HIV-1 HXB2 strain derivatives in MT-4 T cells or peripheral blood mononuclear cells (PBMCs) yielded similar results to those observed in this study, despite targeting a region within env that had previously been identified as highly relevant (183). Only when virus competition assays were employed, the codon-optimized variants demonstrated a notable advantage over the wt virus in MT-4 cells.

In conclusion, the introduction of CpG-rich sequences in the form of reporters within Gag demonstrated no adverse impact on HIV-1 derivative replication or stability. This is consistent with reports published during the course of this study indicating that a specific region of *env* is crucial for the efficiency of ZAP recognition and mRNA degradation.

4.2 Advantages of SNAP-tag over FPs in the context of Gag-labeled HIV-1 derivatives

The field of virology relies on the use of microscopy for the visualization of various stages within the replication cycle. The introduction of EM revealed morphological details in the context of infection. However, dynamics and localization of viral proteins within the various steps inside and outside cells were only observable with the emergence of fluorescence microscopy (184). The most commonly employed labeling method involved the fusion of a fluorescent protein to the protein of interest. In 1995, Baulcombe initially proposed the concept of incorporating GFP into the expression cassette of a potato virus-based vector as a reporter for viral infections (185). Since then, a multitude of advancements to label proteins of interest have been created, including a significantly expanded range of distinct fluorescent proteins with varying emission and excitation spectra. In addition to the aforementioned advancements in technology involving fluorescent proteins, alternative strategies for protein labeling have also been employed. One such strategy is based on self-labeling proteins, like the SNAP-tag. It is noteworthy that, while self-labeling tags are commonly employed for the tracking and localization of cellular proteins and their turnover, only a limited number of applications within virological research have been published. To the best of my knowledge, there have only been three instances where viruses have been directly labeled with SNAP-tag: Hepatitis C virus in 2014 (186), Chikungunya Virus in 2017 (187) and HIV-1 in 2011 (139).

4.2.1 Overall advantages of SNAP-tag for HIV-1 labeling compared to standard approaches

An improvement on the replication kinetics of SNAP-tagged HIV-1 derivatives was previously reported by Eckhardt *et al*. in 2011, in which the authors described HIV-1^{SNAP} (139). In contrast to the HIV-1^{isnapf} construct, which has been thoroughly characterized in this study, the SNAP-tag was fused to the C-terminus of MA, without the PR cleavage site that was introduced by Hübner *et al*. in 2007 (140). However, introduction of the additional cleavage site to generate HIV-1^{iSNAP} also did not lead in notable differences regarding infectivity (141). HIV-1$^{iSNAPf(opt)}$ represents a modified version of the previously reported derivative, featuring an improved SNAP variant (SNAPf), an added cleavage site for viral protease between MA and SNAPf, and codon optimization, as discussed in the previous section.

In the context of HIV-1, derivatives expressing the SNAPf-tag demonstrated overall higher infectivity, faster replication kinetics, and improved stability compared to those expressing sfGFP in the TZM-bl reporter cell line and C8166 T cells. While the wide distribution of data points for HIV-1^{iSNAPf} measurements in these experiments must be considered when interpreting the results, a difference between HIV-1^{iSNAP} and HIV-1^{iSNAPf} was observed (Figure 8). This was unexpected, given that only ten mutations separate SNAP and SNAPf. The mutations were introduced by directed evolution based on random mutagenesis with the objective of optimizing the affinity of an AGT mutant towards BG substrates (136). One of the mutations was the exchange of glutamic acid with arginine, so a negative charge was replaced with a positively charged amino acid. This resulted in lower affinity to negatively charged BG substrates (143). One potential explanation for these observed differences is that the aforementioned adaptations may have resulted in a more favorable folding kinetic of SNAPf within Gag.

In prolonged cultivation experiments in infected A3.01 T cells, the HIV-1$^{iSNAPf(opt)}$ derivative exhibited markedly elevated replication capacity relative to HIV-1$^{isfGFP(opt)}$. This was evidenced by comparable levels of particle production to those observed with the wt HIV-1$_{NL4-3}$, albeit with a slightly delayed and reduced peak activity. No virus released of sfGFP-expressing variants was detected until day 12 of the experiment. This was accompanied by a partial loss of the sfGFP-tag, while SNAPf remained stable until the end of the experiment.

Although the SNAP-tag is of approximately 25% lower mass than sfGFP, the actual protein size does not differ substantially, with a hydrodynamic radius (rH) of 2.6-2.8 nm for sfGFP (188) and 1.95 nm for SNAP-tag (134). The crystal structures of both tags reveal a key difference in the placement and distance between their C- and N-termini (marked in magenta) (Figure 27). The termini of sfGFP are in relatively close proximity, whereas those of the SNAP-tag are significantly more distant. When these tags are inserted into the Gag polyprotein, sfGFP would be expected to

extend outward, whereas the SNAP-tag may integrate more smoothly in the extended linker sequence between the MA and CA domain (Figure 27). A better fit within the molecular structure may result in reduced disruptions to the Gag assembly process. In conjunction with the observation of larger Gag lattice accumulations at the plasma membrane of HIV^{iGFP} expressing cells (104, 151), it can be speculated that disturbance of lateral Gag-Gag interactions by a protruding GFP domain may impair or delay the assembly process.

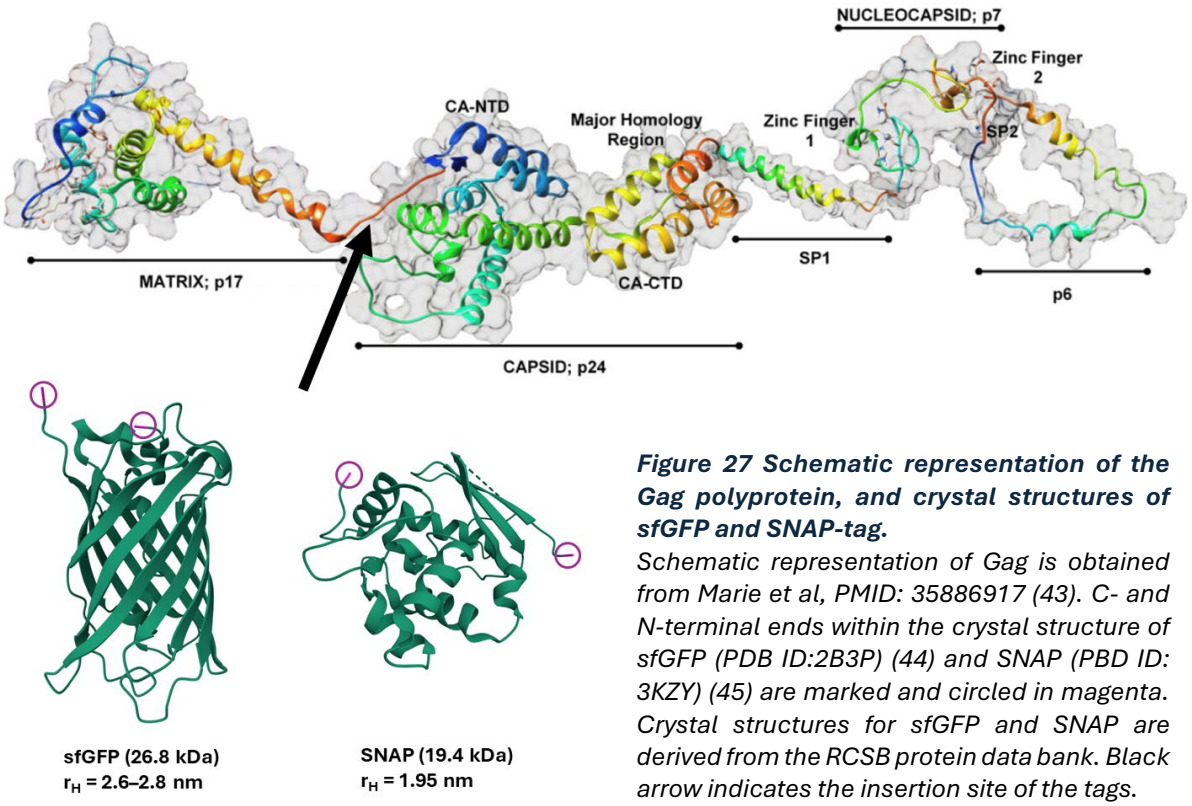

Figure 27 Schematic representation of the Gag polyprotein, and crystal structures of sfGFP and SNAP-tag.
Schematic representation of Gag is obtained from Marie et al, PMID: 35886917 (43). C- and N-terminal ends within the crystal structure of sfGFP (PDB ID:2B3P) (44) and SNAP (PBD ID: 3KZY) (45) are marked and circled in magenta. Crystal structures for sfGFP and SNAP are derived from the RCSB protein data bank. Black arrow indicates the insertion site of the tags.

CLEM images of HIV-1$^{iSNAPf(opt)}$ within the VS context conducted in the course of this work did not reveal any evidence of abnormal Gag.iSNAPf(opt) patches or irregular budding sites (Figure 18). However, also HIV-1$^{isfGFP(opt)}$ did not reveal any elevated Gag levels at the plasma membrane. The images obtained in this thesis used a basic CLEM approach involving cell dehydration, embedding in Epon, and the production of thin sections. Cryo-CLEM with freeze substitution offers better preservation of molecular structures, leading to a higher overall resolution. This technique could reveal more detailed morphological features of the immature Gag lattice of HIV-1$^{iSNAPf(opt)}$ compared to GFP-tagged derivatives. Additionally, the small sample size of only a few correlated cell pairs in this thesis needs to be considered.

Prolonged passaging of HIV-1$^{iSNAPf(opt)}$ in A3.01 T cells demonstrated stable integration of SNAP for a minimum of 19 passages (Figure 12). Western blot analysis did not reveal any truncated versions of Gag.SNAPf in the replicate that remained double positive after 30 passages. Attempts to

perform bulk sequencing of Gag from passaged HIV-1 particles were unsuccessful. Sequencing the complete HIV-1 genome of passaged HIV-1$^{iSNAPf(opt)}$ particles could provide insights into whether passaging led to compensatory mutations in Gag or other parts of the HIV-1 genome. In particular, the sequence of Env would be of interest, as Van Duyne *et al*. reported a compensatory mutation in *Env* selected under dolutegravir inhibition that enhanced HIV-1 cell-to-cell transmission (189). The same mutation was also independently discovered in our laboratory (personal communication by Dr. Vojtech Zila) in long-term cultivated HIV-1 infected SupT1 T cells in the absence of inhibitor selection. In the case that the same or other mutations were detected, the effect on cell-to-cell transmission could be investigated with the system developed in this thesis by pulse-chase labeling cell-to-cell transmission of HIV-1$^{iSNAPf(opt)}$ purified from passage 30.

4.2.2 Pulse-chase labeling viral infection with highly fluorogenic substrates

Pulse-chase approaches represent a powerful biochemical tool, offering particular utility in the study of synthesis, turnover, and dynamics in living cells. The initial step involves covalently labeling the protein or molecule of interest, a process known as the pulse. Subsequently, the expression of unlabeled molecules is monitored with a second label, facilitating observation of protein trafficking and turnover over time. The traditional approach to labeling has been based on the use of radioactive isotypes, a technique that originated in the 1950s (190). In the early stages of HIV-1 research, pulse-chase labeling approaches involving radioactive isotopes were used to explore the synthesis and processing of various viral components. For instance, in 1988, Willey and colleagues applied this approach to study processing of the Env precursor glycoprotein gp160 (191). The first application of pulse-chase labeling of proteins by using SNAP-tag technology was reported by Jansen *et al*. in 2007 (192). Labeling proteins at different time points with distinct fluorophores allows for clear differentiation between existing and newly synthesized proteins, providing an effective method for studying dynamic processes within cells. The SNAP-based pulse-chase labeling technique provides researchers with enhanced flexibility in monitoring protein dynamics over time, due to the broad selection of compatible fluorophores. The use of various BG-conjugated fluorophores enables longer imaging durations as feasible with FPs and the ability to observe different generations of two different proteins within a single sample simultaneously when combined with other self-labeling proteins like Halo-tag. (193). Bodor *et al*. were the first to propose comprehensive protocols for pulse-chase labeling of SNAP-tag fusion proteins, and additionally introduced quench-chase-pulse labeling (194). The pulse-chase labeling of HIV-1$^{iSNAPf(opt)}$ in this study followed a modified protocol where Gag.SNAPf was initially labeled at the onset of imaging, and newly synthesized Gag.SNAPf was subsequently tracked for 18-24 hours using a second SNAP substrate. Bodor *et al*. highlighted that avoiding continuous

imaging offers the advantage of allowing protein turnover to occur in tissue culture instead of during microscopy. However, the major accomplishment of this thesis was the continuous monitoring of new Gag.SNAPf(opt) expression, facilitated by the incorporation of the no-wash SNAP substrate SNAP23 into the experimental setup. The combination of pulse-chase and no-wash labeling approaches that I established is, to the best of my knowledge, a novel contribution to the toolbox of virology. This method could be applied to other virus families or different HIV-1 proteins, providing new perspectives through continuous live observation of protein turnover in cellular populations.

Overall, I demonstrated that both HIV-1$^{iSNAPf(opt)}$ and HIV-1^{iSNAPf} performed better than HIV-1^{isfGFP} in all experimental conditions. The SNAP-tagged variants had enhanced single-round and multiple-round infectivity, replication kinetics, and particle yields, closely matching those of wt HIV-1. The SNAP-tag remained stable over weeks of continuous co-culture. Achieving highly stable expression of the tag within a fully replication-competent HIV-1 context marks a major breakthrough for studying HIV-1 transmission and spread in tissue culture.

4.3 Dynamics of productive HIV-1 cell-to-cell transmission

The second key aim of this study was to develop a live microscopy system for visualizing cell-to-cell viral transmission using the fully replication-competent HIV-1 derivative, HIV-1$^{iSNAPf(opt)}$. Previous research has predominantly utilized HIV-1 derivatives labeled with GFP within the Gag region, inserted between the MA and CA domains, to examine the dynamics of cell-to-cell transmission through fluorescence microscopy. While this approach yielded valuable insights into the quantitative and morphological aspects of VS formation and productive infection, it also had notable limitations. When investigating productive infection in correlation to VS, the majority of studies employing this derivative have focused on the transfer of fluorescently labeled Gag and/or Env proteins, and subsequently correlated these observations with the overall cell population. However, the cell-to-cell transmission observed in individual cell pairs at specific time points could not be definitively linked to productive infection, as it was unclear whether the observed events were directly responsible for infection, due to the inability to distinguish between transferred and newly produced viral proteins in a fully infectious HIV-1 context.

The initial quantitative analysis of HIV-1 cell-to-cell transmission was conducted by Hübner *et al*. in 2009, utilizing HIV Gag-iGFP (≙ HIV-1^{iGFP}) (96). To distinguish transfer from productive infection, Jurkat donor cells were not only transfected with HIV Gag-iGFP but also with HIV NL-GI, in which GFP is expressed in place of Nef. This enabled the visualization of viral transfer as puncta and productive infection as diffuse GFP in target cells. An illustrative example was provided wherein a

donor Jurkat cell was in contact with a MT4 target cell for a period of 18 hours. Fourteen hours later, an increase in diffuse GFP was observed, which was concluded to represent productive infection. In total, 6.25 % of the tracked conjugates resulted in diffuse GFP expression (7 out of 112). Among all the synapses examined, five showed evidence of virus transfer. The time intervals for detecting new Gag.SNAPf expression in my experiments could be divided into two clusters: one occurring between 30 minutes and 4 hours, and the other taking over 12 hours. The findings of Hübner are primarily consistent with the second cluster. However, it needs to be considered that, the readout methodology differs. In the context of HIV-1 infection, Gag is expressed earlier and to higher levels than Nef, making a tagged Gag derivative a more sensitive readout compared to a Nef associated label. In addition, sfGFP displays faster maturation and increased brightness compared to eGFP used by Hübner et al. These differences should result in faster detection of productive infection events in our setup compared to the previous work. They are, however, not likely to explain the events in which Gag.SNAPf appeared very early after cell contact. It is also noteworthy that I did not detect contacts between a donor and target cell for more than three hours, which contrasts with the observations reported by Hübner *et al.* (Figure 26 A). It needs to be kept in mind, however, that the imaging period in my study was limited to 24 hours, which is considerably shorter than the duration employed in the aforementioned study. In a subsequent, more method-oriented report of the same group, Jurkat cells were transfected with HIV Gag-iGFP, mixed with primary CD4+ T cells, followed by three hours of co-culture (94). Viral transfer was subsequently confirmed by flow cytometry, through the assessment of GFP-positive CD4+ T cells. About 15–20% of primary CD4+ T cells tested positive under these conditions, though this experimental configuration could only detect Gag.iGFP transfer. If I had employed HIV-1$^{iSNAPf(opt)}$ with continuous exposure to only a single BG-conjugated SNAP dye, without prestaining the donor cell population, the same cluster of cells with detection times between 30 minutes and 4 hours would have been observed. However, because I could differentiate between transferred and newly synthesized Gag.SNAPf, I discovered that this signal represented new Gag.SNAPf expression, not viral transfer. This implies that similar occurrences might have been present in prior studies but were not recognized as such. Studies have shown that stable conjugates between HIV-1-infected donor T cells and target cells *in vitro* have an average lifespan of around 60 minutes. In comparison, interactions between uninfected T cells are usually brief, lasting less than ten minutes (91). These observations are consistent with the median contact time of roughly 50 minutes between donor and target cells in this study. However, individual contact times were notably shorter than this median. Two possible explanations could account for this discrepancy. One possibility is that cells may partially migrate out of the initial two-dimensional focal plane,

meaning stable contacts persist, but the tracking system fails to detect them as continuous. This would indicate that the cells remain in contact with one another, yet the tracking mechanism does not recognize this contact as long-lasting due to the absence of a trackable segment. To account for this, a gap of four frames was integrated into the tracking algorithm, allowing for the reappearance of a tracked segment within twelve minutes to still be considered continuous contact. When no contact was observed for tracked segments, or when cells were out of focus for more than twelve minutes, they were recorded as detached. Another possible explanation for this could be the formation of something analogous to a kinapse, a phenomenon known from studies of the immunological synapse between T and B cells. A kinapse refers to a dynamic, moving junction between T cells and antigen-presenting cells (APCs) (195). The *in vivo* relevance of immunological kinapses has been supported by research from Azar *et al.*, who emphasized the importance of T cell activation status and the type of APC (196). Recent findings suggest that Env accumulates dynamically at the VS, driven by a rapid recycling process (133). Given that Env binding to CD4 drives VS formation, this quick turnover might possibly contribute to the formation of a "virological kinapse".

To investigate Gag and Env distribution during cell-to-cell transmission and VS formation, Wang *et al*. used an HIV-1 derivative tagged in Env, HIV Env-iSFGF-ΔV1V2, co-transfected with HIV Gag-iCherry (197). The formation of VS was broken down into distinct stages. First, the cells initiate the cell-to-cell contact, followed by Env accumulation within 5-10 minutes. Gag then gets redistributed to the contact site, causing both Env and Gag to accumulate for up to an hour, which leads to the formation of the characteristic synaptic button. They observed two types of Env accumulation: one lasting no more than 10 minutes and another with an average duration of 30 minutes Since the minimal time resolution of their setup was 10 minutes, shorter periods of Env accumulation might have gone unnoticed. When using a frame rate of 0.33, matching the conditions of this thesis, they observed Gag and Env accumulation six minutes post-contact and detected a short-lived VS, consistent with my observations using HIV-1$^{iSNAPf(opt)}$. Additionally, they reported co-transfer of Gag and Env through the VS within two minutes, supporting my findings that a single contact can achieve particle transfer and productive infection due to the efficiency of the process, irrespective of contact duration.

It is important to note that the documented quantitative data on cell-to-cell transmission is also influenced by external factors beyond the selection of the reporter. Differences in experimental methods for detecting virus transfer and subsequent target cell infection, such as flow cytometry, microscopy, or other molecular techniques, can lead to varying conclusions. Additionally, factors

like the type of cells used (e.g., primary T cells versus different T cell lines), the timing of observations, the infection method and rate for donor cells, and other variables must be considered for accurate and direct comparisons.

My analysis further revealed that when a donor cell contacted multiple target cells, a common event due to the seeding density of $1x10^5/cm^2$, the outcomes of Gag.SNAPf(opt) expression varied between the target cells. Despite having the same contact time with a specific donor cell, some target cells expressed new Gag.SNAPf(opt), whereas others did not. This variation was also observed in cases where donor cells engaged multiple target cells simultaneously in polysynapses. This finding suggests that the target cell could play a more important role in the outcome of a transfer event than previously recognized. Earlier research has primarily focused on factors within the donor cell and viral components (107, 198–200). Notably, one study that focused more on the target cell site reported increased susceptibility for productive HIV-1 cell-to-cell transmission to naïve and memory CD4+ T cells with higher density of cortical actin (201).

4.3.1 Early Gag.SNAPf expression in context of cell-to-cell transmission

The most striking observation made during the live monitoring of productive HIV-1 cell-to-cell transmission was the early appearance of Gag.SNAPf(opt) in target cells that had interacted with productively infected donor T cells. This early detection is in contrast with the established durations for reverse transcription and integration of the viral genome. Statistical analyses demonstrated that reverse transcription and integration in CD4+ T cells are expected to take 4.6 and 6.8 hours, respectively, with the overall process typically completed within 11.4 hours (151). *In vitro*, the estimated duration for a full intracellular cycle of HIV-1 infection is approximately 24 hours, with Gag expression detectable between 9- and 12-hours post-infection (152). Thus, early Gag.SNAPf(opt) expression in this study was anticipated within this timeframe. Furthermore, the early Gag.SNAPf(opt) expression was detected even when the RT inhibitor EFV was present, which prevents viral cDNA production. This indicates that early Gag.SNAPf(opt) expression occurred independently of reverse transcription, supported by the observation that no early expression was seen when the fusion inhibitor T20 was introduced (Figure 24). A recent report published at the beginning of the year by Köppke *et a.l* reported direct translation of incoming HIV-1 genomes (177). Given that HIV-1 is a positive-sense RNA virus, direct translation of Gag by the host cell machinery is theoretically possible. To explore this, the authors created a minimal lentiviral vector incorporating a destabilizing domain (DD) linked to a reporter nano-luciferase (Nluc). By adding Shield1, a cell-permeable ligand, this vector can be stabilized in a reversible and dose-dependent manner. The researchers found that reporter activity increased over time even when reverse transcription was blocked by NVP, suggesting that reporter proteins were produced independently

of reverse transcription. The researchers ruled out plasmid carry-over and incomplete inhibition of reverse transcription as explanations. This direct translation was observed across various cell types, including A3.01 T cells which were used in my study, and was independent of the entry pathway. Nonetheless, the effect was weaker in primary cells like macrophages and CD4+ T cells. Another study using ribosome profiling reported translational activity in the Gag ORF as early as one hour after infection (202). However, since this report has only been available on bioRxiv since April 2022, its findings should be considered preliminary and taken with caution. A key difference between the research by Köppke and colleagues and my study is that Köppke's work focused solely on cell-free HIV-1 infection. In contrast, during cell-to-cell transmission, the directed budding of viruses towards the contact zone results in a high local MOI. This increases the likelihood of viral particles bypassing entry and post-entry bottlenecks (100, 101). The elevated MOI at the VS could facilitate the simultaneous transfer of multiple viral particles. Consequently, the increased efficiency of VS-transmission of HIV-1 could also enhance the effect of direct translation in the target cells as multiple copies of the genome are available for translation at the same time.

For future research, it would be valuable to develop a system that can clearly distinguish between productive infection and direct translation, as my pulse-labeling approach cannot differentiate between these two processes. Mazurov and colleagues recently introduced an ultra-sensitive assay for quantifying HIV-1 cell-to-cell transmission by measuring the expression of Nluc in target cells (203). The Nluc gene was inserted in an antisense orientation within the HIV-1 provirus. The presence of an intron in this configuration blocks Nluc expression in virus-producing cells, as it is efficiently spliced only when mRNA is synthesized from the sense strand. Thus, only the mRNA that undergoes reverse transcription during transmission to target cells will generate Nluc. Combining an anti-sense fluorescent reporter with the pulse-chase labeling system of HIV-1$^{iSNAPf(opt)}$ could enable precise identification of events occurring without reverse transcription.

4.4 Conclusion and future implications of the developed system

This dissertation presents a novel method for visualizing HIV-1 cell-to-cell transmission, employing pulse-chase labeling to distinguish viral transfer from productive infection. I developed and characterized HIV-1$^{iSNAPf(opt)}$, which was demonstrated to be fully replication competent. The replication dynamics of this derivative were comparable to those of wt HIV-1, and the SNAPf(opt)-tag was demonstrated to remain stably incorporated into Gag over an extended period of passaging in A3.01 T cells. Despite attempts to improve replication and infectivity through codon optimization of sfGFP and SNAPf to prevent RNA degradation, no notable enhancements were achieved. A pulse-chase labeling method was used to simultaneously monitor Gag.SNAPf transfer and new expression in target cells with continuous observation. Additionally, a semi-automated analytical pipeline was employed for quantitative analysis of VS dynamics. This analysis revealed that a single contact was sufficient to trigger new Gag expression in target cells, detectable as early as 30 minutes after VS formation.

A potential application of the pulse-chase labeling method in studying cell-to-cell transmission is to examine the interactions with the cytoskeleton and the involvement of translation machinery components. VS-formation relies on tubulin, and MTOC polarization towards the contact site in donor cells has been documented (89). It has been demonstrated that viral particles can be transferred to multiple target cells at the same time, even if MTOC polarization is only directed towards a single target cell (204). Given the frequent observation of polysynapses, it would be useful to investigate whether MTOC polarization correlates with the appearance of new Gag.SNAPf expression and productive infection. This could be accomplished by the addition of a tubulin marker to donor cells before they are mixed with membrane-labeled target cells. adding a tubulin marker to the donor cell population prior to mixing with membrane-labeled target cells. The main challenge for this approach would be the requirement to adapt imaging and image analysis pipeline to a 3D analysis of cells at high spatial resolution without compromising the possibility for prolonged observation times.

The stable integration of SNAPf(opt) into fully replication-competent HIV-1$^{iSNAPf(opt)}$ across multiple infection cycles highlights its value for studying viral transmission over multiple rounds of infection. One promising application of this approach could be in examining viral spread within three-dimensional environments. Immle and colleagues have created a system for observing cell-to-cell transmission in 3D by embedding a mixed cell population within a collagen matrix (205). Combining the two approaches, pulse-chase labeling of cell-to-cell transmission in 3D

could be accomplished. However, a key challenge would be potential interference of fluorescent dyes with collagen fibers, which might affect the background and signal-to-noise ratio.

Another potentially interesting advancement of the approach would be the integration of a microfluidics system. This system would enable sequential staining of Gag expression at various time points and at the same time allow for the controlled introduction and removal of specific inhibitors affecting different stages of replication. During the optimization process, I conducted an initial assessment of imaging slides that permit direct application of tubes with minimal disruption to the cell layer and motility. However, without a microfluidics system attached the lack of a continuous fresh medium supply led to a significant decline in cell viability. Another aspect that remains a topic of debate within the scientific community is the mechanism of HIV-1 entry following transfer through the VS. Although fusional uptake is considered the primary method for viral particles, evidence points to both fusional and endosomal uptake (93, 206, 207). Since fusion-mediated entry is inhibited at temperatures below 23°C (208), live pulse-chase labeling experiments could be conducted at 37°C and 22°C. Subsequently Gag.SNAPf(opt) expression within contacted target cells can be assessed and compared.

Recent data have shown that resting T cells can be productively infected by cell-to-cell transmission without activation (209). In this study, intracellular staining for HIV-1 Gag in resting autologous primary CD4+ target T cells was employed to measure productive target cell infection. This finding suggests that HIV-1$^{iSNAPf(opt)}$, which allows for tracking of Gag.SNAPf(opt), could be used to extend the pulse-chase labeling technique to study resting T cells. This would enable live microscopy to confirm the published results and directly link HIV-1 transfer to resting T cells with the occurrence of productive infection.

In conclusion, the results demonstrate that HIV-1$^{iSNAPf(opt)}$ is a powerful tool for studying HIV-1 replication and transmission in a fully infectious context. This is a major advancement, given that prior methods using HIV^{iGFP} were constrained by its impaired replication. This is the first demonstration of distinct contact events being directly linked to new Gag.SNAPf(opt) expression in target cells. However, further investigation is required to determine the proportion of this expression that leads to productive infection versus transient translation of incoming viral RNA.

5. Conferences and contributions

5.1 Publications

Microscopy-based assay for semi-quantitative detection of SARS-CoV-2 specific antibodies in human sera: A semi-quantitative, high throughput, microscopy-based assay expands existing approaches to measure SARS-CoV-2 specific antibody levels in human sera. **(2021)** Pape C, Remme R, Wolny A, Olberg S, Wolf S, Cerrone L, Cortese M, Klaus S, Lucic B, **Ullrich S**, Anders-Össwein M, Wolf S, Cerikan B, Neufeldt CJ, Ganter M, Schnitzler P, Merle U, Lusic M, Boulant S, Stanifer M, Bartenschlager R, Hamprecht FA, Kreshuk A, Tischer C, Kräusslich HG, Müller B, Laketa V. **Bioessays, doi: 10.1002/bies.202000257**

SARS-CoV-2 RNA Extraction Using Magnetic Beads for Rapid Large-Scale Testing by RT-qPCR and RT-LAMP. **(2020)** Klein S, Müller TG, … Winter SL, Zimmermann L, Naumoska T, Bubeck F, Kirrmaier D, **Ullrich S**, Barreto Miranda I, Anders S, Grimm D, Schnitzler P, Knop M, Kräusslich HG, Dao Thi VL, Börner K, Chlanda P. **Viruses, doi: 10.3390/v12080863**

5.2 Conference contributions

All conference contributions were presented as:

“A novel pulse-chase fluorescence imaging approach for the analysis of HIV-1 cell-to-cell transmission and spread”

Stephanie Ullrich[1], Maria Anders-Össwein[1], Samy Sid Ahmed[2], Vibor Laketa[1,4], Richard Wombacher[3], Kai Johnsson[3,5], Hans-Georg Kräusslich[1,4], Oliver T. Fackler[2,4], Barbara Müller[1]

1 Department of Infectious Diseases, Virology, University Hospital Heidelberg, Heidelberg, German, 2 Department of Infectious Diseases, Integrative Virology, University Hospital Heidelberg, Heidelberg, Germany, 3Department of Chemical Biology, Max Planck Institute for Medical Research, Heidelberg, Germany, 4 German Center for Infectious Disease Research, partner site Heidelberg, 5 Institute of Chemical Sciences and Engineering, École Polytechnique Fédérale de Lausanne (EPFL), 1015 Lausanne

5.2.1 Oral presentations

- Retroviruses, Cold Spring Harbor Laboratory, New-York, 22nd to 27th May 2023
- 12th international Retroviral Symposium: Assembly, Maturation and Uncoating, Snowbird, Utah 6th to 9th September 2023
- Flash-talk at EMBO | EMBL Symposium: Seeing is believing imaging the molecular processes of life, Heidelberg, 4th to 6th October 2023

5.2.2 Poster presentations

- Retreat SFB 1129, July 2023
- 12th international Retroviral Symposium: Assembly, Maturation and Uncoating, Snowbird, Utah 6th to 9th September 2023
- Flash-talk at EMBO | EMBL Symposium: Seeing is believing imaging the molecular processes of life, Heidelberg, 4th to 6th October 2023
- Retreat SFB 1129, July 2024

6. Acknowledgements

Scientific research is always a collaborative effort, and this project was no exception. Many people have contributed to my success and helped me reach the goal of earning my doctoral degree, and I would like to express my gratitude to them.

First, I would like to thank Prof. Dr. Barbara Müller for giving me the opportunity to work in her group and for her excellent supervision over the past five years. She was always open to scientific discussions and helped me grow both as a person and a scientist by providing the perfect balance between guidance and independence, allowing me to develop my skills as a researcher. Her trust in me, particularly by allowing me to present my work at scientific conferences, was invaluable. It gave me the chance to learn how to present my research effectively and establish connections within the scientific community. Additionally, I want to thank Prof. Dr. Hans-Georg Kräusslich for providing valuable scientific input during lab seminars and TAC meetings. His ability to quickly identify the core issues and prioritize key points during my presentations greatly helped me stay focused on what mattered most: avoiding getting lost in details. I appreciate his support as the first supervisor examining my thesis and for being a part of my TAC and defense committee.

A significant part of the project's success is attributed to the valuable input from Prof. Dr. Oliver T. Fackler. As a member of my TAC committee, he allowed me to present my data in his lab seminars, and the feedback I received from him and members of his group was crucial in developing my thesis in a direction that yielded scientific relevance in a project that was primarily comprised of establishing a method. Thank you for your support and for examining my thesis. Furthermore, I would like to thank Prof. Dr. Friedrich Frischknecht for providing a non-virologist perspective during TAC meetings, which offered valuable new insights. I also want to thank Dr. Marco Binder and Dr. Venera Weinhardt for being part of my defense committee.

Thank you to Dr. Charlotta Funaya for processing and acquiring thin sections and tomograms for my CLEM data. I always felt really welcomed in the EM facility and enjoyed the discussions with her and Dr. Réza Shahidi to solve problems we faced during the process. Many thanks to my collaborators Prof. Dr. Kai Johnson and Dr. Richard Wombacher for providing me the SNAP23 dye; without your help, I could not have developed the pulse-chase labeling approach in the way I presented it in this thesis. It was the key breakthrough in this project. I also want to acknowledge the arivis team who helped me to develop the automated analysis pipeline.

A very special thank you to Maria Anders-Oesswein. She taught me everything I needed to know in the lab and did all the preliminary experiments involving the tagged derivatives before I joined

the team. We became very close throughout the project, and I could always count on her, no matter what the issue was. I will never forget our time pipetting thousands of serum samples during the peak of the pandemic while the rest of Germany was in lockdown. A very special thank you also to all the other “Müllers.” Rene and Annica made me feel welcome from the very beginning, and Sandra, Lisa, Nuno, Snehith, and Anja all contributed to the positive atmosphere in our group, always offering support when needed.

I also want to thank all the members of the Kräusslich and Fackler groups for their scientific discussions and support, both in and outside the lab. Special thanks to Dr. Samy Sid Ahmed for his helpful ideas and contributions to this project. Some colleagues became more than just lab mates during my Ph.D. journey: Jana, Charlotte, Ann-Kathrin, and Sarah, you helped me to not lose my mind when lab life became frustrating. Same goes for Jian and Samara, I will really miss you guys. Thank you to Anja, Irena, and Florian for proofreading my thesis and helping me to elevate my writing to the next level.

Last but not least, I want to thank my family for always supporting me. Papi, I know you are watching from above and are proud of me. Vincent, your encouragement throughout the highs and lows of this project has been priceless, I could not have done it without you. Finally, I would like to thank my friends Irena, Betti, and Laura. I am very grateful to have you and that we maintained our friendship, even though we are now spread throughout Germany.

7. List of figures and abbreviations

7.1 Figures

7.2 Abbreviations

Name	Abbreviation
Acquired immune deficiency syndrome	AIDS
Antigen-presenting cells	APC
Benzyl guanine	BG
Blue cell units	BCU
Broadly neutralizing antibodies	bNAbs
Cabotegravir	CAB
Capsid	CA
C-C chemokine receptor type 5	CXCR4
Central nervous system	CNS
Combined antiretroviral therapy	cART
Condensed ribonucleoprotein particle	RNP
C-X-C motif chemokine receptor 4	CCR5
Double-stranded	ds
Dulbecco's Modified Eagle's Medium	DMEM
Electron multiplying charge-coupled device (EMCCD)	EMCCD
Endosomal complex required for transport	ESCRT
Envelope	Env
Field of view	FoV
Food and Drug Administration	FDA
Glycoprotein	gp
Green fluorescent protein	GFP
Group Specific Antigen	Gag
HIV-associated neurocognitive disorders.	HAND
Human immunodeficiency virus type 1	HIV-1
Human T cell leukemia virus type 1	HTLV-I
Immunofluorescence	IF
Integrase	IN
Intercellular adhesion molecule 1	ICAM-1
Isopropyl-β-d-thiogalactopyranosid	IPTG
Lymphocyte function-associated antigen	LFA-1
Matrix	MA
Murine leukemia virus	MLV
Natural killer	NK
Negative Factor	Nef
Nuclear pore complex	NPC
Nucleocapsid	NC
Open reading frame	ORF
Phenylalanine-glycine	FG
Polyethylenimine	PEI
Polymerase	Pol
Pre-integration complex	PIC
Protease	PR
Regulator of Virion	Rev
Related simian immunodeficiency virus	SIVcpz

Name	Abbreviation
Reverse transcriptase	(RT)
Reverse transcription complex	RTC
Rilpivirine	RPV
Roswell Park Memorial Institute Medium	RPMI
SDS-Polyacrylamide Gel Electrophoresis	SDS-PAGE
Single-stranded	ss
Spacer peptides	SP
Spinning dics confocal microscopy	SDCM
Super folder GFP	sfGFP
SYBR Green based Product Enhanced Reverse Transcriptase	SG-Pert
The non-nucleoside reverse transcriptase inhibitor	NNRTI
Trans activator of Transcription	Tat
transmission electron microscopy	TEM
tunneling nanotubes	TNT
Viral Protein R	Vpr
Viral Protein U	Vpu
Virion Infectivity Factor	Vif
Virological synapse	VS
World health organization	WHO
Zidovudine	AZT
Zinc-finger antiviral protein	ZAP

8. Literature Cited

1. White DO, Fenner F. Medical virology. 4th ed., [4th print.]. San Diego (Calif.): Academic Press; 1998.

2. Baltimore D. Expression of animal virus genomes. Bacteriol Rev 1971; 35(3):235–41.

3. Human immunodeficiency virus 1 Taxonomy ID. NCBI:txid11676.

4. TEMIN HM, MIZUTANI S. Viral RNA-dependent DNA Polymerase: RNA-dependent DNA Polymerase in Virions of Rous Sarcoma Virus. Nature 1970; 226(5252):1211–3.

5. BALTIMORE D. Viral RNA-dependent DNA Polymerase: RNA-dependent DNA Polymerase in Virions of RNA Tumour Viruses. Nature 1970; 226(5252):1209–11.

6. Hindmarsh P, Leis J. Retroviral DNA Integration. Microbiol Mol Biol Rev 1999; 63(4):836–43.

7. Barré-Sinoussi F, Chermann JC, Rey F, Nugeyre MT, Chamaret S, Gruest J et al. Isolation of a T-Lymphotropic Retrovirus from a Patient at Risk for Acquired Immune Deficiency Syndrome (AIDS). Science 1983; 220(4599):868–71.

8. Gottlieb MS, Schroff R, Schanker HM, Weisman JD, Fan PT, Wolf RA et al. Pneumocystis carinii Pneumonia and Mucosal Candidiasis in Previously Healthy Homosexual Men. N Engl J Med 1981; 305(24):1425–31.

9. Gao F, Bailes E, Robertson DL, Chen Y, Rodenburg CM, Michael SF et al. Origin of HIV-1 in the chimpanzee Pan troglodytes troglodytes. Nature 1999; 397(6718):436–41.

10. Faria NR, Rambaut A, Suchard MA, Baele G, Bedford T, Ward MJ et al. HIV epidemiology. The early spread and epidemic ignition of HIV-1 in human populations. Science 2014; 346(6205):56–61.

11. Keele BF, van Heuverswyn F, Li Y, Bailes E, Takehisa J, Santiago ML et al. Chimpanzee Reservoirs of Pandemic and Nonpandemic HIV-1. Science 2006; 313(5786):523–6.

12. Sharp PM, Bailes E, Robertson DL, Gao F, Hahn BH. Origins and evolution of AIDS viruses. Biol Bull 1999; 196(3):338–42.

13. Simon F, Mauclère P, Roques P, Loussert-Ajaka I, Müller-Trutwin MC, Saragosti S et al. Identification of a new human immunodeficiency virus type 1 distinct from group M and group O. Nat Med 1998; 4(9):1032–7. Available from: URL: https://www.nature.com/articles/nm0998_1032.

14. Plantier J-C, Leoz M, Dickerson JE, Oliveira F de, Cordonnier F, Lemée V et al. A new human immunodeficiency virus derived from gorillas. Nat Med 2009; 15(8):871–2.

15. Sharp PM, Hahn BH. The evolution of HIV-1 and the origin of AIDS. Philos Trans R Soc Lond B Biol Sci 2010; 365(1552):2487–94.

16. World Health Organization. HIV statistics, globally and by WHO region, 2023. Geneva: World Health Organization; 2023. Available from: URL: https://iris.who.int/handle/10665/376793.

17. Pantaleo G, Graziosi C, Demarest JF, Butini L, Montroni M, Fox CH et al. HIV infection is active and progressive in lymphoid tissue during the clinically latent stage of disease. Nature 1993; 362(6418):355–8.

18. Pantaleo G, Fauci AS. New Concepts in the Immunopathogenesis of HIV Infection. Annu. Rev. Immunol. 1995; 13(1):487–512.

19. Fiebig EW, Wright DJ, Rawal BD, Garrett PE, Schumacher RT, Peddada L et al. Dynamics of HIV viremia and antibody seroconversion in plasma donors: implications for diagnosis and staging of primary HIV infection. AIDS 2003; 17(13):1871–9.

20. Cohen MS, Shaw GM, McMichael AJ, Haynes BF. Acute HIV-1 Infection. N Engl J Med 2011; 364(20):1943–54.

21. Brenchley JM, Paiardini M, Knox KS, Asher AI, Cervasi B, Asher TE et al. Differential Th17 CD4 T-cell depletion in pathogenic and nonpathogenic lentiviral infections. Blood 2008; 112(7):2826–35.

22. Daar ES, Pilcher CD, Hecht FM. Clinical presentation and diagnosis of primary HIV-1 infection. Curr Opin HIV AIDS 2008; 3(1):10–5.

23. Finzi D, Siliciano RF. Viral dynamics in HIV-1 infection. Cell 1998; 93(5):665–71.

24. Piatak M, Saag MS, Yang LC, Clark SJ, Kappes JC, Luk KC et al. High levels of HIV-1 in plasma during all stages of infection determined by competitive PCR. Science 1993; 259(5102):1749–54.

25. Finzi D, Hermankova M, Pierson T, Carruth LM, Buck C, Chaisson RE et al. Identification of a reservoir for HIV-1 in patients on highly active antiretroviral therapy. Science 1997; 278(5341):1295–300.

26. Siliciano RF, Greene WC. HIV latency. Cold Spring Harb Perspect Med 2011; 1(1):a007096.

27. Stevenson M. HIV-1 pathogenesis. Nat Med 2003; 9(7):853–60. Available from: URL: https://www.nature.com/articles/nm0703-853.

28. Nakashima H, Matsui T, Harada S, Kobayashi N, Matsuda A, Ueda T et al. Inhibition of replication and cytopathic effect of human T cell lymphotropic virus type III/lymphadenopathy-associated virus by 3'-azido-3'-deoxythymidine in vitro. Antimicrob Agents Chemother 1986; 30(6):933–7.

29. Weichseldorfer M, Reitz M, Latinovic OS. Past HIV-1 Medications and the Current Status of Combined Antiretroviral Therapy Options for HIV-1 Patients. Pharmaceutics 2021; 13(11).

30. Richman DD, Margolis DM, Delaney M, Greene WC, Hazuda D, Pomerantz RJ. The challenge of finding a cure for HIV infection. Science 2009; 323(5919):1304–7.

31. Domingo P, Vidal F. Combination antiretroviral therapy. Expert Opin Pharmacother 2011; 12(7):995–8.

32. Yuan NY, Kaul M. Beneficial and Adverse Effects of cART Affect Neurocognitive Function in HIV-1 Infection: Balancing Viral Suppression against Neuronal Stress and Injury. J Neuroimmune Pharmacol 2021; 16(1):90–112.

33. Cabenuva (Cabotegravir Extended-Release Injectable Suspension; Rilpivirine Extended-Release Injectable Suspension) Highlights of Prescribing ...; 2022.

34. Nachega JB, Scarsi KK, Gandhi M, Scott RK, Mofenson LM, Archary M et al. Long-acting antiretrovirals and HIV treatment adherence. Lancet HIV 2023; 10(5):e332-e342.

35. Wain-Hobson S. HIV genome variability in vivo. AIDS 1989; 3 Suppl 1:S13-8.

36. Sakuragi J-I. Morphogenesis of the Infectious HIV-1 Virion. Front Microbiol 2011; 2:242.

37. Novikova M, Zhang Y, Freed EO, Peng K. Multiple Roles of HIV-1 Capsid during the Virus Replication Cycle. Virol Sin 2019; 34(2):119–34. Available from: URL: https://pubmed.ncbi.nlm.nih.gov/31028522/.

38. Korniy N, Goyal A, Hoffmann M, Samatova E, Peske F, Pöhlmann S et al. Modulation of HIV-1 Gag/Gag-Pol frameshifting by tRNA abundance. Nucleic Acids Res 2019; 47(10):5210–22.

39. Freed EO. HIV-1 replication. Somat Cell Mol Genet 2001; 26(1-6):13–33. Available from: URL: https://link.springer.com/article/10.1023/a:1021070512287.

40. Checkley MA, Luttge BG, Freed EO. HIV-1 envelope glycoprotein biosynthesis, trafficking, and incorporation. J Mol Biol 2011; 410(4):582–608.

41. Cullen BR. Regulation of HIV-1 gene expression. FASEB J 1991; 5(10):2361–8.

42. Strebel K. HIV accessory proteins versus host restriction factors. Curr Opin Virol 2013; 3(6):692–9.

43. Marie V, Gordon ML. The HIV-1 Gag Protein Displays Extensive Functional and Structural Roles in Virus Replication and Infectivity. International Journal of Molecular Sciences 2022; 23(14).

44. Pedelacq JD, Cabantous S, Tran TH, Terwilliger TC, Waldo GS. Crystal structure of a superfolder green fluorescent protein; 2005.

45. Bannwarth M, Schmitt S, Pojer F, Schiltz M, Johnsson K. Crystal structure of SNAP-tag; 2010.

46. Shaw GM, Hunter E. HIV transmission. Cold Spring Harb Perspect Med 2012; 2(11):a006965. Available from: URL: https://perspectivesinmedicine.cshlp.org/content/2/11/a006965.short.

47. Barral MFM, Oliveira GR de, Lobato RC, Mendoza-Sassi RA, Martínez AMB, Gonçalves CV. Risk factors of HIV-1 vertical transmission (VT) and the influence of antiretroviral therapy (ART) in pregnancy outcome. Rev Inst Med Trop Sao Paulo 2014; 56(2):133–8.

48. Bour S, Geleziunas R, Wainberg MA. The human immunodeficiency virus type 1 (HIV-1) CD4 receptor and its central role in promotion of HIV-1 infection. Microbiol Rev 1995; 59(1):63–93.

49. Chen B. Molecular Mechanism of HIV-1 Entry. Trends Microbiol 2019; 27(10):878–91.

50. Deng H, Liu R, Ellmeier W, Choe S, Unutmaz D, Burkhart M et al. Identification of a major co-receptor for primary isolates of HIV-1. Nature 1996; 381(6584):661–6.

51. Feng Y, Broder CC, Kennedy PE, Berger EA. HIV-1 entry cofactor: functional cDNA cloning of a seven-transmembrane, G protein-coupled receptor. Science 1996; 272(5263):872–7.

52. Berger EA, Doms RW, Fenyö EM, Korber BT, Littman DR, Moore JP et al. A new classification for HIV-1. Nature 1998; 391(6664):240.

53. Naghavi MH. HIV-1 capsid exploitation of the host microtubule cytoskeleton during early infection. Retrovirology 2021; 18(1):19.

54. Stolp B, Fackler OT. How HIV takes advantage of the cytoskeleton in entry and replication. Viruses 2011; 3(4):293–311.

55. Hulme AE, Perez O, Hope TJ. Complementary assays reveal a relationship between HIV-1 uncoating and reverse transcription. Proc Natl Acad Sci U S A 2011; 108(24):9975–80.

56. Cosnefroy O, Murray PJ, Bishop KN. HIV-1 capsid uncoating initiates after the first strand transfer of reverse transcription. Retrovirology 2016; 13(1):58.

57. Xu H, Franks T, Gibson G, Huber K, Rahm N, Strambio De Castillia C et al. Evidence for biphasic uncoating during HIV-1 infection from a novel imaging assay. Retrovirology 2013; 10:70.

58. Francis AC, Melikyan GB. Single HIV-1 Imaging Reveals Progression of Infection through CA-Dependent Steps of Docking at the Nuclear Pore, Uncoating, and Nuclear Transport. Cell Host Microbe 2018; 23(4):536-548.e6.

59. Arhel N. Revisiting HIV-1 uncoating. Retrovirology 2010; 7:96.

60. Burdick RC, Delviks-Frankenberry KA, Chen J, Janaka SK, Sastri J, Hu W-S et al. Dynamics and regulation of nuclear import and nuclear movements of HIV-1 complexes. PLOS Pathogens 2017; 13(8):e1006570.

61. Zila V, Margiotta E, Turoňová B, Müller TG, Zimmerli CE, Mattei S et al. Cone-shaped HIV-1 capsids are transported through intact nuclear pores. Cell 2021; 184(4):1032-1046.e18.

62. Müller TG, Zila V, Peters K, Schifferdecker S, Stanic M, Lucic B et al. HIV-1 uncoating by release of viral cDNA from capsid-like structures in the nucleus of infected cells. Elife 2021; 10.

63. Di Nunzio F, Danckaert A, Fricke T, Perez P, Fernandez J, Perret E et al. Human nucleoporins promote HIV-1 docking at the nuclear pore, nuclear import and integration. PLoS ONE 2012; 7(9):e46037.

64. Burdick RC, Li C, Munshi M, Rawson JMO, Nagashima K, Hu W-S et al. HIV-1 uncoats in the nucleus near sites of integration. Proc Natl Acad Sci U S A 2020; 117(10):5486–93.

65. Zurnic Bönisch I, Dirix L, Lemmens V, Borrenberghs D, Wit F de, Vernaillen F et al. Capsid-Labelled HIV To Investigate the Role of Capsid during Nuclear Import and Integration. J Virol 2020; 94(7).

66. Sever B, Otsuka M, Fujita M, Ciftci H. A Review of FDA-Approved Anti-HIV-1 Drugs, Anti-Gag Compounds, and Potential Strategies for HIV-1 Eradication. International Journal of Molecular Sciences 2024; 25(7):3659. Available from: URL: https://www.mdpi.com/1422-0067/25/7/3659.

67. Hu W-S, Hughes SH. HIV-1 reverse transcription. Cold Spring Harb Perspect Med 2012; 2(10).

68. Whitcomb JM, Kumar R, Hughes SH. Sequence of the circle junction of human immunodeficiency virus type 1: implications for reverse transcription and integration. J Virol 1990; 64(10):4903–6.

69. Hughes SH. Reverse Transcription of Retroviruses and LTR Retrotransposons. In: Craig NL, Chandler M, Gellert M, editors. Mobile DNA III. Washington: ASM Press; 2015. p. 1051–77.

70. Bowerman B, Brown PO, Bishop JM, Varmus HE. A nucleoprotein complex mediates the integration of retroviral DNA. Genes Dev. 1989; 3(4):469–78. Available from: URL: https://genesdev.cshlp.org/content/3/4/469.short.

71. Lusic M, Siliciano RF. Nuclear landscape of HIV-1 infection and integration. Nat Rev Microbiol 2017; 15(2):69–82.

72. Engelman AN, Singh PK. Cellular and molecular mechanisms of HIV-1 integration targeting. Cell Mol Life Sci 2018; 75(14):2491–507.

73. Engelman A, Mizuuchi K, Craigie R. HIV-1 DNA integration: mechanism of viral DNA cleavage and DNA strand transfer. Cell 1991; 67(6):1211–21.

74. Ali A, Mishra R, Kaur H, Chandra Banerjea A. HIV-1 Tat: An update on transcriptional and non-transcriptional functions. Biochimie 2021; 190:24–35. Available from: URL: https://www.sciencedirect.com/science/article/pii/S0300908421001759.

75. Freed EO. HIV-1 assembly, release and maturation. Nat Rev Microbiol 2015; 13(8):484–96.

76. Sundquist WI, Krausslich H-G. HIV-1 Assembly, Budding, and Maturation. Cold Spring Harb Perspect Med 2012; 2(8):a015420-a015420.

77. Martin-Serrano J, Bieniasz PD. A bipartite late-budding domain in human immunodeficiency virus type 1. J Virol 2003; 77(22):12373–7.

78. Adamson CS, Freed EO. Human immunodeficiency virus type 1 assembly, release, and maturation. Adv Pharmacol 2007; 55:347–87.

79. Briggs JAG, Riches JD, Glass B, Bartonova V, Zanetti G, Kräusslich H-G. Structure and assembly of immature HIV. Proc Natl Acad Sci U S A 2009; 106(27):11090–5.

80. Gupta P, Balachandran R, Ho M, Enrico A, Rinaldo C. Cell-to-cell transmission of human immunodeficiency virus type 1 in the presence of azidothymidine and neutralizing antibody. J Virol 1989; 63(5):2361–5.

81. Sattentau Q. Avoiding the void: cell-to-cell spread of human viruses. Nat Rev Microbiol 2008; 6(11):815–26.

82. Owusu IA, Quaye O, Passalacqua KD, Wobus CE. Egress of non-enveloped enteric RNA viruses. J Gen Virol 2021; 102(3).

83. Rivera-Serrano EE, González-López O, Das A, Lemon SM. Cellular entry and uncoating of naked and quasi-enveloped human hepatoviruses. Elife 2019; 8.

84. Christian RT, Ludovici PP, Jeter WS. Cell-to-cell transmission of herpes simplex virus in primary human amnion cells. Proc Soc Exp Biol Med 1971; 138(3):1109–15.

85. Iwasaki Y, Clark HF. Cell to cell transmission of virus in the central nervous system. II. Experimental rabies in mouse. Lab Invest 1975; 33(4):391–9.

86. Fais S, Capobianchi MR, Abbate I, Castilletti C, Gentile M, Cordiali Fei P et al. Unidirectional budding of HIV-1 at the site of cell-to-cell contact is associated with co-polarization of intercellular adhesion molecules and HIV-1 viral matrix protein. AIDS 1995; 9(4):329–35.

87. Igakura T, Stinchcombe JC, Goon PKC, Taylor GP, Weber JN, Griffiths GM et al. Spread of HTLV-I between lymphocytes by virus-induced polarization of the cytoskeleton. Science 2003; 299(5613):1713–6.

88. Jolly C, Kashefi K, Hollinshead M, Sattentau QJ. HIV-1 cell to cell transfer across an Env-induced, actin-dependent synapse. J Exp Med 2004; 199(2):283–93.

89. Jolly C, Mitar I, Sattentau QJ. Requirement for an intact T-cell actin and tubulin cytoskeleton for efficient assembly and spread of human immunodeficiency virus type 1. J Virol 2007; 81(11):5547–60.

90. Jolly C, Booth NJ, Neil SJD. Cell-cell spread of human immunodeficiency virus type 1 overcomes tetherin/BST-2-mediated restriction in T cells. J Virol 2010; 84(23):12185–99.

91. Jolly C. T cell polarization at the virological synapse. Viruses 2010; 2(6):1261–78.

92. Bracq L, Xie M, Benichou S, Bouchet J. Mechanisms for Cell-to-Cell Transmission of HIV-1. Front Immunol 2018; 9:260.

93. Sloan RD, Kuhl BD, Mesplède T, Münch J, Donahue DA, Wainberg MA. Productive entry of HIV-1 during cell-to-cell transmission via dynamin-dependent endocytosis. J Virol 2013; 87(14):8110–23.

94. Dale BM, McNerney GP, Hübner W, Huser TR, Chen BK. Tracking and quantitation of fluorescent HIV during cell-to-cell transmission. Methods 2011; 53(1):20–6.

95. Pearce-Pratt R, Malamud D, Phillips DM. Role of the cytoskeleton in cell-to-cell transmission of human immunodeficiency virus. J Virol 1994; 68(5):2898–905.

96. Hübner W, McNerney GP, Chen P, Dale BM, Gordon RE, Chuang FYS et al. Quantitative 3D video microscopy of HIV transfer across T cell virological synapses. Science 2009; 323(5922):1743–7.

97. Jolly C, Welsch S, Michor S, Sattentau QJ. The Regulated Secretory Pathway in CD4+ T cells Contributes to Human Immunodeficiency Virus Type-1 Cell-to-Cell Spread at the Virological Synapse. PLOS Pathogens 2011; 7(9):e1002226.

98. Rudnicka D, Feldmann J, Porrot F, Wietgrefe S, Guadagnini S, Prévost M-C et al. Simultaneous cell-to-cell transmission of human immunodeficiency virus to multiple targets through polysynapses. J Virol 2009; 83(12):6234–46.

99. Dimitrov DS, Willey RL, Sato H, Chang LJ, Blumenthal R, Martin MA. Quantitation of human immunodeficiency virus type 1 infection kinetics. J Virol 1993; 67(4):2182–90.

100. Sattentau QJ. Cell-to-Cell Spread of Retroviruses. Viruses 2010; 2(6):1306–21.

101. Law KM, Komarova NL, Yewdall AW, Lee RK, Herrera OL, Wodarz D et al. In Vivo HIV-1 Cell-to-Cell Transmission Promotes Multicopy Micro-compartmentalized Infection. Cell Rep 2016; 15(12):2771–83.

102. Richardson MW, Carroll RG, Stremlau M, Korokhov N, Humeau LM, Silvestri G et al. Mode of transmission affects the sensitivity of human immunodeficiency virus type 1 to restriction by rhesus TRIM5alpha. J Virol 2008; 82(22):11117–28.

103. Sourisseau M, Sol-Foulon N, Porrot F, Blanchet F, Schwartz O. Inefficient human immunodeficiency virus replication in mobile lymphocytes. J Virol 2007; 81(2):1000–12.

104. Chen P, Hübner W, Spinelli MA, Chen BK. Predominant mode of human immunodeficiency virus transfer between T cells is mediated by sustained Env-dependent neutralization-resistant virological synapses. J Virol 2007; 81(22):12582–95.

105. Iwami S, Takeuchi JS, Nakaoka S, Mammano F, Clavel F, Inaba H et al. Cell-to-cell infection by HIV contributes over half of virus infection. Elife 2015; 4.

106. Murooka TT, Deruaz M, Marangoni F, Vrbanac VD, Seung E, Andrian UH von et al. HIV-infected T cells are migratory vehicles for viral dissemination. Nature 2012; 490(7419):283–7.

107. Law KM, Satija N, Esposito AM, Chen BK. Cell-to-Cell Spread of HIV and Viral Pathogenesis. Adv Virus Res 2016; 95:43–85.

108. Agosto LM, Uchil PD, Mothes W. HIV cell-to-cell transmission: effects on pathogenesis and antiretroviral therapy. Trends Microbiol 2015; 23(5):289–95.

109. Agosto LM, Zhong P, Munro J, Mothes W. Highly active antiretroviral therapies are effective against HIV-1 cell-to-cell transmission. PLOS Pathogens 2014; 10(2):e1003982.

110. Abela IA, Berlinger L, Schanz M, Reynell L, Günthard HF, Rusert P et al. Cell-cell transmission enables HIV-1 to evade inhibition by potent CD4bs directed antibodies. PLOS Pathogens 2012; 8(4):e1002634.

111. Dufloo J, Bruel T, Schwartz O. HIV-1 cell-to-cell transmission and broadly neutralizing antibodies. Retrovirology 2018; 15(1):51.

112. Li H, Zony C, Chen P, Chen BK. Reduced Potency and Incomplete Neutralization of Broadly Neutralizing Antibodies against Cell-to-Cell Transmission of HIV-1 with Transmitted Founder Envs. J Virol 2017; 91(9).

113. Malbec M, Porrot F, Rua R, Horwitz J, Klein F, Halper-Stromberg A et al. Broadly neutralizing antibodies that inhibit HIV-1 cell to cell transmission. J Exp Med 2013; 210(13):2813–21.

114. Sowinski S, Jolly C, Berninghausen O, Purbhoo MA, Chauveau A, Köhler K et al. Membrane nanotubes physically connect T cells over long distances presenting a novel route for HIV-1 transmission. Nat Cell Biol 2008; 10(2):211–9.

115. Valdebenito S, Ono A, Rong L, Eugenin EA. The role of tunneling nanotubes during early stages of HIV infection and reactivation: implications in HIV cure. NeuroImmune Pharm Ther 2023; 2(2):169–86.

116. Okafo G, Prevedel L, Eugenin E. Tunneling nanotubes (TNT) mediate long-range gap junctional communication: Implications for HIV cell to cell spread. Sci Rep 2017; 7(1):16660.

117. Mukerji J, Olivieri KC, Misra V, Agopian KA, Gabuzda D. Proteomic analysis of HIV-1 Nef cellular binding partners reveals a role for exocyst complex proteins in mediating enhancement of intercellular nanotube formation. Retrovirology 2012; 9:33.

118. Symeonides M, Murooka TT, Bellfy LN, Roy NH, Mempel TR, Thali M. HIV-1-Induced Small T Cell Syncytia Can Transfer Virus Particles to Target Cells through Transient Contacts. Viruses 2015; 7(12):6590–603.

119. Kowalski M, Potz J, Basiripour L, Dorfman T, Goh WC, Terwilliger E et al. Functional regions of the envelope glycoprotein of human immunodeficiency virus type 1. Science 1987; 237(4820):1351–5.

120. Compton AA, Schwartz O. They Might Be Giants: Does Syncytium Formation Sink or Spread HIV Infection? PLOS Pathogens 2017; 13(2):e1006099.

121. Roy NH, Chan J, Lambelé M, Thali M. Clustering and mobility of HIV-1 Env at viral assembly sites predict its propensity to induce cell-cell fusion. J Virol 2013; 87(13):7516–25.

122. Whitaker EE, Matheson NJ, Perlee S, Munson PB, Symeonides M, Thali M. EWI-2 Inhibits Cell-Cell Fusion at the HIV-1 Virological Presynapse. Viruses 2019; 11(12).

123. Burrell CJ, Howard CR, Murphy FA. History and Impact of Virology. Fenner and White's Medical Virology 2016:3–14.

124. SHIMOMURA O, JOHNSON FH, SAIGA Y. Extraction, purification and properties of aequorin, a bioluminescent protein from the luminous hydromedusan, Aequorea. J Cell Comp Physiol 1962; 59:223–39.

125. Kremers G-J, Gilbert SG, Cranfill PJ, Davidson MW, Piston DW. Fluorescent proteins at a glance. J Cell Sci 2011; 124(Pt 2):157–60.

126. McDonald D, Vodicka MA, Lucero G, Svitkina TM, Borisy GG, Emerman M et al. Visualization of the intracellular behavior of HIV in living cells. J Cell Biol 2002; 159(3):441–52.

127. Desai TM, Marin M, Sood C, Shi J, Nawaz F, Aiken C et al. Fluorescent protein-tagged Vpr dissociates from HIV-1 core after viral fusion and rapidly enters the cell nucleus. Retrovirology 2015; 12:88.

128. Müller B, Daecke J, Fackler OT, Dittmar MT, Zentgraf H, Kräusslich H-G. Construction and characterization of a fluorescently labeled infectious human immunodeficiency virus type 1 derivative. J Virol 2004; 78(19):10803–13.

129. Dale BM, McNerney GP, Thompson DL, Hubner W, los Reyes K de, Chuang FY et al. Cell-to-Cell Transfer of HIV-1 via Virological Synapses Leads to Endosomal Virion Maturation that Activates Viral Membrane Fusion. Cell Host Microbe 2011; 10(6):551–62. Available from: URL: https://www.sciencedirect.com/science/article/pii/S1931312811003702.

130. Albanese A, Arosio D, Terreni M, Cereseto A. HIV-1 pre-integration complexes selectively target decondensed chromatin in the nuclear periphery. PLoS ONE 2008; 3(6):e2413.

131. Jouvenet N, Simon SM, Bieniasz PD. Imaging the interaction of HIV-1 genomes and Gag during assembly of individual viral particles. Proc Natl Acad Sci U S A 2009; 106(45):19114–9.

132. Nakane S, Iwamoto A, Matsuda Z. The V4 and V5 Variable Loops of HIV-1 Envelope Glycoprotein Are Tolerant to Insertion of Green Fluorescent Protein and Are Useful Targets for Labeling. J Biol Chem 2015; 290(24):15279–91.

133. Wang L, Sandmeyer A, Hübner W, Li H, Huser T, Chen BK. A Replication-Competent HIV Clone Carrying GFP-Env Reveals Rapid Env Recycling at the HIV-1 T Cell Virological Synapse. Viruses 2021; 14(1).

134. Sakin V, Paci G, Lemke EA, Müller B. Labeling of virus components for advanced, quantitative imaging analyses. FEBS Lett 2016; 590(13):1896–914.

135. Keppler A, Gendreizig S, Gronemeyer T, Pick H, Vogel H, Johnsson K. A general method for the covalent labeling of fusion proteins with small molecules in vivo. Nat Biotechnol 2003; 21(1):86–9. Available from: URL: https://www.nature.com/articles/nbt765.

136. Gronemeyer T, Chidley C, Juillerat A, Heinis C, Johnsson K. Directed evolution of O6-alkylguanine-DNA alkyltransferase for applications in protein labeling. Protein Eng Des Sel 2006; 19(7):309–16.

137. Keppler A, Pick H, Arrivoli C, Vogel H, Johnsson K. Labeling of fusion proteins with synthetic fluorophores in live cells. Proc Natl Acad Sci U S A 2004; 101(27):9955–9.

138. Sun X, Zhang A, Baker B, Sun L, Howard A, Buswell J et al. Development of SNAP-tag fluorogenic probes for wash-free fluorescence imaging. Chembiochem 2011; 12(14):2217–26.

139. Eckhardt M, Anders M, Muranyi W, Heilemann M, Krijnse-Locker J, Müller B. A SNAP-tagged derivative of HIV-1--a versatile tool to study virus-cell interactions. PLoS ONE 2011; 6(7):e22007.

140. Hübner W, Chen P, Del Portillo A, Liu Y, Gordon RE, Chen BK. Sequence of human immunodeficiency virus type 1 (HIV-1) Gag localization and oligomerization monitored with live confocal imaging of a replication-competent, fluorescently tagged HIV-1. J Virol 2007; 81(22):12596–607.

141. Eckhardt M. Quantitative analysis of the early steps of virus host cell interaction of human immunodeficiency virus type 1 and hepatitis C virus. Heidelberg University Library; 2010. Available from: URL: http://archiv.ub.uni-heidelberg.de/volltextserver/id/eprint/10683.

142. Hughes PW. Follow That Protein: SNAP-Tagging Permits High-Resolution Protein Localization. Plant Cell 2020; 32(10):3039–40.

143. Wilhelm J, Kühn S, Tarnawski M, Gotthard G, Tünnermann J, Tänzer T et al. Kinetic and Structural Characterization of the Self-Labeling Protein Tags HaloTag7, SNAP-tag, and CLIP-tag. Biochemistry 2021; 60(33):2560–75.

144. Hein B, Willig KI, Wurm CA, Westphal V, Jakobs S, Hell SW. Stimulated emission depletion nanoscopy of living cells using SNAP-tag fusion proteins. Biophys J 2010; 98(1):158–63.

145. Erdmann RS, Baguley SW, Richens JH, Wissner RF, Xi Z, Allgeyer ES et al. Labeling Strategies Matter for Super-Resolution Microscopy: A Comparison between HaloTags and SNAP-tags. Cell Chem Biol 2019; 26(4):584-592.e6.

146. Gao G, Guo X, Goff SP. Inhibition of retroviral RNA production by ZAP, a CCCH-type zinc finger protein. Science 2002; 297(5587):1703–6.

147. Luo X, Wang X, Gao Y, Zhu J, Liu S, Gao G et al. Molecular Mechanism of RNA Recognition by Zinc-Finger Antiviral Protein. Cell Rep 2020; 30(1):46-52.e4.

148. Zhu Y, Chen G, Lv F, Wang X, Ji X, Xu Y et al. Zinc-finger antiviral protein inhibits HIV-1 infection by selectively targeting multiply spliced viral mRNAs for degradation. Proc Natl Acad Sci U S A 2011; 108(38):15834–9.

149. Takata MA, Gonçalves-Carneiro D, Zang TM, Soll SJ, York A, Blanco-Melo D et al. CG dinucleotide suppression enables antiviral defence targeting non-self RNA. Nature 2017; 550(7674):124–7.

150. Ficarelli M, Antzin-Anduetza I, Hugh-White R, Firth AE, Sertkaya H, Wilson H et al. CpG Dinucleotides Inhibit HIV-1 Replication through Zinc Finger Antiviral Protein (ZAP)-Dependent and -Independent Mechanisms. J Virol 2020; 94(6).

151. Wang L, Eng ET, Law K, Gordon RE, Rice WJ, Chen BK. Visualization of HIV T Cell Virological Synapses and Virus-Containing Compartments by Three-Dimensional Correlative Light and Electron Microscopy. J Virol 2017; 91(2).

152. Bohne J, Kräusslich H-G. Mutation of the major 5' splice site renders a CMV-driven HIV-1 proviral clone Tat-dependent: connections between transcription and splicing. FEBS Lett 2004; 563(1-3):113–8.

153. Müller B, Anders M, Akiyama H, Welsch S, Glass B, Nikovics K et al. HIV-1 Gag processing intermediates trans-dominantly interfere with HIV-1 infectivity. J Biol Chem 2009; 284(43):29692–703.

154. Salahuddin SZ, Markham PD, Wong-Staal F, Franchini G, Kalyanaraman VS, Gallo RC. Restricted expression of human T-cell leukemia--lymphoma virus (HTLV) in transformed human umbilical cord blood lymphocytes. Virology 1983; 129(1):51–64.

155. Pear WS, Nolan GP, Scott ML, Baltimore D. Production of high-titer helper-free retroviruses by transient transfection. Proc Natl Acad Sci U S A 1993; 90(18):8392–6.

156. Wei X, Decker JM, Liu H, Zhang Z, Arani RB, Kilby JM et al. Emergence of resistant human immunodeficiency virus type 1 in patients receiving fusion inhibitor (T-20) monotherapy. Antimicrob Agents Chemother 2002; 46(6):1896–905.

157. Folks T, Benn S, Rabson A, Theodore T, Hoggan MD, Martin M et al. Characterization of a continuous T-cell line susceptible to the cytopathic effects of the acquired immunodeficiency syndrome (AIDS)-associated retrovirus. Proc Natl Acad Sci U S A 1985; 82(13):4539–43.

158. Paul-Gilloteaux P, Heiligenstein X, Belle M, Domart M-C, Larijani B, Collinson L et al. eC-CLEM: flexible multidimensional registration software for correlative microscopies. Nat Methods 2017; 14(2):102–3.

159. Schindelin J, Arganda-Carreras I, Frise E, Kaynig V, Longair M, Pietzsch T et al. Fiji: an open-source platform for biological-image analysis. Nat Methods 2012; 9(7):676–82.

160. Chaumont F de, Dallongeville S, Chenouard N, Hervé N, Pop S, Provoost T et al. Icy: an open bioimage informatics platform for extended reproducible research. Nat Methods 2012; 9(7):690–6.

161. Nadai Y, Eyzaguirre LM, Constantine NT, Sill AM, Cleghorn F, Blattner WA et al. Protocol for nearly full-length sequencing of HIV-1 RNA from plasma. PLoS ONE 2008; 3(1):e1420.

162. Pizzato M, Erlwein O, Bonsall D, Kaye S, Muir D, McClure MO. A one-step SYBR Green I-based product-enhanced reverse transcriptase assay for the quantitation of retroviruses in cell culture supernatants. J Virol Methods 2009; 156(1-2):1–7.

163. Kärber G. Beitrag zur kollektiven Behandlung pharmakologischer Reihenversuche. Archiv f. experiment. Pathol. u. Pharmakol 1931; 162(4):480–3. Available from: URL: https://link.springer.com/article/10.1007/bf01863914.

164. SPEARMAN C. THE METHOD OF 'RIGHT AND WRONG CASES' ('CONSTANT STIMULI') WITHOUT GAUSS'S FORMULAE. British Journal of Psychology, 1904-1920 1908; 2(3):227–42.

165. O'Doherty U, Swiggard WJ, Malim MH. Human immunodeficiency virus type 1 spinoculation enhances infection through virus binding. J Virol 2000; 74(21):10074–80.

166. Padilla-Parra S, Marin M, Gahlaut N, Suter R, Kondo N, Melikyan GB. Fusion of mature HIV-1 particles leads to complete release of a gag-GFP-based content marker and raises the intraviral pH. PLoS ONE 2013; 8(8):e71002.

167. Hanne J, Göttfert F, Schimer J, Anders-Össwein M, Konvalinka J, Engelhardt J et al. Stimulated Emission Depletion Nanoscopy Reveals Time-Course of Human Immunodeficiency Virus Proteolytic Maturation. ACS Nano 2016; 10(9):8215–22.

168. Balleza E, Kim JM, Cluzel P. Systematic characterization of maturation time of fluorescent proteins in living cells. Nat Methods 2018; 15(1):47–51.

169. Pédelacq J-D, Cabantous S, Tran T, Terwilliger TC, Waldo GS. Engineering and characterization of a superfolder green fluorescent protein. Nat Biotechnol 2006; 24(1):79–88.

170. Radestock B, Morales I, Rahman SA, Radau S, Glass B, Zahedi RP et al. Comprehensive mutational analysis reveals p6Gag phosphorylation to be dispensable for HIV-1 morphogenesis and replication. J Virol 2013; 87(2):724–34.

171. Grubbs FE. Sample Criteria for Testing Outlying Observations. Ann. Math. Statist. 1950; 21(1):27–58.

172. Hierholzer JC, Killington RA. Virus isolation and quantitation. In: Mahy BWJ, Kangro HO, editors. Virology methods manual. London, San Diego: Academic Press; 1996. p. 25–46.

173. Lardon N, Wang L, Tschanz A, Hoess P, Tran M, D'Este E et al. Systematic Tuning of Rhodamine Spirocyclization for Super-resolution Microscopy. J Am Chem Soc 2021; 143(36):14592–600.

174. Berg S, Kutra D, Kroeger T, Straehle CN, Kausler BX, Haubold C et al. ilastik: interactive machine learning for (bio)image analysis. Nat Methods 2019; 16(12):1226–32.

175. Murray JM, Kelleher AD, Cooper DA. Timing of the components of the HIV life cycle in productively infected CD4+ T cells in a population of HIV-infected individuals. J Virol 2011; 85(20):10798–805.

176. van 't Wout AB, Lehrman GK, Mikheeva SA, O'Keeffe GC, Katze MG, Bumgarner RE et al. Cellular gene expression upon human immunodeficiency virus type 1 infection of CD4(+)-T-cell lines. J Virol 2003; 77(2):1392–402.

177. Köppke J, Keller L-E, Stuck M, Arnow ND, Bannert N, Doellinger J et al. Direct translation of incoming retroviral genomes. Nat Commun 2024; 15(1):299.

178. Abernathy E, Glaunsinger B. Emerging roles for RNA degradation in viral replication and antiviral defense. Virology 2015; 479-480:600–8.

179. Roy CN, Benitez Moreno MA, Kline C, Ambrose Z. CG Dinucleotide Removal in Bioluminescent and Fluorescent Reporters Improves HIV-1 Replication and Reporter Gene Expression for Dual Imaging in Humanized Mice. J Virol 2021; 95(19):e0044921.

180. Kmiec D, Nchioua R, Sherrill-Mix S, Stürzel CM, Heusinger E, Braun E et al. CpG Frequency in the 5' Third of the env Gene Determines Sensitivity of Primary HIV-1 Strains to the Zinc-Finger Antiviral Protein. mBio 2020; 11(1).

181. Buckmaster MV, Goff SP. Riplet Binds the Zinc Finger Antiviral Protein (ZAP) and Augments ZAP-Mediated Restriction of HIV-1. J Virol 2022; 96(16):e0052622.

182. Hayakawa S, Shiratori S, Yamato H, Kameyama T, Kitatsuji C, Kashigi F et al. ZAPS is a potent stimulator of signaling mediated by the RNA helicase RIG-I during antiviral responses. Nat Immunol 2011; 12(1):37–44.

183. Jordan-Paiz A, Franco S, Martinez MA. Reducing HIV-1 env gene CpG frequency increases the replication capacity of the HXB2 virus strain. Virus Res 2022; 310:198685.

184. Liu S-L, Wang Z-G, Xie H-Y, Liu A-A, Lamb DC, Pang D-W. Single-Virus Tracking: From Imaging Methodologies to Virological Applications. Chem Rev 2020; 120(3):1936–79.

185. Baulcombe DC, Chapman S, Santa Cruz S. Jellyfish green fluorescent protein as a reporter for virus infections. Plant J 1995; 7(6):1045–53.

186. Eyre NS, Fiches GN, Aloia AL, Helbig KJ, McCartney EM, McErlean CSP et al. Dynamic imaging of the hepatitis C virus NS5A protein during a productive infection. J Virol 2014; 88(7):3636–52.

187. Remenyi R, Roberts GC, Zothner C, Merits A, Harris M. SNAP-tagged Chikungunya Virus Replicons Improve Visualisation of Non-Structural Protein 3 by Fluorescence Microscopy. Sci Rep 2017; 7(1):5682.

188. Laber JR, Dear BJ, Martins ML, Jackson DE, DiVenere A, Gollihar JD et al. Charge Shielding Prevents Aggregation of Supercharged GFP Variants at High Protein Concentration. Mol Pharm 2017; 14(10):3269–80.

189. van Duyne R, Kuo LS, Pham P, Fujii K, Freed EO. Mutations in the HIV-1 envelope glycoprotein can broadly rescue blocks at multiple steps in the virus replication cycle. Proc Natl Acad Sci U S A 2019; 116(18):9040–9.

190. CLERMONT Y, LEBLOND CP. Renewal of spermatogonia in the rat. Am J Anat 1953; 93(3):475–501.

191. Willey RL, Bonifacino JS, Potts BJ, Martin MA, Klausner RD. Biosynthesis, cleavage, and degradation of the human immunodeficiency virus 1 envelope glycoprotein gp160. Proc Natl Acad Sci U S A 1988; 85(24):9580–4.

192. Jansen LET, Black BE, Foltz DR, Cleveland DW. Propagation of centromeric chromatin requires exit from mitosis. J Cell Biol 2007; 176(6):795–805.

193. Gautier A, Juillerat A, Heinis C, Corrêa IR, Kindermann M, Beaufils F et al. An engineered protein tag for multiprotein labeling in living cells. Chem Biol 2008; 15(2):128–36.

194. Bodor DL, Rodríguez MG, Moreno N, Jansen LET. Analysis of protein turnover by quantitative SNAP-based pulse-chase imaging. Curr Protoc Cell Biol 2012; Chapter 8:Unit8.8.

195. Dustin ML. T-cell activation through immunological synapses and kinapses. Immunol Rev 2008; 221:77–89.

196. Azar GA, Lemaître F, Robey EA, Bousso P. Subcellular dynamics of T cell immunological synapses and kinapses in lymph nodes. Proc Natl Acad Sci U S A 2010; 107(8):3675–80.

197. Wang L, Izadmehr S, Kamau E, Kong X-P, Chen BK. Sequential trafficking of Env and Gag to HIV-1 T cell virological synapses revealed by live imaging. Retrovirology 2019; 16(1):2.

198. Casartelli N, Sourisseau M, Feldmann J, Guivel-Benhassine F, Mallet A, Marcelin A-G et al. Tetherin restricts productive HIV-1 cell-to-cell transmission. PLOS Pathogens 2010; 6(6):e1000955.

199. Bruce JW, Park E, Magnano C, Horswill M, Richards A, Potts G et al. HIV-1 virological synapse formation enhances infection spread by dysregulating Aurora Kinase B. PLOS Pathogens 2023; 19(7):e1011492.

200. Gardiner JC, Mauer EJ, Sherer NM. HIV-1 Gag, Envelope, and Extracellular Determinants Cooperate To Regulate the Stability and Turnover of Virological Synapses. J Virol 2016; 90(14):6583–97.

201. Permanyer M, Pauls E, Badia R, Esté JA, Ballana E. The cortical actin determines different susceptibility of naïve and memory CD4+ T cells to HIV-1 cell-to-cell transmission and infection. PLoS ONE 2013; 8(11):e79221.

202. Labaronne E, Décimo D, Bertrand L, Guiguettaz L, Sohier TJ, Cluet D et al. Extensive uORF translation from HIV-1 transcripts conditions DDX3 dependency for expression of main ORFs and elicits specific T cell immune responses in infected individuals; 2022.

203. Mazurov D, Herschhorn A. Ultrasensitive quantification of HIV-1 cell-to-cell transmission in primary human CD4+ T cells measures viral sensitivity to broadly neutralizing antibodies. mBio 2024; 15(1):e0242823.

204. Sol-Foulon N, Sourisseau M, Porrot F, Thoulouze M-I, Trouillet C, Nobile C et al. ZAP-70 kinase regulates HIV cell-to-cell spread and virological synapse formation. EMBO J 2007; 26(2):516–26.

205. Imle A, Kumberger P, Schnellbächer ND, Fehr J, Carrillo-Bustamante P, Ales J et al. Experimental and computational analyses reveal that environmental restrictions shape HIV-1 spread in 3D cultures. Nat Commun 2019; 10(1):2144.

206. Bosch B, Grigorov B, Senserrich J, Clotet B, Darlix J-L, Muriaux D et al. A clathrin-dynamin-dependent endocytic pathway for the uptake of HIV-1 by direct T cell-T cell transmission. Antiviral Res 2008; 80(2):185–93.

207. Martin N, Welsch S, Jolly C, Briggs JAG, Vaux D, Sattentau QJ. Virological synapse-mediated spread of human immunodeficiency virus type 1 between T cells is sensitive to entry inhibition. J Virol 2010; 84(7):3516–27.

208. Herold N, Anders-Ößwein M, Glass B, Eckhardt M, Müller B, Kräusslich H-G. HIV-1 entry in SupT1-R5, CEM-ss, and primary CD4+ T cells occurs at the plasma membrane and does not require endocytosis. J Virol 2014; 88(24):13956–70. Available from: URL: https://pubmed.ncbi.nlm.nih.gov/25253335/.

209. Reuschl A-K, Mesner D, Shivkumar M, Whelan MVX, Pallett LJ, Guerra-Assunção JA et al. HIV-1 Vpr drives a tissue residency-like phenotype during selective infection of resting memory T cells. Cell Rep 2022; 39(2):110650.

9. Appendix

A

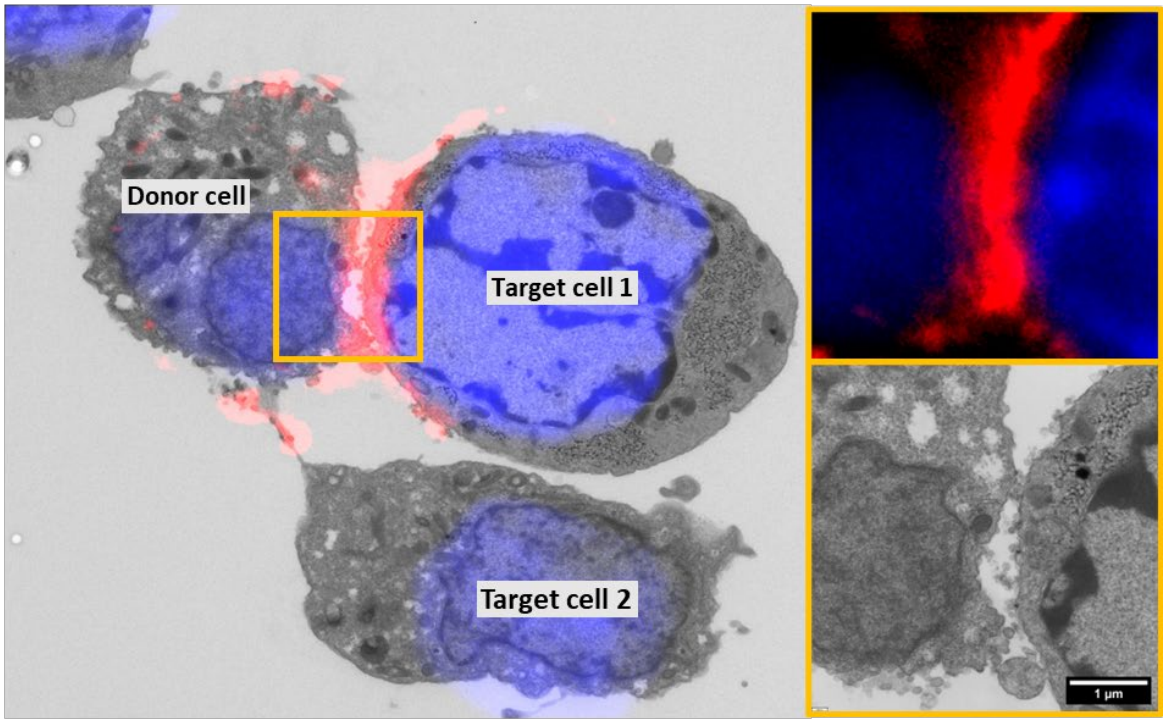

B

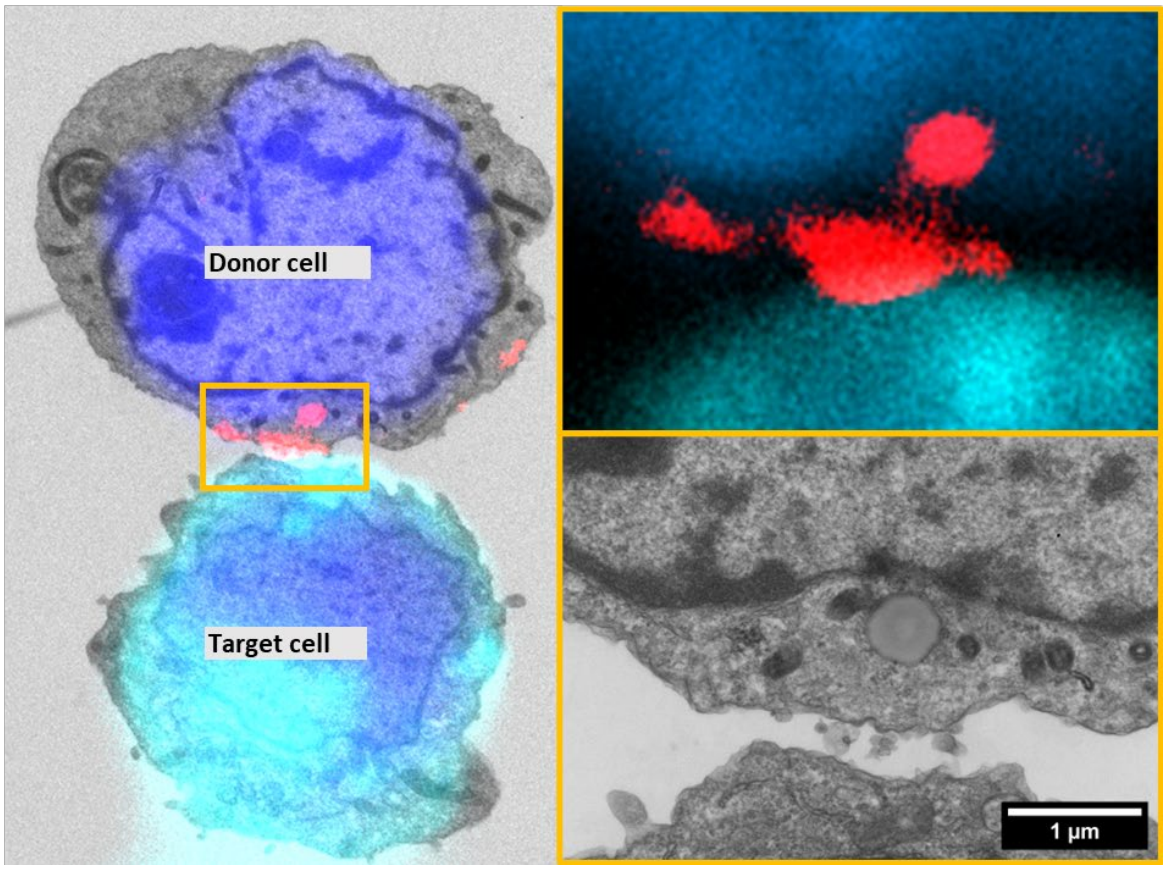

C

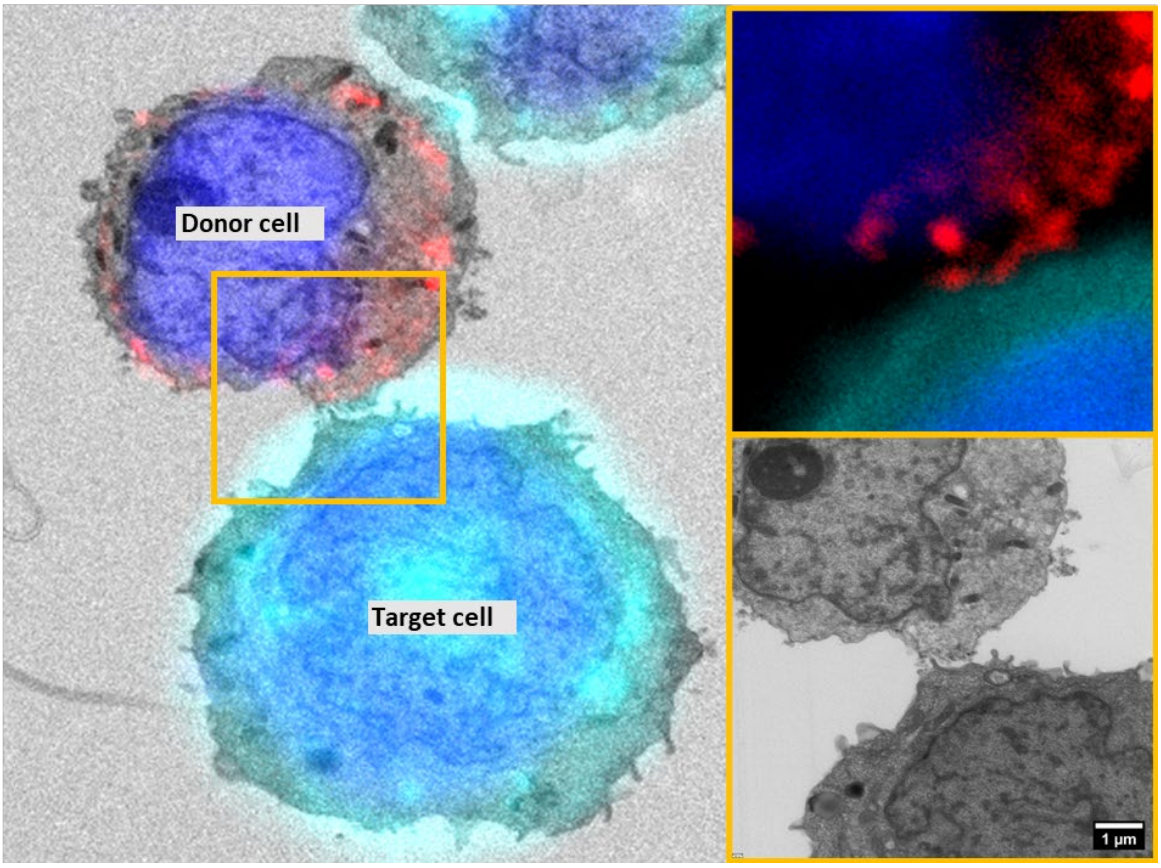

Supplementary Figure 1 CLEM analysis of the HIV-1$^{iSNAPf(opt)}$ VS.
A3.01 T cells were infected with HIV-1$^{iSNAPf(opt)}$. At 18 hours post-infection, Gag.SNAPf(opt) was labeled using 600 nM SPY555-BG, washed, and mixed with membrane-labeled uninfected A3.01 cells (target cells) at a ratio of 1:4 and seeded onto gridded MatTek dishes. Subsequently, the cells were fixed for an additional 90 minutes with 4% PFA and 0.2% GA, washed, and stained with Hoechst 33258. Subsequently, Dr. Funaya proceeded to dehydrate the cells, embed them in Epon, and section them. The resulting sections were imaged using a JEOL JEM-1400 transmission electron microscope and a Tecnai F20 electron microscope. Contact events identified by fluorescence were relocated using the grid, and EM and fluorescence images were correlated using the eC-CLEM plugin in Icy software. Correlation of a HIV-1$^{iSNAPf(opt)}$ infected donor cell with an uninfected target cell. A-C represent individual cell pairs from two different experiments.

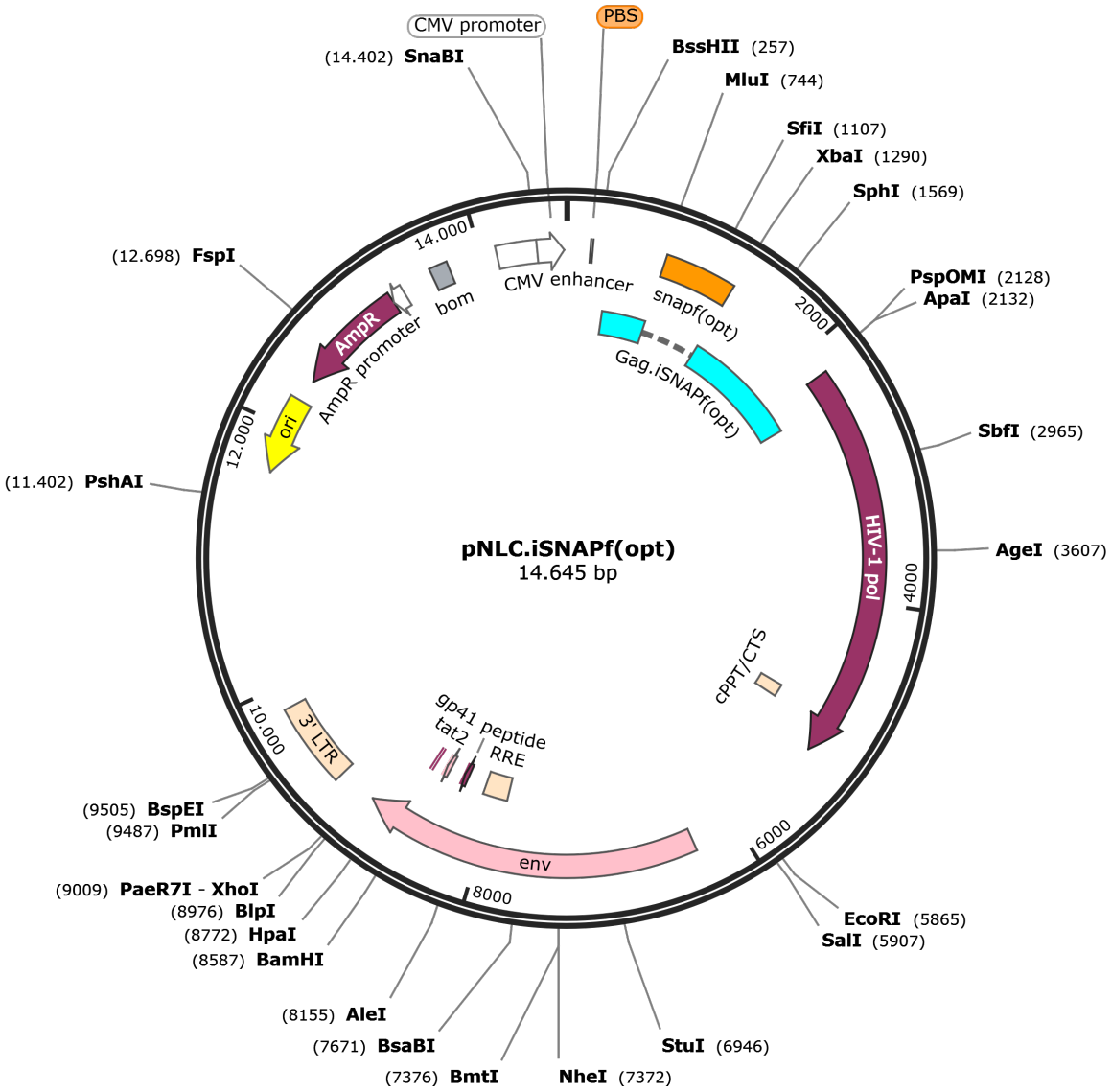

Supplementary Figure 2 Plasmid map of pNLC.iSNAPf(opt).
The plasmid is based on the wildtype proviral plasmid pNLC4-3 with iSNAPf(opt) integrated between the MA and CA as internal domains.

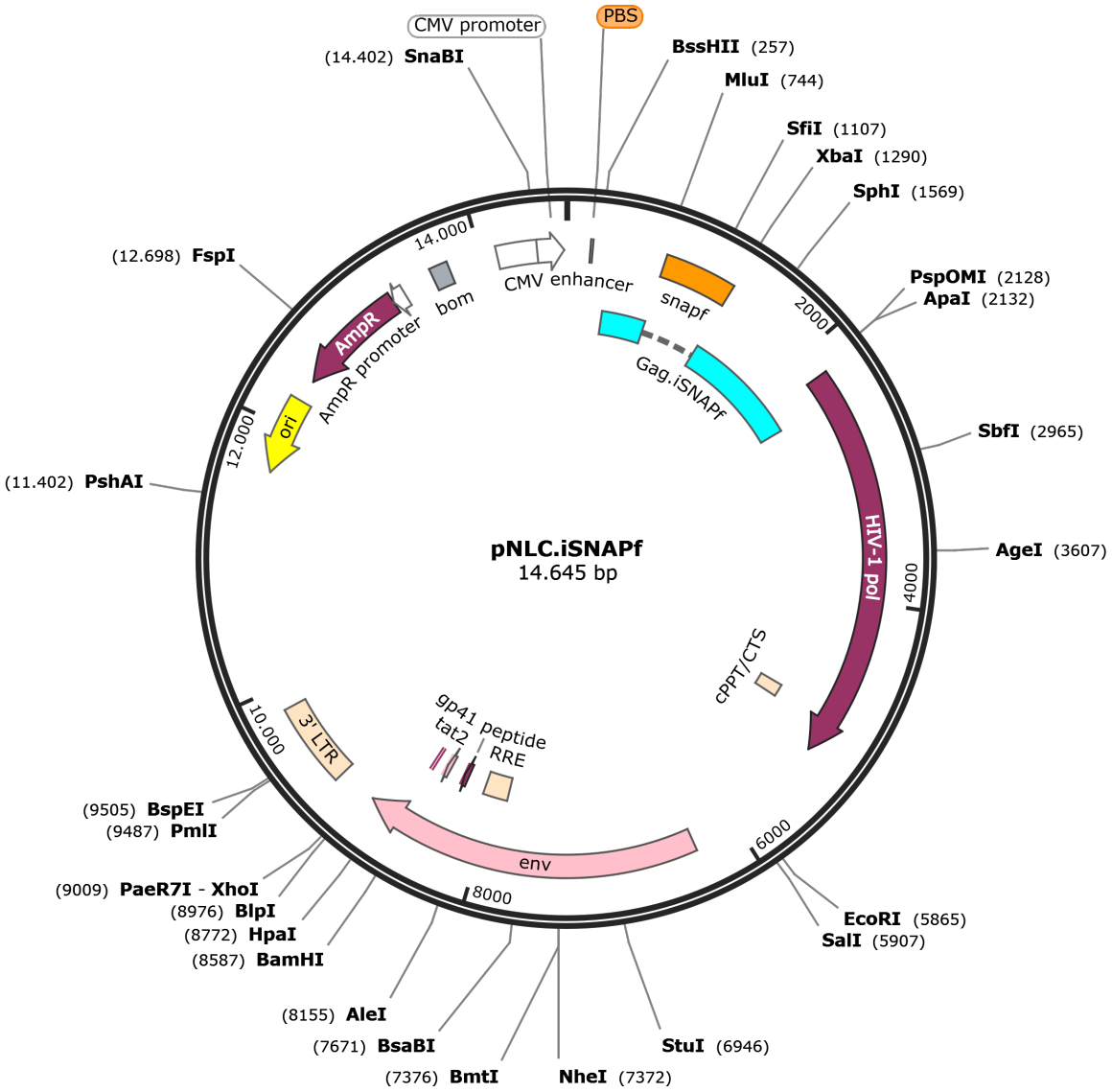

Supplementary Figure 3 Plasmid map of pNLC.iSNAPf.
The plasmid is based on the wildtype proviral plasmid pNLC4-3 with iSNAPf integrated between the MA and CA as internal domains.

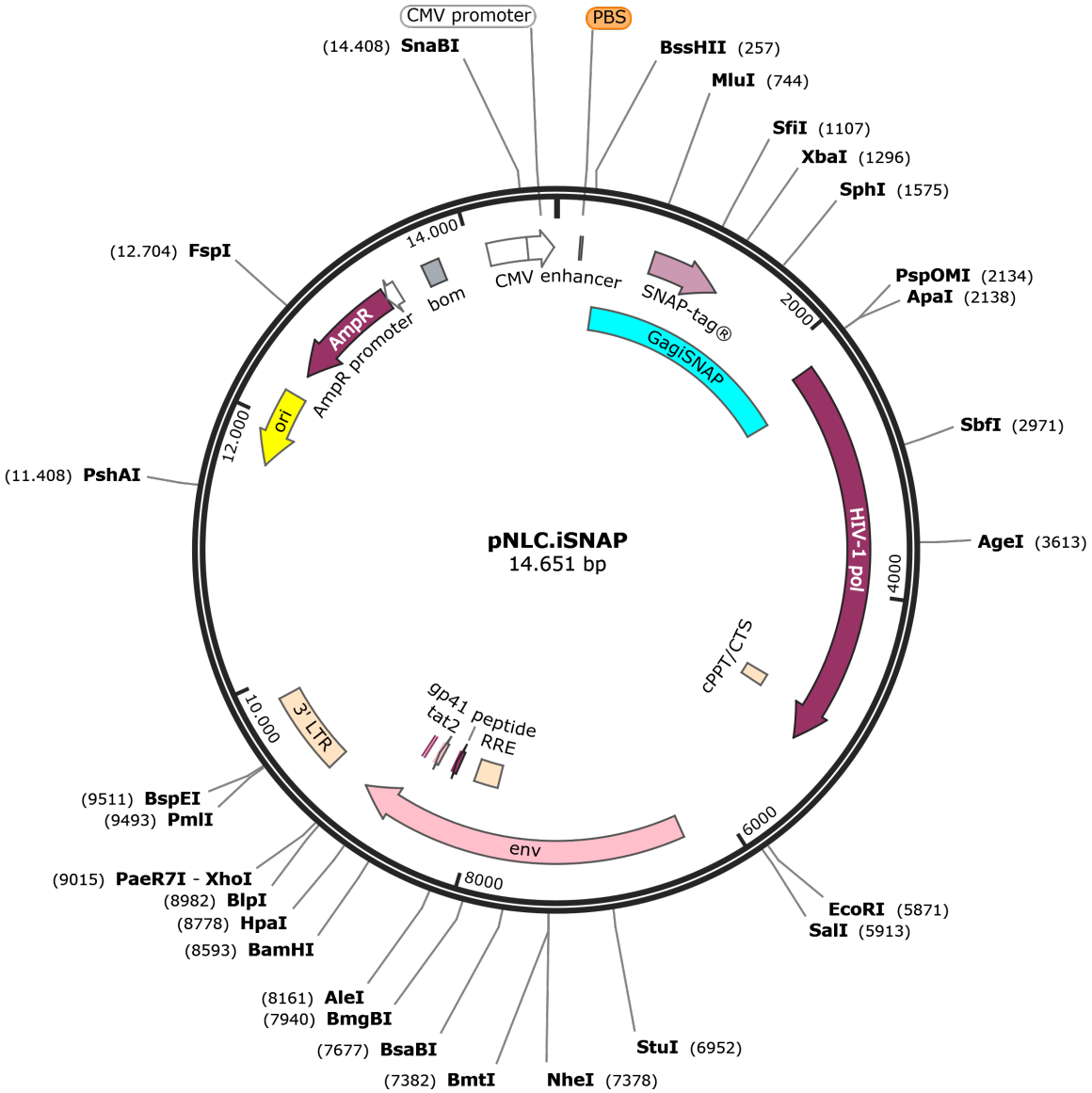

Supplementary Figure 4 Plasmid map of pNLC.iSNAP.
The plasmid is based on the wildtype proviral plasmid pNLC4-3 with iSNAP integrated between the MA and CA as internal domains.

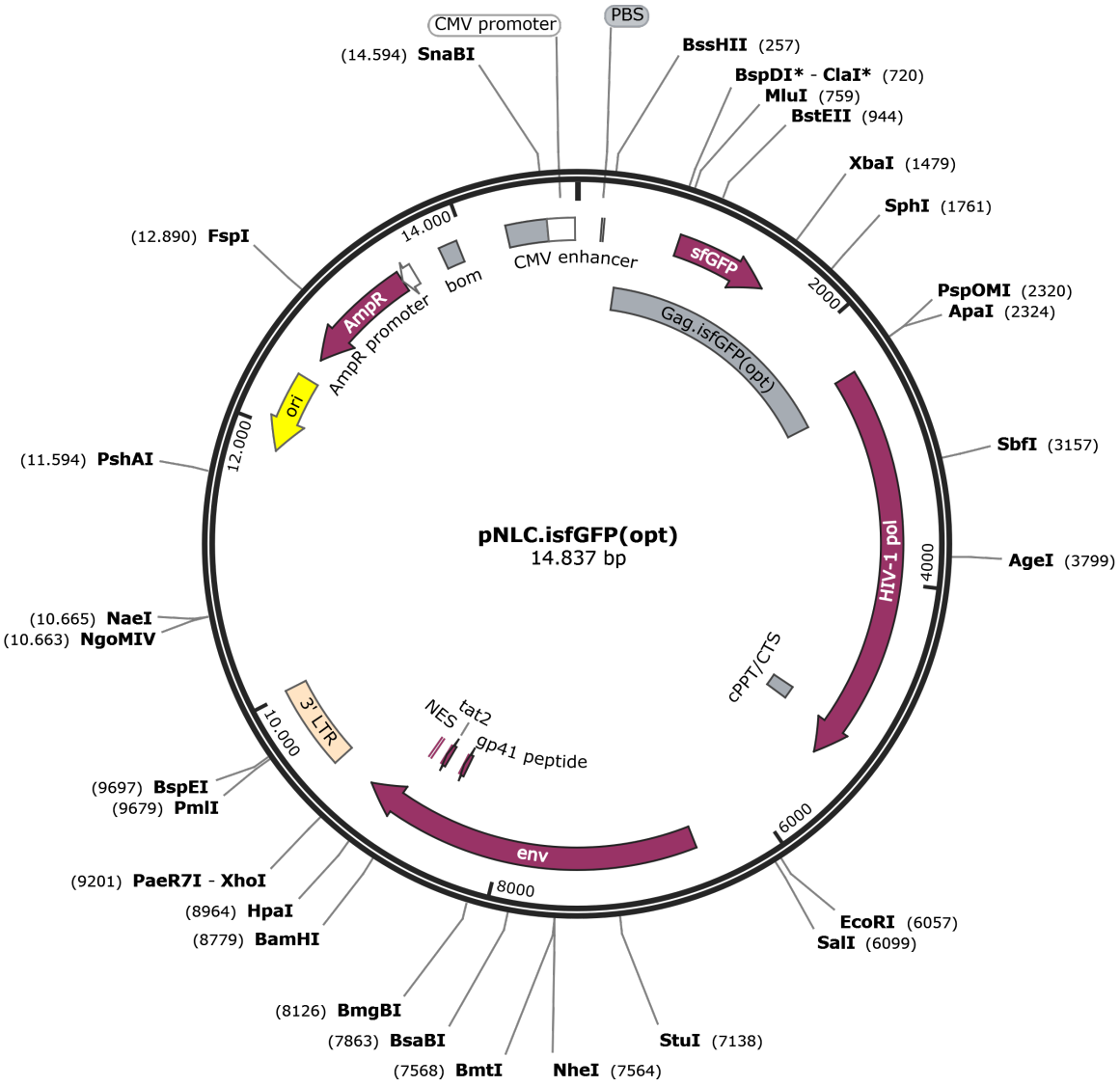

Supplementary Figure 5 Plasmid map of pNLC.isfGFP(opt)

The plasmid is based on the wildtype proviral plasmid pNLC4-3 with isfGFP(opt) integrated between the MA and CA as internal domains.

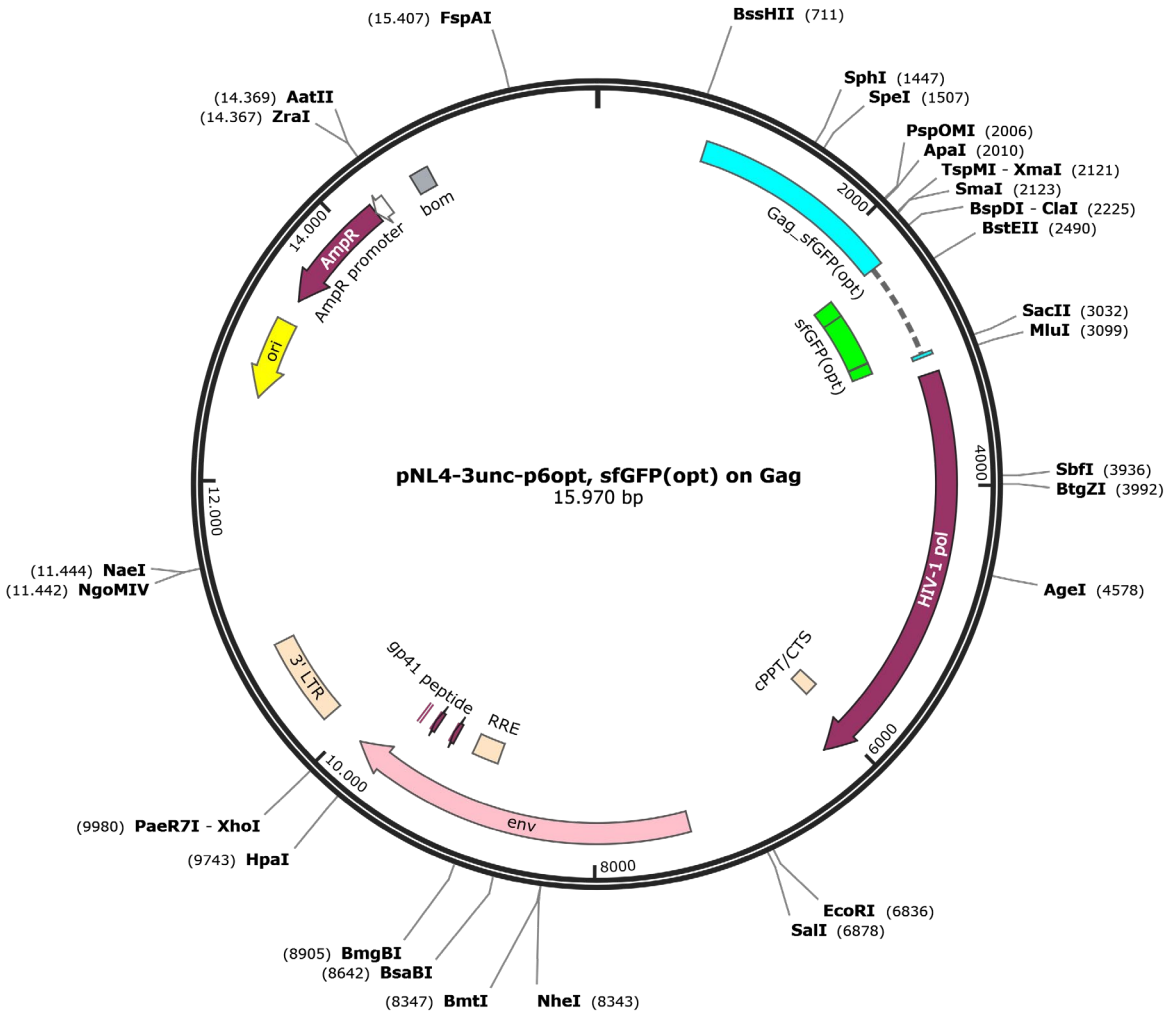

Supplementary Figure 6 Plasmid map of pNL4-3unc-p6opt, sfGFP(opt) on Gag.
This plasmid is based on the proviral plasmid pNL4-3. sfGFP(opt) is inserted at the C-terminal end of Gag, where the Gag and Pol ORFs are genetically uncoupled to prevent any impact on the processing of Pol.

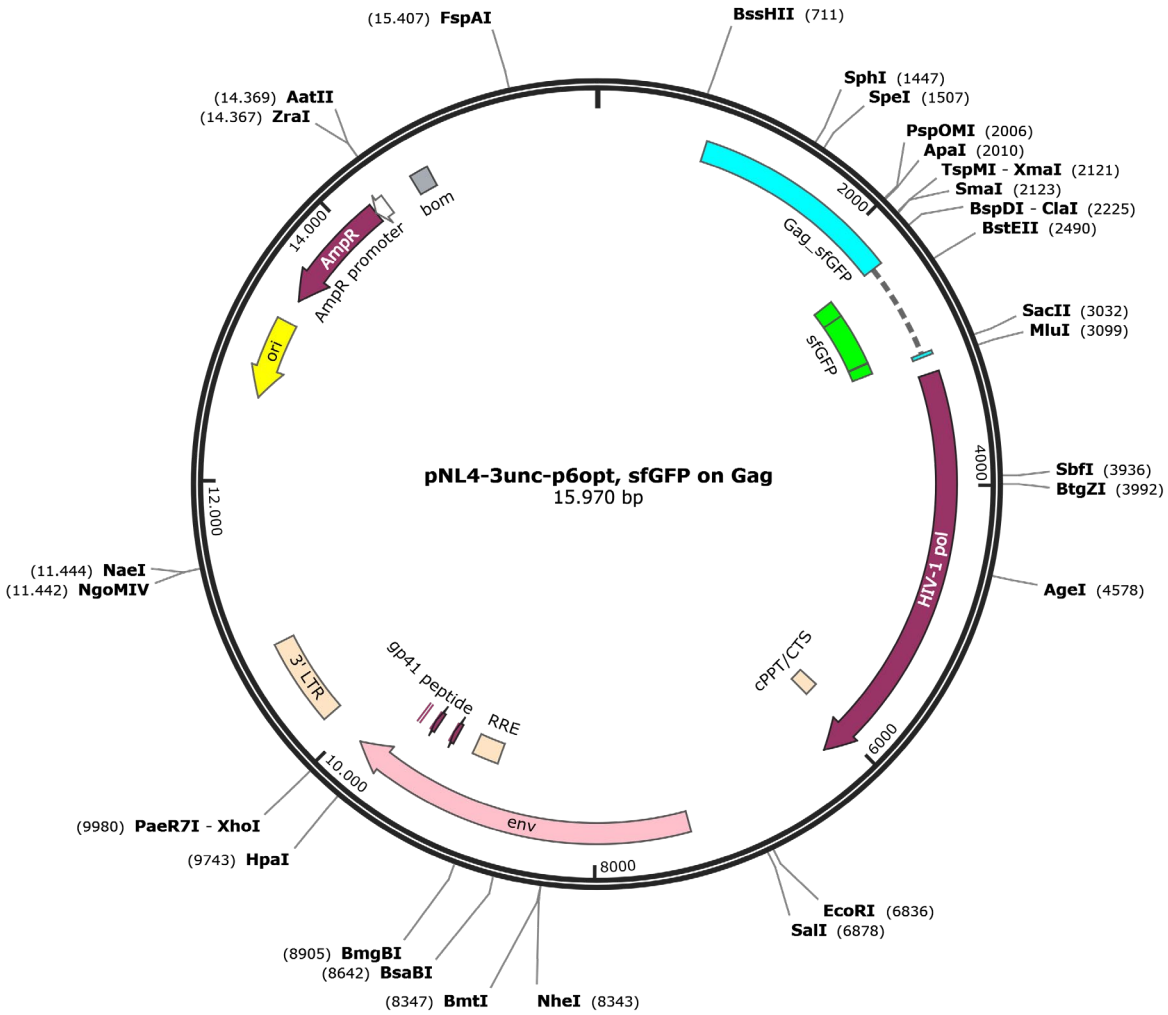

Supplementary Figure 7 Plasmid map of pNL4-3unc-p6opt, sfGFP on Gag.
This plasmid is based on the proviral plasmid pNL4-3. sfGFP(opt) is inserted at the C-terminal end of Gag, where the Gag and Pol ORFs are genetically uncoupled to prevent any impact on the processing of Pol.